

GEOGRAPHICA ANNONICA

Volume 25, Issue 1 (March 2021)





UNIVERSITY OF NOVI SAD | FACULTY OF SCIENCES
DEPARTMENT OF GEOGRAPHY, TOURISM & HOTEL MANAGEMENT

INTERNATIONAL SCIENTIFIC JOURNAL

GEOGRAPHICA PANNONICA

Volume 25, Issue 1, March 2021

INTERNATIONAL SCIENTIFIC JOURNAL
GEOGRAPHICA PANNONICA

UNIVERSITY OF NOVI SAD | FACULTY OF SCIENCES | DEPARTMENT OF GEOGRAPHY, TOURISM & HOTEL MANAGEMENT

EDITOR IN CHIEF

Lazar Lazić, lazarus@uns.ac.rs

EDITORS

Jasmina Đorđević, jasminadjordjevic@live.com

Imre Nagy, nagy@rkk.hu

Milka Bubalo Živković, milka.bubalo.zivkovic@dgt.uns.ac.rs

Aleksandra Dragin, sadragin@gmail.com

Mladen Jovanović, mladjenov@gmail.com

Minučer Mesaroš, minucher@gmail.com

TECHNICAL EDITOR

Dragan Milošević, dragan.milosevic@dgt.uns.ac.rs

Jelena Dunjić, dunjicjelena1@gmail.com

EDITORIAL BOARD

Slobodan B. Marković

University of Novi Sad
Faculty of Science
Novi Sad, Serbia

Tobias Heckmann

Department of Geography, Physical Geography
Catholic University Eichstaett-Ingolstadt
Eichstätt, Germany

Petru Urdea

West University of Timișoara
Department of Geography
Timișoara, Romania

Tamás Weidinger

Eötvös Loránd University
Institute of Geography and Earth Science
Department of Meteorology
Budapest, Hungary

Marko Krevs

University of Ljubljana
Faculty of Art, Department of Geography
Ljubljana, Slovenia

Konstantinos Andriotis

Middlesex University
London, United Kingdom

Michael Lehnert

Palacky University Olomouc
Faculty of science, Department of Geography
Olomouc, Czech Republic

Szabó Szilárd

University of Debrecen
Department of Physical Geography and Geoinformatics
Debrecen, Hungary

Tajan Trobec

University of Ljubljana
Department of Geography
Ljubljana, Slovenia

Crețan Remus

West University of Timișoara
Department of Geography
Timișoara, Romania

ADVISORY BOARD

Ulrich Hambach

Geowissenschaften Universität Bayreuth
LS Geomorphologie
Bayreuth, Germany

Milivoj Gavrilov

University of Novi Sad
Faculty of Science
Novi Sad, Serbia

Matej Ogrin

University of Ljubljana
Department of Geography
Ljubljana, Slovenia

Nina Nikolova

"St. Kliment Ohridski" University of Sofia
Faculty of Geology and Geography
Department of Climatology, Hydrology and
Geomorphology
Sofia, Bulgaria

Zorana Lužanin

University of Novi Sad
Faculty of Science
Novi Sad, Serbia

Damir Demonja

Institute for Development
and International Relations, IRMO,
Zagreb, Croatia

Praveen Kumar Rai

Banaras Hindu University
Department of Geography
Varanasi, India

Petr Šimáček

Palacky University Olomouc
Faculty of science, Department of Geography
Olomouc, Czech Republic

Ivana Bajšanski

University of Novi Sad
Faculty of Technical Sciences
Novi Sad, Serbia

Ondrej Slach

University of Ostrava
Department of Human Geography and Regional
Development (Faculty of Science)
Ostrava, Czech Republic

EDITORIAL OFFICE

Faculty of Sciences
Department of Geography, Tourism and Hotel Management
Trg Dositeja Obradovića 3, 21000 Novi Sad, Serbia
tel. +381 21 450-105
fax +381 21 459-696
Official site: www.dgt.uns.ac.rs

CONTACTS

Lazar Lazić, PhD, full professor

Department of Geography, Tourism and Hotel Management, Serbia, lazarus@uns.ac.rs

Dragan Milošević, teaching assistant

Department of Geography, Tourism and Hotel Management, Serbia, dragan.milosevic@dgt.uns.ac.rs

Official mail of the Journal

gpscijournal@dgt.uns.ac.rs

Internet portal

www.dgt.uns.ac.rs/pannonica.html

Instructions to authors

www.dgt.uns.ac.rs/pannonica/instructions.htm

Contents

Michal Lehnert, Petr Šimáček, David Fiedor, Martin Jurek

Spatial Variability of Soil Temperature in an Urban Area:
a Case Study for a Medium-sized European City 1
[DOI: 10.5937/gp25-29415](https://doi.org/10.5937/gp25-29415)

Hamida Ngoma, Wang Wen, Brian Ayugi, Rizwan Karim, Exavery Kisesa Makula

Mechanisms associated with September to November (SON) rainfall
over Uganda during the recent decades 10
[DOI: 10.5937/gp25-29932](https://doi.org/10.5937/gp25-29932)

Phillip Okello Ochieng, Guirong Tan, Victor Ongoma, Isaiah Nyandega

Influence of Convectively Coupled Equatorial Kelvin Waves
on March-May Precipitation over East Africa 24
[DOI: 10.5937/gp25-31132](https://doi.org/10.5937/gp25-31132)

Pavel Konstantinov, Diana Tattimbetova, Mikhail Varentsov, Natalia Shartova

Summer Thermal Comfort in Russian Big Cities (1966-2015) 35
[DOI: 10.5937/gp25-29440](https://doi.org/10.5937/gp25-29440)

Sabahudin Smajić, Merima Kovačević, Dragoslav Pavić

Identification and Geovisualization of Landscape Transformation of Surface Mine Areas
in the Đurđevik Coal Basin (Bosnia and Herzegovina) 42
[DOI: 10.5937/gp25-29151](https://doi.org/10.5937/gp25-29151)

Ageliki Anagnostou, George Ekonomou, Dimitris Kallioras

The Nexus of Tourism Spending with Economic Performance:
A Panel Data Analysis for the Eurozone Area 53
[DOI: 10.5937/gp25-29541](https://doi.org/10.5937/gp25-29541)

Spatial Variability of Soil Temperature in an Urban Area: a Case Study for a Medium-sized European City

Michal Lehnert^{A*}, Petr Šimáček^A, David Fiedor^A, Martin Jurek^A

Received: November 16, 2020 | Revised: December 15, 2020 | Accepted: December 15, 2020

doi: 10.5937/gp25-29415

Abstract

Even though soil temperature in urban environment influences a range of processes, it has been studied rather sparsely in comparison with surface temperature or air temperature. Our research extends the soil temperature observation in Olomouc (Czechia) and uses semi-stationary measurement to describe detailed spatial variability of soil temperature in the area of a medium-sized Central European city. Differences in soil temperature 20 cm below grass-covered surface may exceed 3°C due to soil type, shadow cast by buildings and grass characteristics, which means that the representativeness of the data on soil temperature from a meteorological station within a city may be limited. Further research and a conceptual approach towards the study of soil temperature in urban landscape is needed.

Keywords: soil temperature; urban climate; Olomouc

Introduction

Soil temperature influences a range of significant processes in the landscape; however, it remains studied rather infrequently. Data on temperature and thermal regimes of soils are essential for many scientific as well as technical contexts and applications, from pedology and ecology to agronomy and construction (e.g. Šulgin, 1972; Bedrna et al., 1989; Jenny, 1994; Probert, 2000; Gens, 2010; Duray et al. 2015). In recent years, the study of thermal regimes of soils and soil temperature has also gained attention in the research of urban and suburban climate (urban climate science); due to climate change a progressive field requiring (fine-scale) climatic models that demand accurate input data on the characteristics and physical properties of land surface and its adequate parametrisation (Masson et al., 2020).

In the studies of urban climate, emphasis is given to the characteristics of anthropogenic surface

and their accurate parametrisation (Mohajeri et al., 2017). Soils represent a considerable part of active surface in urban areas (Kopp & Raška, 2017); however, their characteristics are strongly generalized (Sievers et al., 1983; Bokwa et al., 2019; Feranec et al., 2019; Resler et al., 2020) considering the range of factors influencing temperature and thermal regimes of soils (Lehnert, 2014) and the general variability of soils in urban areas (Milošević et al. 2014; Sobocká et al., 2020). This leads to significant inaccuracies in the presumed radiative balance of active surface, and to differences between simulated and observed/real heat fluxes (Christen and Vogt, 2004).

Unlike many studies on surface temperature (in Central Europe e.g. Schwarz et al., 2012; Dobrovolný, 2013; Gemés et al., 2016; Geletič et al., 2019; Fricke et al., 2020), only a limited number of empirical studies have been carried out with focus on soil tempera-

^A Palacky University Olomouc, Faculty of science, Department of Geography, Olomouc, Czech Republic; m.lehnert@upol.cz, petr.simacek@upol.cz, david.fiedor@upol.cz, martin.jurek@upol.cz

* Corresponding author: Michal Lehnert; e-mail: m.lehnert@upol.cz

ture in urban environment. Harman (2003) presented a theory presuming lower average temperature of the soil surface in built-up areas compared to areas outside of housing development. On the contrary, Lokoshchenko and Korneva (2015) used long-term measurements in Moscow (Russia) to calculate that the mean difference in soil temperature between central areas of the city and rural surroundings equals to 0.6–0.8°C and the mean difference between urban periphery and rural surroundings equals to 0.4–0.6°C. The differences were most pronounced in the winter season and less pronounced in the summer. Similarly, Tang et al. (2011) observed soil temperature 1.2°C higher in urban area compared with its rural surroundings, using stationary measurement of temperature in homogenised soil placed into plastic tubes in Nanjing (China). Tang et al.

(2011) also used semi-stationary measurements (600 research points in two days of August 2010) to detect larger spatial variability of soil temperature within a city. In our previous study (Lehnert, 2013b) we analysed stationary (station) measurements in Olomouc and its surroundings but we did not detect any clear influence of the city on soil temperature but we showed that spatial variability of soil temperature in urban and sub-urban landscape could be studied in further detail by means of field measurements (Lehnert et al., 2015). Considering the growing interest in the topic of temperature and thermal regimes of soils in urban environment, we aim in this case study to assess spatial variability of average daily soil temperature in the city of Olomouc, Czechia using two days of detailed field measurements of soil temperature.

Methods

Study area

The research was carried out in the city of Olomouc in the eastern part of the Czech Republic (Figure 1). Olomouc is a mid-sized city (100 thousand inhabitants, area of 103 km²) located mostly in the flat floodplain of the Morava river, with mean elevation of 245 m a.s.l. Haplic and gleyic Fluvisols prevail, complemented in the urban landscape of Olomouc by larger areas of urban Anthrosols. Olomouc has a moderate climate (Cfb temperate oceanic climate according to Köppen classification) with average annual temperature of 8.9°C and annual sum of precipitation 547 mm (Vysoudil et al., 2012). A long-term research of urban climate is underway in Olomouc and the urban heat island (UHI) effect of more than 2.0°C has been detected (Lehnert et al., 2018). The city structure is typical of a wide range of the types of urban development, from the preserved historical centre with compact streets to quarters of detached houses with gardens, mid-rise blocks of flats, recently built shopping zones and suburban settlements. In the surroundings of the city, agricultural landscape prevails.

Field measurement

The field measurement was designed with the aim to cover locations that would represent the variability of urban environment and types of housing development (Figure 1). Potential research locations were identified using the leading factor (compact development, flat terrain, grass surface) and subsequently a defined set of research locations was established by means of expert selection. Each research point was placed inside the area of the research location far enough from its fringe, it was covered with vegetation representative for the whole location and preliminary measurements

were carried out before the main measurement campaign to ensure that soil moisture and soil temperature data measured at that point were characteristic for the whole research location.

Measurements were carried out using digital penetration thermometers Hanna HI 145 (Figure 2) with an accuracy of 0.3°C in the used temperature range. The thermometers were chosen considering their fast sampling response, acceptable accuracy tested through comparison with meteorological station measurement, and financial accessibility (Lehnert 2013a). Thermometer inertia was taken into account, soil temperature record was taken only after stabilisation of the value measured on the probe (usually 2–5 minutes after insertion into soil). In order to obtain representative data records, soil temperature was measured at each research point at least twice and always using at least two thermometers, following the recommendation of Buchan (2001).

The case study measurement campaign was carried out in the city of Olomouc in two days of spring, 5 and 7 May 2015, at 25 research points (Table 1). The weather during the experiment days is described in Table 2 and synoptic situation in Europe is illustrated by charts in Appendix A, showing a transition of a cold front across Central Europe on 6 May, 2020. The measurement was carried out in the times used for the determination of average soil temperature 07, 14 and 21 Central European Time ±30 minutes necessary for all the measurement teams to cover all locations of measurement. Eventual inaccuracy of measurement due to this temporal span does not exceed 0.1°C at the 98% probability level, as demonstrated before by stationary soil temperature measurement in Olomouc (Lehnert, 2013a).

Figure 2. Semi-stationary soil temperature measurement in Olomouc and surroundings
Source: Lehnert, 2013a

Figure 1. Study area and soil temperature measurement sites in Olomouc

Table 1. Characteristics of the research points of the field experiment*

Point	Elevation (m a.s.l.)	Soil type (FAO WRB)	LCZ	Grass height (cm)	Soil moisture (% vol.)	
					5 May 2015	7 May 2015
BE1	217	FL ha	89	6-10	16	14
BE2	217	FL ha	8D	6-10	13	18
BE3	216	FL ha	9	11-15	15	16
BE4	216	FL ha	9	1-5	7	14
BE5	216	FL ha	9	11-15	18	21
EN1	212	AT	59	6-10	13	15
EN2	212	FL ha	59	1-5	12	20
EN3	213	FL ha	5	1-5	15	16
EN4	214	FL ha	5	11-15	17	16
EN5	214	AT	5	16-20	13	20
NU1	233	AT	8	11-15	14	18
NU2	238	CH ar	89	6-10	24	20
NU3	250	CH ar	59	1-5	20	18
NU4	236	AT	5	11-15	20	19
NU5	237	CH ar	5	11-15	13	16
ST1	215	AT	5	11-15	14	11
ST2	214	AT	9	6-10	19	16
ST3	214	FL ha	DB	6-10	10	15
ST4	214	FL ha	85	11-15	14	20
ST5	214	FL ha	59	1-5	12	28
UD1	222	CM lv	5B	6-10	15	25
UD2	212	AT	5	1-5	24	18
UD3	213	FL ha	5	6-10	12	23
UD4	214	FL ha	5	6-10	13	18
UD5	213	FL ha	D	6-10	19	22

* Base map sources: COSMC 2020, Natural Earth 2020

Notes:

- 1) FAO WRB – World Reference Base for Soil Resources by the Food and Agriculture Organization of the United Nations: FL ha – Fluvisol haplic, AT – Anthrosol, CH ar – Chernozem arenic, CM lv – Cambisol luvic
- 2) LCZ – Local Climate Zones (see Stewart & Oke, 2012 for further details)
- 3) Vegetation cover of soil (vertical view) 76–100% in all cases except UD4, where it was 50–75%.

Table 2. Weather conditions on 5–7 May 2015 at the meteorological station Olomouc-Holice

		5 May 2015	6 May 2015	7 May 2015
Air temperature (°C)	max.	23.8	19.0	20.1
	avg.	19.1	15.1	13.8
	min.	12.5	14.0	9.6
Relative humidity (%)	avg.	74	88	59
Precipitation (mm)		11.7	1.4	0.0
Wind speed (m s ⁻¹)		2.3	1.3	3.3
Sunshine duration (hrs)		3.2	0.0	10.7

Source: Czech Hydrometeorological Institute.

Results

On the reference meteorological station Olomouc-Holice of the Czech Hydrometeorological Institute, average daily soil temperature in 20 cm depth was 14.2°C on 5 May, 2015 and 14.7°C on 7 May, 2015 (Table 3). Based on soil temperature measurements at various depths, a trend typical for the season of increasing soil temperature occurred at depths of 20, 50 and 100 cm, while short-term weather patterns influenced the near-surface layers of the soil. Vertical profile of soil temperature during the measurement campaign can be derived from the reference station Olomouc-Holice. Horizontal spatial variability of soil temperature, however, can only be obtained through detailed field measurement.

On the first day of the experiment (5 May 2015), values of average daily soil temperature in 20-cm depth

Values higher than the temperature at the reference station were observed namely within the research sector EN. The average daily soil temperature in 20-cm depth, calculated as the average of all research points, was 14.4°C, a good fit with the average daily soil temperature at the reference station Olomouc-Holice (14.2°C).

Results from the second day of the field experiment (7 May 2015) indicate rise by 0.3°C in average daily soil temperature in comparison with the records from the first day of the experiment (on the reference station Olomouc-Holice, the rise was by 0.5°C). In detail, soil temperature was higher on 20 from the 25 research points on the second day (Figure 3), while the overall spatial variability in average daily soil temperature within the city was smaller on the sec-

Table 3. Soil temperature [°C] at the reference station Olomouc-Holice on 5–7 May, 2015

T _{depth(cm)}	5 May 2015	6 May 2015	7 May 2015
T ₀₅	15.9	16.0	15.5
T ₁₀	15.5	15.9	15.3
T ₂₀	14.2	15.1	14.7
T ₅₀	12.3	13.1	13.3
T ₁₀₀	10.8	11.0	11.2

Source: Czech Hydrometeorological Institute.

at the research locations in the city showed a –1.8°C to +1.4°C deviation from the average daily temperature of 14.2°C at the reference station Olomouc-Holice, so the overall soil temperature range in average daily soil temperature was 3.2°C at the study locations within the city. Figure 3 shows that the lowest average daily soil temperature (in 20-cm depth) was detected at research point UD5 followed by NU4 and NU5, while the highest average daily soil temperature was detected at research point EN1 followed by EN5 and EN2.

ond day. On 7 May 2015, average daily soil temperature at the research points deviated –1.7°C to +1.1°C from the average daily soil temperature at the reference station Olomouc-Holice (14.7°C), thus the overall temperature range was 2.8°C. The lowest average daily soil temperature was detected at research points NU4 (13.0°C) and NU5 (13.3°C), the highest at the research point EN2 (15.8°C). The average daily soil temperature derived from the whole set of research points within the city was 14.7°C, equal to the value at the

Figure 3. Soil temperature in 20-cm depth at research points of the field experiment in Olomouc, 5 and 7 May 2015
Base map source: COSMC 2020

Discussion and conclusion

The field experiment was incited by previous studies analysing temperature characteristics in the urban environment of Olomouc (Geletič & Vysoudil, 2012; Lehnert et al., 2018; Lehnert et al., 2020) and pedological research in the area (e.g. Chmelová & Šarapatka, 2002). Spatial variability of soil temperature within the city was illustrated on the example of two days with different weather conditions and using semi-stationary field measurement. This study explicitly expresses the differences in average daily soil temperature across the city in comparison with the background reference station. The range of soil temperature differences may exceed 3.0°C on a sunny day. The average of soil temperature from all research points is in good fit with the value at the reference station, a confirmation of the relevance of the field experiment and of the adequate location of the meteorological station Olomouc-Holice for soil temperature measurement. The results of the experiment also confirm the assumption that it is not possible to find any simple relation between soil temperature and city parts, urban building types etc., which is similar to the complexity of differences in soil temperature between urban and suburban landscape (Lehnert et al., 2015).

Detected spatial variability in soil temperature in urban environment may result in various practical applications – it may influence the composition/diversity of low vegetation in individual parts of the city (Čeplová et al., 2017), it may influence evaporation (Feldhake & Boyer, 1986), technical parameters of buildings and underground utilities (Low et

reference station and thus again confirming a good fit in the selection of the reference station as well as the relevance of the field experiment.

A comparison of soil temperature at the individual research points and at the reference station Olomouc-Holice reveals that there are characteristic differences at most locations for both days; therefore, the detected differences are not random and indicate that there is a pattern of spatial differences in soil temperature across the city (of Olomouc). The results also demonstrate a considerable variability in soil temperature at the scale of individual city quarters (research sectors), which means that it is rather difficult to identify areas with higher/lower soil temperature on the basis of the methodology used in the experiment (see Discussion). Nevertheless, the results from 7 May 2015, when cloudiness was lower and sun irradiation was more intense, reveal higher soil temperature in the sector of Envelopa (EN1–EN5) with low-rise buildings and subterranean anthropogenic sources of heat.

al., 2013), or in the context of thermal characteristics of soils and of active surface it may be included into and influence the accuracy of (fine-scale) meteorological models (Maronga et al., 2020). The detected spatial variability of soil temperature also points to the issue of representativeness of stationary meteorological measurements not only in the urban environment. The vast majority of stations that observe soil temperature are located on the basis of requirements for meteorological observation (air temperature, precipitation, wind direction and velocity etc.) or based on research parameters for urban climate studies (Vysoudil et al., 2012). When selecting locations for soil temperature measurements, research of the field of soil temperature in the area should be performed and physical characteristics of soils should be determined prior to selecting the definitive location, one that would properly represent the characteristic soil temperature pattern and regime in the area (Shein et al., 2009). Otherwise, local differences in soil temperature may completely override the regional differences, failing the representativeness of the results for a wider area (Lehnert, 2013b).

Spatiotemporal variability of soil temperature cannot be determined neither on the basis of spatiotemporal variability of air temperature (Zheng et al. 1993; Kang et al., 2000; Dolschak et al., 2015) nor on the basis of surface temperature, therefore further research and a methodological and conceptual approach to the study of temperature and thermal regimes of soils (not only for fine-scale climatological modelling) is essential.

This approach must respect the specifics of urban landscape and a substantial variability of soils in urban areas, where pedogenesis and the resulting spatial variability of soils is largely interconnected with human activity.

For further analyses of temperature and thermal regimes of soils in urban environment in the con-

text of their applicability, the concept of pedo-urban complexes or urban pedotope (Sobocká, 2010; Sobocká et al., 2020) seems applicable and it may be to a large extent compatible with the concept of local climate zones (Stewart & Oke, 2012), a concept well established in the study of urban climate.

Acknowledgement

This research was supported by an internal grant from Palacký University, Olomouc ref. IGA_PrF_2020_029 Spatial analysis of selected environmental and social issues in urban and suburban areas.

References

- Bedrna, Z., Fulajtár, E., Zrubec, F., & Juráni, B. (1989). *Pôdne režimy*. Veda, Bratislava.
- Bokwa, A., Geletič, J., Lehnert, M., Žuvela-Aloise, M., Hollósi, B., Gál, T., Skarbit, N., Dobrovolný, P., Hajto, M.J., Kielar, R. & Walawender, J. P. (2019). Heat load assessment in Central European cities using an urban climate model and observational monitoring data. *Energy and Buildings*, 201, 53-69.
- Buchan, G. D. (2001): Soil temperature regime. In: Smith, K. A., Mullins, C. E. [eds.]: *Soil and Environmental analysis: Physical methods* (pp. 539-594). New York, Marcel Dekker.
- Čeplová, N., Kalusová, V., & Lososová, Z. (2017). Effects of settlement size, urban heat island and habitat type on urban plant biodiversity. *Landscape and Urban Planning*, 159, 15-22.
- Chmelová, R., & Šarapatka, B. (2002). Soil erosion by water: Contemporary research methods and their use. *Geographica*, 37, 23-30.
- Christen, A., & Vogt, R. (2004). Energy and radiation balance of a central European city. *International Journal of Climatology: A Journal of the Royal Meteorological Society*, 24(11), 1395-1421.
- COSMC – Czech Office for Surveying, Mapping and Cadastre (2020): Esri ArcGIS Server View Service - Orthophoto CR. Publicly available at: <https://ags.cuzk.cz/ArcGIS/rest/services/ortofoto/MapServer>
- Dobrovolný, P. (2013). The surface urban heat island in the city of Brno (Czech Republic) derived from land surface temperatures and selected reasons for its spatial variability. *Theoretical and Applied Climatology*, 112(1-2), 89-98.
- Dolschak, K., Gartner, K., & Berger, T. W. (2015). A new approach to predict soil temperature under vegetated surfaces. *Modeling Earth Systems and Environment*, 1(4), 32.
- Duray, B., Nagy, I., Andres, L., & Milošević, D. (2015). Soil pollution in the Hungarian-Romanian border region (Valley of Körös-Cris rivers). *Carpathian Journal of Earth and Environmental Sciences*, 10(3), 207-216.
- Feldhake, C. M., & Boyer, D. G. (1986). Effect of soil temperature on evapotranspiration by C3 and C4 grasses. *Agricultural and Forest Meteorology*, 37(4), 309-318.
- Feranec, J., Kopecká, M., Szatmari, D., Holec, J., Šťastný, P., Pazúr, R., & Bobálová, H. (2019). A review of studies involving the effect of land cover and land use on the urban heat island phenomenon, assessed by means of the MUKLIMO model. *Geografie*, 124, 83-101.
- Fricke, C., Pongrácz, R., Gál, T., Savić, S., & Unger, J. (2020). Using local climate zones to compare remotely sensed surface temperatures in temperate cities and hot desert cities. *Moravian Geographical Reports*, 28(1), 48-60.
- Geletič, J., Lehnert, M., Savić, S., & Milošević, D. (2019). Inter-/intra-zonal seasonal variability of the surface urban heat island based on local climate zones in three central European cities. *Building and Environment*, 156, 21-32.
- Geletič, J., & Vysoudil, M. (2012): Analysis of surface temperatures in urban and suburban landscapes from satellite thermal images: A case study of olomouc and its environs, Czech Republic [Analýza povrchové teploty v městské a příměstské krajině na základě analýzy satelitních termálních snímků, Olomouc a okolí (Česká Republika)]. *Moravian Geographical Reports*, 20 (1), pp. 2-15.
- Gémes, O., Tobak, Z., & Van Leeuwen, B. (2016). Satellite based analysis of surface urban heat island intensity. *Journal of Environmental Geography*, 9(1-2), 23-30.
- Gens, A. (2010). Soil-environment interactions in geotechnical engineering. *Géotechnique*, 60(1), 3-74.
- Harman, I. N. (2003): *The energy balance of urban areas*. Dissertation. Reading: University of Reading.

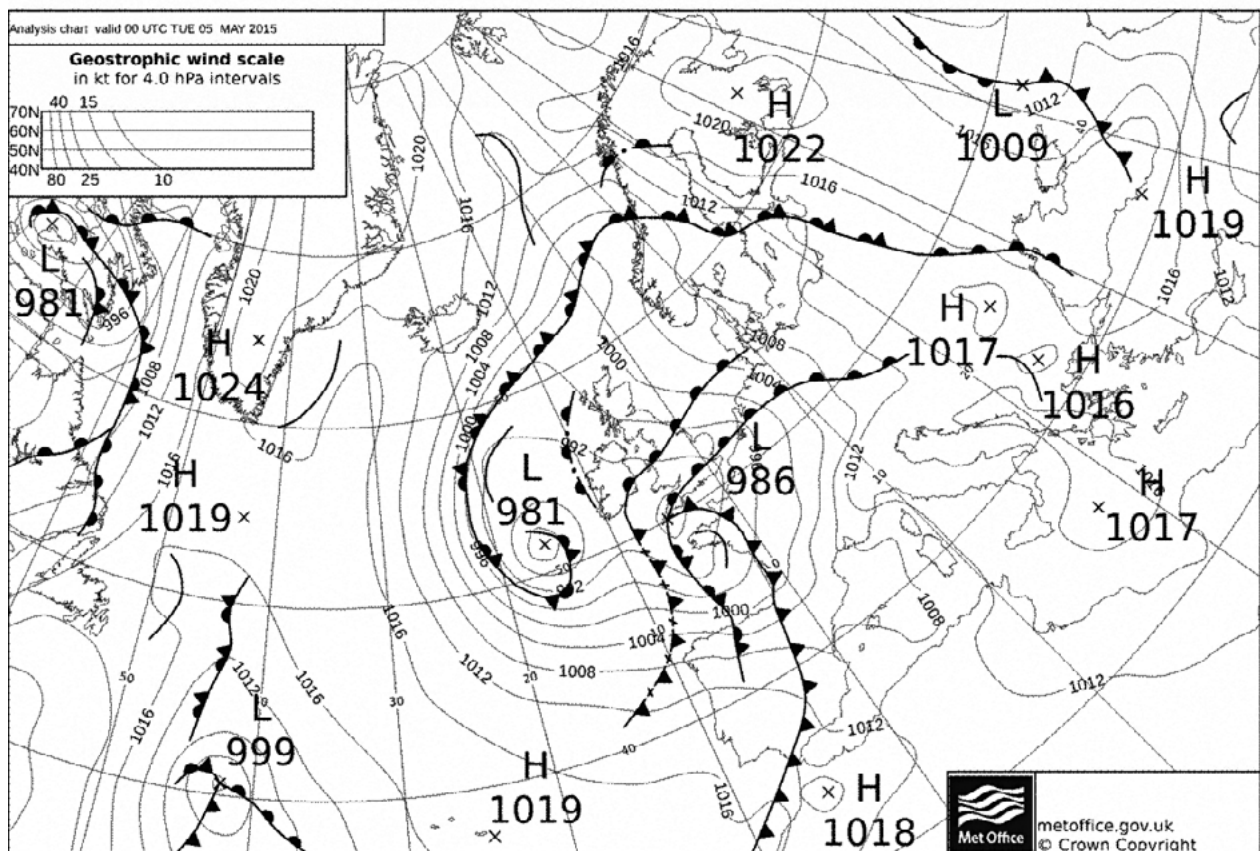
- Jenny, H. (1994): *Factors of soil formation: a system of quantitative pedology*. New York: Dover Publications, Inc.
- Kang, S., Kim, S., Oh, S., & Lee, D. (2000). Predicting spatial and temporal patterns of soil temperature based on topography, surface cover and air temperature. *Forest Ecology and Management*, 136(1-3), 173-184.
- Kopp, J. & Raška P. (2017). *Ekohydrologický management mikrostruktur v městské krajiny*. Západočeská univerzita v Plzni, Plzeň.
- Lehnert, M. (2013a). *Vliv vybraných (geo)faktorů na režim teploty půdy v městské a příměstské krajině Olomouce*. Dissertation. Ostravská univerzita v Ostravě, Ostrava.
- Lehnert, M. (2013b). The soil temperature regime in the urban and suburban landscapes of Olomouc, Czech Republic. *Moravian Geographical Reports*, 21(3), 27-36.
- Lehnert, M. (2014). Factors affecting soil temperature as limits of spatial interpretation and simulation of soil temperature. *Acta Universitatis Palackianae Olomucensis-Geographica*, 45(1), 5-21.
- Lehnert, M., Geletič, J., Dobrovolný, P., & Jurek, M. (2018). Temperature differences among local climate zones established by mobile measurements in two central European cities. *Climate Research*, 75(1), 53-64.
- Lehnert, M., Tokar, V., Jurek, M., & Geletič, J. (2020). Summer thermal comfort in Czech cities: measured effects of blue and green features in city centres. *International Journal of Biometeorology*, 1-13. <https://doi.org/10.1007/s00484-020-02010-y>
- Lehnert, M., Vysoudil, M., & Kladivo, P. (2015). Semi-stationary measurement as a tool to refine understanding of the soil temperature spatial variability. *International Agrophysics*, 29(4), 449-457.
- Lokoshchenko, M. A., & Korneva, I.A. (2015). Underground urban heat island below Moscow city. *Urban Climate*, 13, 1-13.
- Low, J. E., Loveridge, F. A., & Powrie, W. (2013). Measuring soil thermal properties for use in energy foundation design. In *Proceedings of the 18th International Conference on Soil Mechanics and Geotechnical Engineering*, Paris, France (pp. 2-6).
- Maronga, B., Banzhaf, S., Burmeister, C., Esch, T., Forkel, R., Fröhlich, D., Fuka, V., Gehrke, K.F., Geletič, J., Giersch, S., & Russo, E. (2020). Overview of the PALM model system 6.0. *Geoscientific Model Development*, 13, 1335-1372.
- Masson, V., Heldens, W., Bocher, E., Bonhomme, M., Bucher, B., Burmeister, C., de Munck, C., Esch, T., Hidalgo, J., Kanani-Sühring, F. & Kwok, Y. T. (2020). City-descriptive input data for urban climate models: Model requirements, data sources and challenges. *Urban Climate*, 31, 100536.
- Milošević, D., Nagy, I., & Stojanović, V. (2014). Soils in the cities: State, problems and remediation techniques. *Researches Reviews of the Department of Geography, Tourism and Hotel Management*, 43(1), 1-16.
- Mohajerani, A., Bakaric, J., & Jeffrey-Bailey, T. (2017). The urban heat island effect, its causes, and mitigation, with reference to the thermal properties of asphalt concrete. *Journal of Environmental Management*, 197, 522-538.
- Natural Earth (2020): Dataset Admin 0 – Countries (version 4.1.0). Publicly available at: <https://www.naturalearthdata.com/>
- Probert, R. J. (2000): The role of temperature in the regulation of seed dormancy and germination. In: Fenner, M. [ed.]: *Seeds: the ecology of regeneration in plant communities* (pp. 261-292). Wallingford, CABI Publishing.
- Resler, J., Eben, K., Geletič, J., Krč, P., Rosecký, M., Sühring, M., Belda, M., Fuka, V., Halenka, T., Huszár, P., & Karlický, J. (2020). Validation of the PALM model system 6.0 in real urban environment; case study of Prague-Dejvice, Czech Republic. *Geoscientific Model Development Discussions*, 1-57.
- Schwarz, N., Schlink, U., Franck, U., & Großmann, K. (2012). Relationship of land surface and air temperatures and its implications for quantifying urban heat island indicators—An application for the city of Leipzig (Germany). *Ecological Indicators*, 18, 693-704.
- Shein, E. V., Bannikov, M. V., Troshina, O. V., & Churkina, O. A. (2009): Temperature field of complex soils (by the example of the Vladimir opolie region). *Eurasian Soil Science*, 42(2): 129-136.
- Sievers, U., Forkel, R., & Zdunkowski, W. (1983). Transport equations for heat and moisture in the soil and their application to boundary layer problems. *Contributions to Atmospheric Physics*, 56, 58-83.
- Sobocká, J. (2010). Specifics of urban soils (Technosols) survey and mapping. *19th World Congress of Soil Science, Soil Solutions for a Changing World, 1-6 August 2010, Brisbane, Australia* (pp. 56-59).
- Sobocká, J., Saksa, M., Feranec, J., Szatmári, D., Holec, J., Bobálová, H., & Rášová, A. (2020). Mapping of urban environmentally sensitive areas in Bratislava city. *Journal of Soils and Sediments*, <https://doi.org/10.1007/s11368-020-02682-4>.
- Stewart, I. D., & Oke, T. R. (2012). Local climate zones for urban temperature studies. *Bulletin of the American Meteorological Society*, 93(12), 1879-1900.
- Šulgin, A. M. (1972). *Klimat počvy i jeho regulirovaniye*. Leningrad, Gidrometeoizdat.
- Tang, C. S., Shi, B., Gao, L., Daniels, J. L., Jiang, H. T., & Liu, C. (2011). Urbanization effect on soil temperature in Nanjing, China. *Energy and Buildings*, 43(11), 3090-3098.

Vysoudil, M., Geletič, J., Lehnert, M., Lipina, P., Pavelková Chmelová, R., & Řepka, M. (2012). Podněbí Olomouce. Univerzita Palackého v Olomouci.

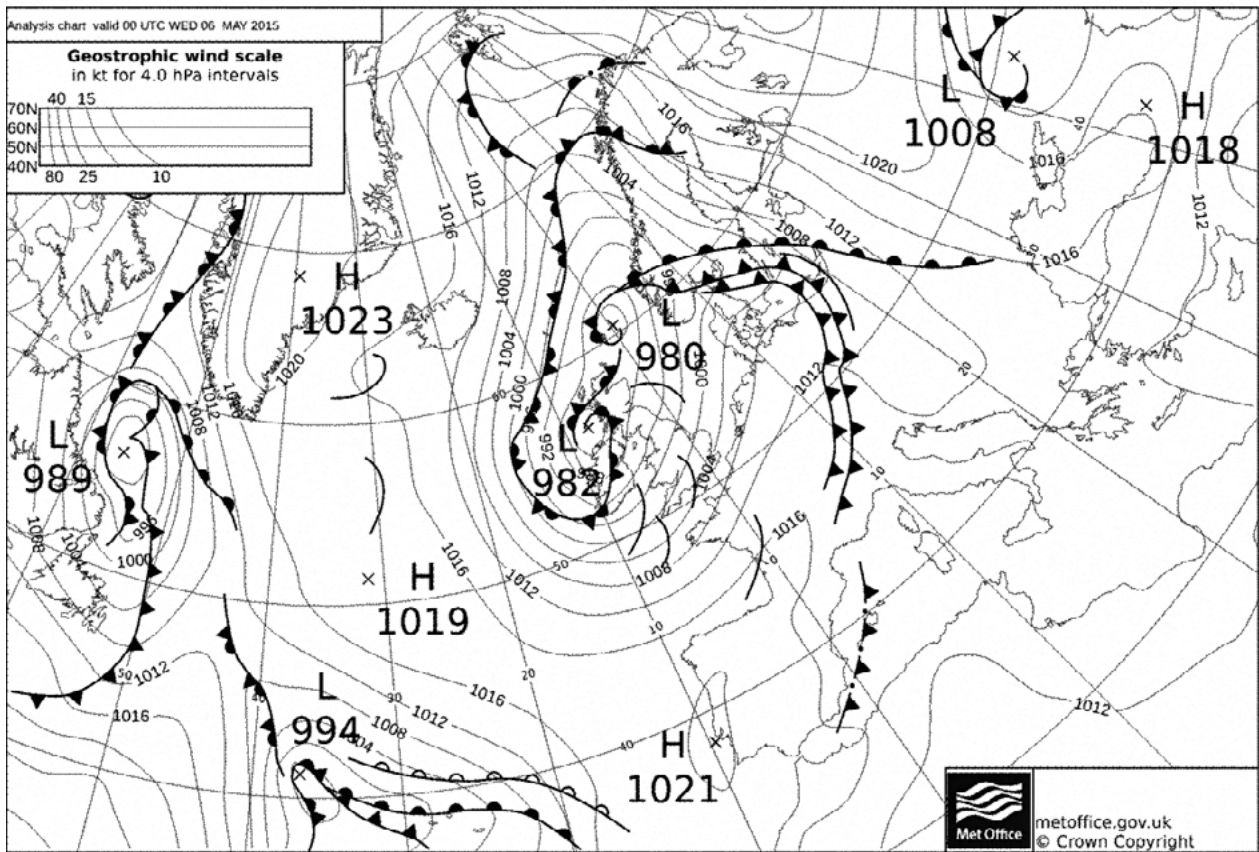
Zheng, D., Hunt, E. R., Running, S. W. (1993): A daily soil temperature model based on air temperature and precipitation for continental applications. *Climate Research*, 2(3): 183–191.

Appendix A

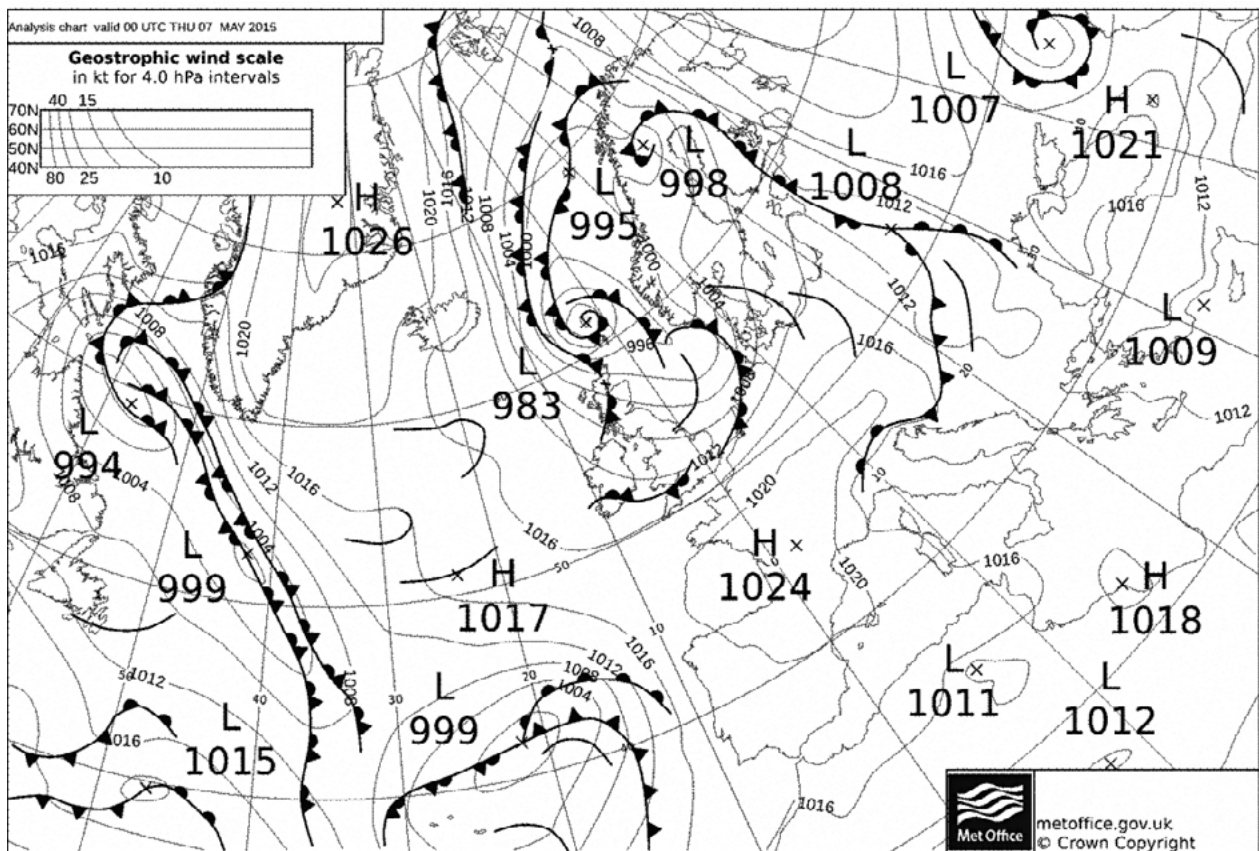
Synoptic charts for Europe, 5–7 May, 2020 (Source: UK Met Office in <https://www.wetterzentrale.de/reanalysis.php>)



5 May, 2020 (00 UTC)



6 May, 2020 (00 UTC)



7 May, 2020 (00 UTC)

Mechanisms associated with September to November (SON) rainfall over Uganda during the recent decades

Hamida Ngoma^{A,C*}, Wang Wen^A, Brian Ayugi^{A,B,E}, Rizwan Karim^A, Exavery Kisesa Makula^{A,D}

Received: December 19, 2020 | Revised: February 14, 2021 | Accepted: February 25, 2021

doi: 10.5937/gp25-29932

Abstract

This study revisits teleconnections associated with the anomalous events of September to November (SON) rainfall over Uganda during 1981-2019, owing to the recent intensification of extreme events. Empirical Orthogonal Function (EOF), Composite and Correlation analysis are employed to examine the variability of SON rainfall over the study domain and associated circulations anomalies. The first EOF mode (dominant mode) displays a positive monopole pattern and explains 67.2% of the variance. The results revealed that SON rainfall is largely influenced by a Walker circulation mode over the Indian Ocean, whereby, wet events are associated with an ascending limb of the Walker circulation on the western part of the Indian Ocean characterized by convergence at low levels and divergence at upper level. The study showed that SON rainfall is positively (negatively) correlated with Indian ocean (Atlantic Ocean) sea surface temperatures (SST). Furthermore, Indian Ocean Dipole (IOD) events have impact on SON rainfall with strong positive correlation, whereas Southern Oscillation Index (SOI) revealed negative correlation. The results also reveal that there is a lag in ENSO and IOD episodes during wet/dry events over the region. ENSO and IOD also tend to extend the rainfall season of SON and thus study of extreme events may not be well captured by studies focusing on SON. Future studies might consider the season of October to December or December to February. These phenomena need to be closely monitored and considered when making seasonal forecasts.

Keywords: Rainfall; Extreme; Circulation; Uganda; East Africa

^A Key Laboratory of Meteorological Disaster, Ministry of Education (KLME)/Joint International Research Laboratory of Climate and Environment Change (ILCEC)/Collaborative Innovation Center on Forecast and Evaluation of Meteorological Disasters (CIC-FEMD), Nanjing University of Information Science and Technology, Nanjing 210044, China; hamynads@gmail.com; wangwen@nuist.edu.cn; rizwan555danyore@gmail.com

^B Jiangsu Key Laboratory of Atmospheric Environment Monitoring and Pollution Control, Collaborative Innovation Center of Atmospheric Environment and Equipment Technology, School of Environmental Science and Engineering, Nanjing University of Information Science and Technology, Nanjing 210044, China; ayugi.o@gmail.com

^C Department of Geography, Geoinformatics and Climatic Sciences, Makerere University, P.O. Box 7062, Kampala, Uganda; hamynads@gmail.com

^D University of Dar es Salaam, Physics Department, P.O. Box 35063, Dar es Salaam, Tanzania; kisesaexavery@yahoo.com

^E Organization of African Academic Doctors (OAAD), Off Kamiti Road P.O. Box 25305-00100, Nairobi, Kenya

* Corresponding author: Hamida Ngoma; e-mail: hamynads@gmail.com

Introduction

Uganda is an agricultural country and the economy largely depends on rainfed agriculture. Abnormal occurrences in rainfall have far-reaching effects on community livelihoods (GOU, 2015). Rainfall over the region exhibits high spatial and temporal variability. This is attributed to the complex topography, varying vegetation patterns and large inland water bodies which regulate the local climate (Basalirwa, 1995; Ogwang et al., 2014). Rainfall over the region is mostly influenced by the equatorial rain band which oscillates northwards and southwards throughout the year (Nicholson, 1996; 2018). This convergence zone over the region is twice a year, thus resulting into bimodal rainfall patterns over the study domain. The long rains occur between March to May (MAM) and short rains between September to November (SON) (Basalirwa, 1995). However, this tends to a unimodal pattern for areas away from the equator. Other factors influencing rainfall over the region include westerlies from Congo basin, monsoons, anticyclones; the Mascarene High, Arabian High, Azores High and the St Helena High, sea surface temperature (SST) anomalies, El-Nino Southern Oscillation (ENSO) and Indian Ocean Dipole (Saji et al., 1999; Indeje et al., 2000; Ogwang et al., 2012; 2015).

Extreme weather events in form of droughts and floods have been reported over the region by previous studies (Ogwang et al., 2015; Nicholson, 2017; Ojara et al., 2020). These are as a result of below normal, above normal or changes in onset, frequency, duration, and intensity of rains in different seasons. This has posed pronounced consequences on the population. Past studies have reported an observed decrease in rainfall during MAM season and an increase during SON (Nsubuga et al., 2014; 2017; Egeru et al., 2019; Ngoma et al., 2021). Nevertheless, SON rains have exhibited higher interannual variability as they are reported to be more influenced by global teleconnections (Saji et al., 1999; Ongoma et al., 2015). Therefore, a clear understanding of the various mechanisms regulating the short rains of SON is paramount so as to improve on seasonal climate forecasts for disaster mitigation and adaptation.

Over the Greater Horn of Africa, various studies have been conducted to investigate the mechanisms influencing climate over the region (Indeje et al., 2000; Hastenrath et al., 2004; Williams & Funk, 2011; Manatsa et al., 2012; 2014; 2015; Ongoma et al., 2015; Nicholson, 2017; 2018; Ayugi et al., 2018). A majority of these studies also focused on the short rains due to its higher interannual variability (Hastenrath et al., 2004; 2011; Manatsa et al., 2014; Ogwang et al., 2014). Hastenrath et al. (2011) reported that the short

rains are mostly influenced by a zonal vertical circulation cell in the central equatorial Indian Ocean known as the Walker circulation. Numerous studies demonstrate that the most important physical mechanism in the variability of the short rains is the intensity of this cell, with the low-level westerlies playing a fundamental role in modulating this cell (Mutai et al., 2012; Limbu & Tan, 2019). It is noted that strong westerlies are favoured by a steep eastward pressure gradient and abnormally weak trade winds in the South Indian Ocean (Nicholson, 2017). The weakening of the equatorial westerlies acts to reduce the subsidence over East Africa. Warm SSTs in the west and cold SSTs in the east are associated with a weakened Walker circulation over the Indian Ocean.

On the other hand, some studies link anomalous wet events of the short rains to effects by the Pacific Ocean (ENSO) (Nicholson & Kim, 1997; Indeje et al., 2000). It is reported that short rains are enhanced during El-Nino years and reduced during La-Nina years. According to Nicholson (2015), ENSO is well correlated with parameters over the Indian Ocean that modulate the short rains, such as the low-level and upper-level zonal winds. It is noted that a higher phase of Southern Oscillation (SO) weakens south easterlies from the Indian Ocean and lowers pressure over the eastern Indian Ocean. It is documented that ENSO plays a significant role in determining the monthly and seasonal rainfall patterns in the East African region (Black et al., 2003; Nicholson & Kim, 1997). Most of these studies were carried out over the entire East Africa or Greater Horn of Africa and a few focused on Uganda. Thus, they do not capture well the localized patterns and the local circulations involved over Uganda.

The recent decades have witnessed an intensification of anomalous events over the study region compared to the last 50 years of observed climatology. For instance, the 2019 short rains over Uganda were considered the most pluvial year observed, affecting thousands of people and destroying the societal infrastructure (ReliefWeb, 2020). The need for accurate forecasting as a way of minimizing the losses remains a paramount process. Towards the detected signature event in 2019, the Climate Outlook Forum (COF53) attributed the events to several factors. They were as follows: the forecasted warmer positive phase of IOD, the Neutral ENSO conditions in the central and east Pacific Oceans, and dynamical factors, among others (UNMA, 2019). The extensive probabilistic features for predictions of the exact cause could be attributed to the deficiency in understanding the teleconnec-

tion's patterns influencing the seasonal rainfall. Recent studies have pointed to these new phenomena that affect the rainfall variation over the larger East African region but no studies conducted over Uganda, despite the large spatial variance (Finney et al., 2019; Wainwright et al., 2020). For instance, the effect of Madden-Julian Oscillation (MJO) and the presence of tropical cyclones in the Western Indian Ocean (WIO) has been detected to contribute to the recent climate extremes. Another recent study by Ogwang et al. (2014) assessed circulation anomalies of October to December extreme rainfall and covered whole East Africa. Furthermore, Ogwang et al. (2016) pointed out

that there was an abrupt change in SON rainfall over Uganda during 1994. Thus, with the expected changes in climate, there is call for the need to revisit the possible mechanisms influencing the SON short rains over Uganda for accurate weather and climate prediction.

This study therefore sought to investigate the mechanisms influencing short rains over Uganda in the recent decades (i.e., 1981 – 2019) and fill in the gap by past studies. Section 2 gives a brief description of the study domain, the data and methods employed in the study. Section 3 presents the findings and discussions of the study. Lastly section 4 gives the summary and presents possible recommendations.

Study Area, Data and Methods

Study Area

Uganda is located in East Africa and stretches from 29.2°E–35.2°E and from 1.5°S–4.5°N (Fig. 1). It is a landlocked country bordered by South Sudan in the North, Kenya in the East, Democratic Republic of Congo (DRC) to the West and Rwanda and Tanzania in the South. The country comprises of complex topography ranging from low lying areas in the north west, middle terrain in the central to high lands and top mountains in the south west (Mts Rwenzori and Mufumbira), and north east (Mts Elgon and Moroto). Various water bodies also cover up some parts of the country including Lakes Victoria, Kyoga, Albert, Edward and George and rivers including the world's longest river, River Nile. The climate of region is equatorial with tropical forests rain forest such as Mabira Forest. All these physical features regulate climate over the region through local induced convection. As mentioned earlier in the introduction section, the climate over the region is mostly influenced by the tropical rain belt which

oscillates from north to south throughout the year (Basalirwa, 1995; Nicholson, 2018).

Data

Observed datasets

Station data over Uganda has many discrepancies (Sylla et al., 2012). This is due to the sparse distribution of ground stations and unreliability of equipment. This study therefore used monthly rainfall estimates from the Climate Hazards Centre for Infrared Precipitation with Station data (CHIRPS) (Funk et al. 2015) as a reference to observed data from 1981 to 2019 relative to the starting period of the datasets. The data is available on <http://https://www.chc.ucsb.edu/data/chirps>. The CHIRPS rainfall data version 2 (CHIRPS.v2) blends 0.05° resolution satellite imagery with in-situ measurements to produce a gridded value from 1981 to present. CHIRPS has been evaluated and utilized by a number of studies over East Africa (Dinku et al., 2018; Ayugi et al., 2019; Ngoma et al., 2021).

Reanalysis Datasets

The study employed ERA5 reanalysis dataset (C3S, 2017) at 0.25° × 0.25° horizontal resolution for winds (zonal u and meridional v), vertical velocity and specific humidity at 850 hPa and 200 hPa for comparison with large-scale circulation. ERA5 is the 5th generation product available from the European Centre for Medium-Range Weather Forecasts (ECMWF). Winds at 850 hPa (200 hPa) was selected because these are linked to low-level (high-level) wind convergence (divergence) that has direct influence on rainfall trends over the study region.

Variables of mean sea level pressure and velocity potential were obtained from the National Centers for Environmental Prediction–National Center for Atmospheric Research (NCEP–NCAR) from <https://psl>.

Figure 1. Location of Uganda in Africa along longitudes 29.2°E and 35.2°E, and latitudes 1.5°S – 4.5°N. Also indicated include the presence of physical features, water bodies and elevation in meters (m).

noaa.gov/data/gridded/data.ncep.reanalysis.html at 2.5° resolution. Version 5 sea surface temperature was obtained from National Oceanic and Atmospheric Administration/National Climatic Data Center, NOAA NCDC at <http://iridl.ldeo.columbia.edu/SOURCES/NOAA/NCDC/ERSST/version5/sst> for the same study period 1981-2019. The study further utilized Southern Oscillation Index (SOI) and Dipole Mode Index (DMI) datasets to investigate the influence of ENSO and Indian Ocean Zonal Mode on SON rainfall over Uganda. These indices were obtained from NOAA at https://psl.noaa.gov/gcos_wgsp/Timeseries/.

Methods

The study employed various methods like Empirical Orthogonal Function (EOF), composite analysis, student t-test and simple correlation. EOF is used to investigate the variability of a single field of climatic data (Lorenz, 1956). The variability in the time evolving field is broken down into a few standing oscillations and a time series (Principal Component) for each oscillation. The first EOF is the leading mode and points to the direction in which the data vectors jointly display the most variability. The second eigenvector is perpendicular to the first eigenvector, which is perpendicular to the third eigenvector and so on, thus called the empirical orthogonal function analysis. Well correlated data may be defined by a small number of orthogonal functions and time coefficients, corresponding to the variances in their spatial and temporal distribution (Bjornsson & Venegas, 1997). EOF is used in this study to show the dominant modes of variability of SON rainfall over the region. This technique has been employed by a number of studies across East Africa (Ogwang et al., 2012; Ayugi et al., 2018; Limbu & Tan, 2019). The data used is normalized in order to prevent areas and seasons of maximum variance from dominating the eigenvectors. The standardized rainfall anomaly (z) is computed as shown in equation 1.

$$Anomaly = \frac{X - \bar{X}}{\sigma} \quad (1)$$

- where X is the SON mean rainfall, \bar{X} is the long-term SON mean rainfall and σ is standard deviation of SON rainfall.

Results and Discussions

Spatiotemporal variability

Figure 2 shows standardized precipitation anomalies for SON rainfall based on CHIRPS data during 1981–2019 over Uganda. High interannual and interdecadal variability is shown over the region with almost equal number of wet and dry events. 19 years

The composite analysis involves identifying and averaging different fields of a variable selected according to their association with key conditions. Composites were separately analyzed for Mean sea level pressure, winds, moisture flux convergence, vertical velocity, and velocity potential. This method was used to detect circulation patterns associated with anomalous events of wet and dry years. Wet (dry) years are defined by values of >1 (<1) standard deviation from the time series of the principal component (PC) of the dominant mode of EOF as explained in studies by Dommenges and Latif (2002) and Makkonen (2006). The results of the composites are used to generate hypotheses for patterns associated with individual scenarios variability.

The composite variables were tested for statistical significance using the t-test (when one or both groups have a sample size of less than 40). The equations for t-test are as shown in equation 2 and 3.

$$t = \frac{\bar{x}_1 - \bar{x}_2}{S_{\bar{x}_1 - \bar{x}_2}} \quad (2)$$

$$S_{\bar{x}_1 - \bar{x}_2} = \sqrt{\frac{(n_1 - 1)}{n_1 + n_2 - 2} S_1^2 + \frac{(n_2 - 1)}{n_1 + n_2 - 2} S_2^2 \left[\frac{1}{n_1} + \frac{1}{n_2} \right]} \quad (3)$$

- where \bar{x} = mean.
- S = standard deviation.

The calculated values of t were compared with those of the theoretical distribution with $N-2$ degrees of freedom at different significance levels. If the calculated value of t is less than the theoretical value, then the significant area identified. Lastly, correlation analysis for Pearson correlation coefficient was employed to study the relationship between SON rainfall and SST, SOI and DMI. The simple correlation has two important properties. First, it is bounded by -1 and 1 , i.e., $-1 < CC < 1$. When the value of correlation coefficient $+1$ or -1 , it indicates a perfect positive or negative correlation between the given pairs of variables, respectively. The square of the correlation coefficient represents the proportion of the variability of one of the two variables that is linearly accounted for or explained by the other.

exhibited wet patterns whereas 20 years experienced dry precipitation anomalies. Significant anomalous events with standardized anomaly of >1 (<-1) occurred during 2011, 2012, 2019 (2005, 2009). Previous studies have attributed these anomalous events to the dipole mode influence of the Indian Ocean sea surface tem-

peratures (Saji et al., 1999; Manatsa et al., 2012). Wet (dry) events are associated with positive (negative) Indian Ocean dipole. Other studies link the interannual variation of SON rains to El Niño Southern Oscillation (ENSO) (Indeje et al., 2000; Ntale and Gan 2003). This is also reflected by the present study with El Niño years coinciding with wet anomalous events of 2010 and 2012 and La Niña years with dry events of 2005, 2009. However, some years reported by previous studies as El-Niño and La-Niña are not reflected in the wet and dry years. An example is 1996-1997 which was a strong El-Niño year but depicting slightly above normal rainfall in Figure 2. This could be attributed to the characteristic of the episodes as reported by a study (Hoell et al., 2014) which found that the short rains are generally reduced during La Niña but that the degree and spatial consistency of the reduction depends on the nature of the episode. Nicholson et al. (2001) also found that the impact of La Niña/El Niño materialized only when cooling/warming of the tropical Indian and Atlantic Oceans occurred in conjunction with the episode. These events are also known to prolong the rainfall season of SON sometimes extending it to January. An example is the heavy rains of 2019 that resulted into flooding and landslides in various parts of the country. The rains started late October and persisted till mid-January 2020 in most parts of the country (ReliefWeb, 2020). This usually leads to destruction of property, damaged infrastructure, poor transport conditions, and increase in food prices.

Furthermore, the spatiotemporal variability of rainfall during SON season was assessed using EOF. Figure 3 (a, b, c) shows the spatial component of the first three eigen vectors and the corresponding principal components (d, e, f). The three modes account for 99.9 % of the entire rainfall variability over the region.

Figure 2. Standardized anomalies of mean SON rainfall (mm/month) over Uganda during 1981-2019 based on CHIRPS datasets averaged along longitudes 29.2°E–35.5°E and latitudes 1.5°S–4.5°N

Independently they explain 67.2%, 21.8% and 10.9% of the total variance. EOF 1 exhibits a monopole variability pattern of entirely positive loading over the study domain, with more strong loadings over the eastern parts of the country, around Lake Victoria, and Lake Kyoga region. This could be attributed to effect of local meso-scale convection thus the modified rainfall patterns. The southwest and north-eastern parts of the country exhibit the weakest loadings. The first EOF 1 timeseries (PC1) captures well the observed patterns of interannual variability of rainfall during SON season as demonstrated in Figure 2. Anomalous events with wet patterns (>1) include 2001, 2011, 2015 and 2019. On the other hand, years characterized with dry patterns (<1) include 1993, 2005, 2009 and 2018. EOF 2 and EOF 3 display a dipole pattern. EOF 2 exhibits positive loading towards the eastern part and negative loading to the west. However, EOF 3 shows positive loading to the north and negative loading to the south of the study region. The timeseries of the second and third modes (PC 2 and PC 3) do not capture well the observed rainfall patterns over Uganda. Thus, this study used PC 1 of the first and dominant mode for identifying wet and dry years with standardized anomaly of +/-1 respectively. The identified years are then utilized in composite analysis to investigate the possible circulations associated with the anomalous events. Table 1 shows wet and dry years from PC1. These results agree with previous studies by Ogwang et al. (2012, 2016) conducted over Uganda for the period 1962-2007, 1901 – 2013 respectively. However, some differences are exhibited in these studies in the percentage variance explained by the dominant modes of the EOFs. One study that utilized ground station datasets depicted low percentage (24%) by the EOF compared to the other that employed gridded datasets from the Climatic Research Unit (CRU). This could be attributed to the uneven distribution of station over the study domain. There is also controversy in the years between revealed as wet and dry years in the recent study and previous studies (Ogwang et al., 2012; Ogwang et al., 2014; Ogwang et al., 2016). The results reveal that some the years reported in previous studies as El-Niño and La-Niña years were not recorded as extremely anomalous years. This could be attributed to the differences in season as some studies focused on October to November rainfall season and also probably inability of gridded datasets to accurately reproduced interannual variability of observed rainfall over the region.

Circulations associated with wet and dry years

Circulation characteristics are important in depicting the dynamical factors associated with the observed weather events for predicting future weather

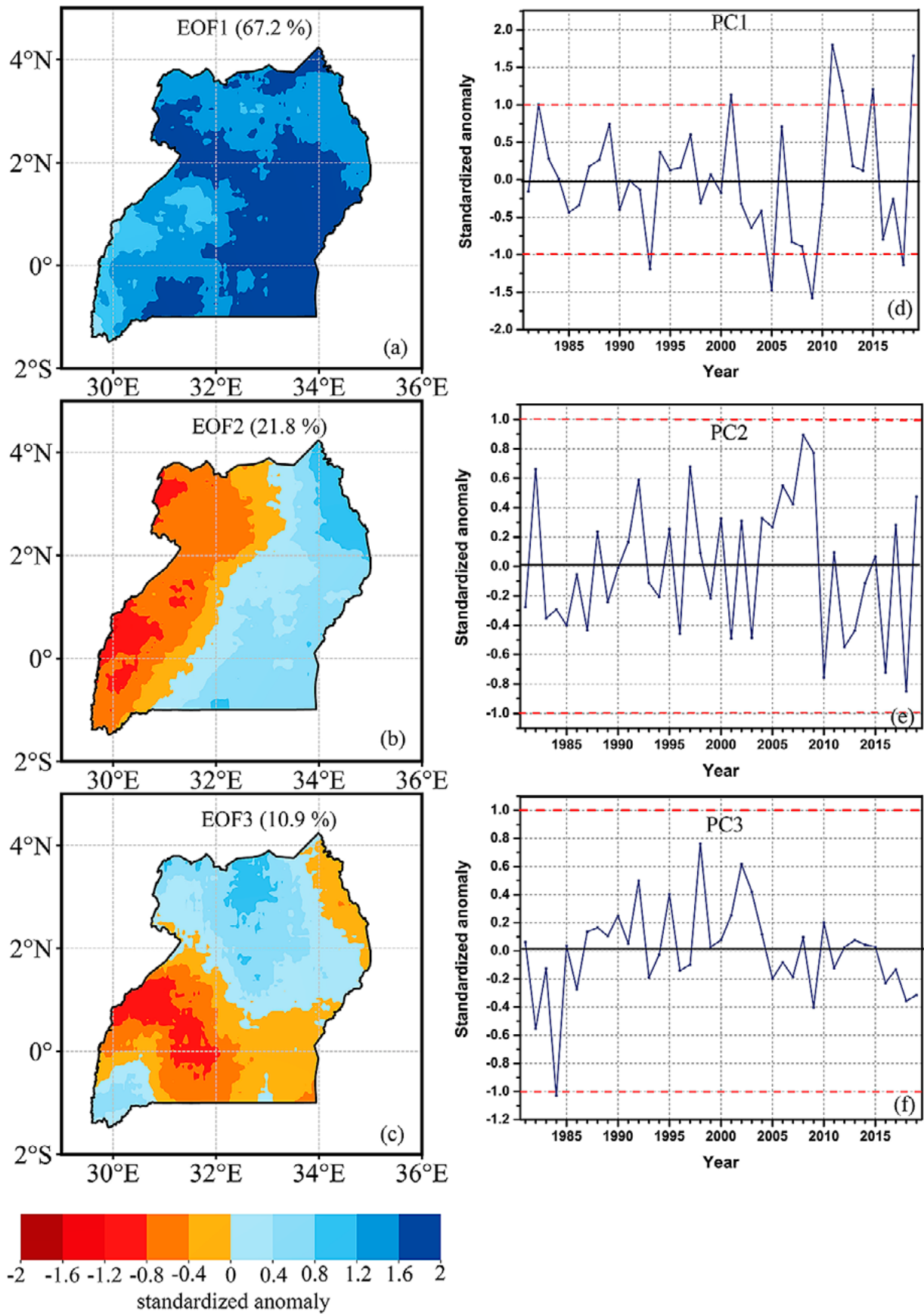


Figure 3. EOF distribution of the first three dominant modes (a, b, c) and Principal components (d, e, f) of SON rainfall over Uganda during 1981-2019 based on CHIRPS data. The first mode represented 67.2 % of the SON rainfall over the region

Table 1. EOF 1 for wet and dry years based on PC 1 for SON rainfall over Uganda between 1981–2019 where z represents standardized anomaly.

Season	Grades	years	Condition: Anomaly (z)	Occurrence (%)
SON	Above normal rainfall (wet)	2001, 2011, 2015, 2019	$z > 1$	10.3
	Below normal rainfall (dry)	1993, 2005, 2009, 2018	$z < 1$	10.3
	Normal rainfall	1981, 1982, 1983, 1984, 1985, 1986, 1987, 1988, 1989, 1990, 1991, 1992, 1994, 1995, 1996, 1997, 1998, 1999, 2000, 2002, 2003, 2004, 2008, 2007, 2008, 2010, 2012, 2013, 2014, 2016, 2017	$1 < z > 1$	79.4

patterns. This study analyzed mean sea level pressure, wind, moisture flux, vertical velocity and velocity potential.

Pressure systems, wind and moisture flux

Figure (4a, b, c) shows mean sea level pressure anomalies during wet, dry and wet-dry years. During wet years (Fig. 4a, c), the Arabian high-pressure system strengthens and is situated over Sudan. The Mascarene High over the south Indian Ocean on the other hand weakens. This positions the rain band over the study region, and is accompanied by north westerlies and westerlies from Congo and easterlies from the Indian Ocean (Fig. 5a, e). In contrary during dry years (Fig. 4b), the Arabian high weakens and the Mascarene High intensified. The ridging is extended over some parts of East Africa and thus moving the loci of cloud clusters associated with westward propagating tropical wave disturbances above the region. This results to weak westerlies towards the study region. As noted by previous studies including Mutai et al. (2012) and Defzuli and Nicholson., (2013), strong westerlies are favored by a steep eastward pressure gradient and abnormally weak trade winds in the South Indian Ocean.

Figure 4. Mean sea level pressure anomalies (hPa) during (a) wet years, (b) dry years and (c), Wet-Dry years based on NCEP reanalysis datasets over Uganda for the period 1981-2019. The shaded area is significant at 0.1 significance level

Figure (5a, b,c,d,e,f) shows wind anomalies during wet, dry, and wet-dry years at 850 hPa and 200 hPa. At the lower level (850 hPa), wind is generally weak and strong at higher level (200 hPa). During wet years, moist westerlies from Congo are observed in conjunction with easterlies from the Indian Ocean. This is accompanied by strong easterlies at upper level. The winds blowing from the Congo forest in DRC are generally warm and moist with high speed, and thus they likely contribute to the observed above-normal rainfall during wet years. The flow converges at lower level

Figure 5. composites of wind anomalies (m/s) at 850hPa (a) and 200 (c) for wet years, 850hPa (b) and 200 hPa (d) for dry years and, 850hPa(d) and 200hPa (e) of wet-dry years for SON rainfall season over Uganda based on CHIRPS and ERA5 data for the period 1981-2019. The shaded area is significant at 0.1 significance level

Figure 6. Moisture flux convergence ($10^{-5} \text{ g kg}^{-1} \text{ s}^{-1}$) at 850 hPa where positive values represent positive moisture flux convergence during wet years (a) and dry years (b)

els and diverges at higher levels, thus wet years are marked by rising motion to the western part of the Indian Ocean and the study area. In contrary, dry years are characterized by weak westerlies and south easterlies from the Indian ocean without convergence at low level. The southeasterlies originating from the Indian Ocean weakens considerably when passing the Kenya and Tanzania highland before entering in Uganda. At upper level, strong westerlies are observed with convergence over the Indian ocean. This reduces water vapor transportation and lowers convection.

Composites of mean moisture flux for wet and dry years is shown in Figure 6. The results reveal that there is more positive anomaly (moisture convergence) and convergent winds during wet years than dry years (Fig.6a). Having sufficient moisture coupled with low-level convergence over the study area results to ascending motion and enhanced convection which later favours anomalous rainfall (anomalous wet condition). During the dry years, the anomalous moisture divergence (negative anomalies) at the lower level dominates in the region (Fig.6b). With low-level divergence and inadequate influx of low-level moisture over the study area, convection is suppressed leading to less rainfall and dry condition. However, moisture divergence is depicted in some parts of the country in the north and around lake regions during both wet and dry years. This is attributed to mesoscale effect of orography and convection from the water bodies.

Vertical velocity and velocity potential

Figure 7 shows composites of vertical velocity anomalies averaged at a fixed longitude (32°E) for wet, dry, and wet-dry years. Figures (7a, c) reveal that wet years are characterized by ascending motion at low level. This is accompanied by the uplifting air on mountains which favors cloud formation and hence precipitation. However, some descending motion is shown in northern areas above 20°N . This could be attributed to complex topography which might induce downdrafts at low levels (Ogwang et al., 2014). Dry years on the

other hand are associated with descending motion at low levels thus subsidence (Fig. 7b). The northern part and areas around the equator are characterized by negative (positive) anomalies at low (mid to high) levels of the study area. This implies that only shallow uplift persists over these areas, while the remaining areas experienced subsidence motion and less rainfall.

Figure 8 represents velocity potential anomalies during wet, dry, and wet-dry years. The results reveal that wet years are characterized by positive velocity potential anomalies and convergence at low level over the western Indian ocean and East Africa (Fig.8a). This is accompanied by negative velocity potential and wind divergence at higher levels (Fig.8c), which reposition the ascending limb of the Walker Circulation. This is completed by the descending limb in the eastern part of the Indian Ocean. Dry years are contrarily associated with negative values and a high centre of divergence over East Africa at low level (Fig.8b). This is accompanied by convergence at upper level (Fig.8d) and thus a descending limb of the Walker circulation. These results are in agreement with previous studies conducted including Ogwang et al. (2012), Nicholson et al. (2017), Ayugi et al. (2018) and Limbu & Tan (2019).

Correlation of rainfall with SST

Simple correlation analysis was done to establish the relationship between SON rainfall over Uganda and sea surface temperature. The results reveal that SON rainfall and SST over the western Indian Ocean (WIO) tend to positively correlate (Fig. 9a). This is further depicted by temporal correlation between the two variables where a correlation coeffi-

Figure 7. Vertical velocity (ω) anomalies during (a) wet years, (b) dry years and (c) wet-dry years at fixed longitude [32°E]. Negative (positive) values indicate upward (downward) motion. Contour interval is 0.01 and units are in Pa s^{-1} . The shaded area is significant at 0.1 significance level

cient of 0.37 significant at 0.05 significance level is shown (Fig. 9b). The positive anomaly in the western part of the Indian Ocean enhances convective activity and rising motion from the lower level, which facilitates the moisture transport to the study area and hence results in precipitation. However, negative correlation is displayed with SST across the Atlantic Ocean (AO) (Fig. 9c, d). Weak positive correlation is only depicted by small parts of the Atlantic Ocean. These results are in agreement with previous studies including Saji et al. (1999) and Ngarukiyimana et al. (2017) over East Africa. However, a stronger positive correlation with Indian Ocean SST is revealed by the present study compared to the findings of Ngarukiyimana et al. (2017) which correlated SST with MAM rainfall. Cross correlation was performed for rainfall and SST temperature over Indian and Atlantic Ocean (Figure 10a & b). The results reveal that there

Figure 8. Composite of velocity potential anomalies (contours in $10^6 \text{m}^2 \text{s}^{-1}$) and divergent winds (vectors in ms^{-1}) at 850 hPa (a, b) for wet and dry years, 200 hPa (b, c) for wet and dry years and 850 hPa (e) and 200 hPa (f) for wet-dry years over Uganda during 1981–2019. The shaded regions are significant at 0.1 significance level

Figure 9. Correlation between standardized SON rainfall anomalies averaged over Uganda and Indian Ocean sea surface temperatures (a, b) and Atlantic Ocean sea surface temperatures (c, d) from 1981–2019. The temporal correlation was obtained by correlating SST over Indian and Atlantic Ocean and SON rainfall averaged over Uganda between longitudes 29°E – 36°E and latitude 1.5°S – 4.5°N . The dotted regions are significant at 0.05 significance level

Figure 10. Cross correlation of mean rainfall and sea surface temperature averaged over Uganda for Indian (a) and Atlantic (b) Ocean, and correlation of OND rainfall (one month lead) and SST of Indian (c) and Atlantic (d) ocean during 1981–2019

is a strong correlation between rainfall and SST over WIO and AT when warm SST anomalies lags 6 months i.e during the previous MAM season and when warm SST anomalies leads 3 months. A stronger and more pronounced correlation is shown when the rainfall season is extended i.e October to December instead of SON (Figure 10 c&d). In addition, the standard deviation of the wet and dry years in the study period is exhibited 1997 which was a strong El-Nino year captured well. These results thus reveal that anomalous SST over IO and AO during SON impact the SON seasonal rainfall by extending the rains to December and the following months which (December to February) which is normally a dry season over Uganda.

Correlation of SOI, DMI and SON rainfall

Southern Oscillation Index (SOI) is based on pressure differences between Tahiti and Darwin. It gives the intensity of El Niño and La Niña events over the Pacific Ocean. Results show that there is negative correlation of SON rainfall and SOI over most parts of Uganda. Positive correlation is depicted by small areas in the west and northern parts of the country (Fig. 10a). Temporal linear correlation coefficient of -0.13 insignificant at 0.05 significance level is displayed for SON rainfall averaged over Uganda and SOI. However, stronger positive correlation is revealed with DMI (Fig. 10c). Most areas in the central and southern parts correlate positively with the DMI. The northern and southern parts of the country exhibit varying patterns with negative correlation. These results are in accordance with a previous study by Phillips and McIntyre (2000) which reported that ENSO affects the southern parts of the country differently from the northern areas. Overall, SON rainfall averaged over Uganda exhibits positive correlation with DMI (0.33), significant at 0.05 significance level and negative correlation with SOI (-0.13) insignificant at 0.05 significance level. These findings are in line with previous studies conducted over East Africa (Saji et al., 1999; Ogwang et al., 2014; Ngarukiyimana et al., 2017). Figure 12 (a&b) represents lead-lag correlation between rainfall and SOI (a), DMI (b) during SON for the period 1981-2019. Correlation with SOI oscillates throughout the months and strong negative correlation is revealed when SOI leads by 2 and 6 months. A stronger and significant negative correlation (-0.36) at 0.05 significance level is also shown for OND rainfall and SON SOI. A strong correlation is shown when DMI lags 4-3 months than rainfall i.e previous MAM season and leads by 6 months (Figure 12b). Results also reveal correlation of 0.49 between DMI during SON and OND rainfall (Figure 12d). However, this correlation is weaker than that found by Ogwang et al. (2015) of 0.6 over East Africa. The weak correlation of rainfall and SOI could be attributed to the lag of warming in the central and Pacific Ocean compared to the western Pacific. Latif and Barnett (1995), indicated that during the warm (cold) events in the tropical Pacific, the tropical Indian Ocean was anomalously warm (cold) while the tropical Atlantic was cold (warm). Black et al. (2003) postulate that ENSO predisposes the Indian Ocean coupled system to an Indian Ocean Zonal Mode (IOZM) event and conclude that only the large events (those that reduce

Figure 11. Correlation between SON rainfall anomalies over Uganda and SOI (a, b) and correlation between SON rainfall anomalies averaged over Uganda and DMI (c, d) during 1981–2019. The dotted areas are significant at 0.01 significance level

the Indian Ocean SST gradient) can produce extreme rainfall. These results are in agreement with a previous study (Mafuru & Guirong, 2020), which found that there is a lag in ENSO events and the upper warm temperature anomalies responsible for inducing rainfall over East Africa.

Figure 12. Cross correlation of SST and mean rainfall during SON averaged over Uganda for Indian(a) and Atlantic(b) Ocean, and correlation of OND rainfall (one month lead) and SST of Indian (c) and Atlantic (d) ocean during 1981-2019

Discussion

With the high spatiotemporal variability of short rains of September to November over Uganda, this study revisited the mechanisms associated with the anomalous events of rainfall during the SON rainfall. EOF analysis revealed equal number of wet and dry years. Wet (dry) years were depicted during 2001, 2011, 2015 and 2019 (1993, 2005, 2009, 2018).

The results demonstrated that the SON rains are mostly influenced by a Walker circulation over the Indian Ocean. Wet (dry) years are associated with an ascending (descending) limb over the western Indian Ocean. This is characterized by the weakening of the Mascarene High and strengthening of the Arabian High over North Africa. This allows in westerly flow from the Congo basin and this converges with easterlies from the Indian Ocean at low level. This convergence is accompanied by divergence at upper level. Indian Ocean SST exhibited positive correlation whereas Atlantic Ocean SST revealed negative correlation with

SON rainfall over the region. This implies that fluctuations in SST over the Indian Ocean have a great influence on SON rainfall over Uganda. In addition, SON rainfall displayed positive (negative) correlation with DMI (SOI). This agrees with past studies which reported that IOD has more influence on the interannual variability of SON rainfall over Uganda. The results further show that there is a lag in ENSO events and anomalous wet and dry events of rainfall over the region.

The results of this study are in contribution to the understanding of the dynamic and thermodynamics factors responsible for varying patterns of rainfall over Uganda in the recent decades. We recommend an in-depth study about the influence of ENSO on rainfall over Uganda as this study could not bring out deeper analysis. This would help in monitoring of these phenomenon and in generating seasonal forecasts to various sectors like agriculture, fishing, disaster management.

Summary and conclusion

Rainfall is the key weather parameter over Uganda. Anomalous events affect the country's economy that largely depends on rainfed agriculture. Precipitation over most parts of the country is bimodal with long rains received during MAM and short rains during SON. However, high interannual variability has been witnessed in the short rains which has prompted some farmers to shift the main growing season to this period due to its increased frequency and sometimes duration.

Various mechanisms have been attributed to the varying patterns of the SON rains. This study therefore investigated the circulations and teleconnection mechanisms associated with anomalous events of SON rainfall during the recent decades. The results revealed that a walker circulation over the Indian Ocean influences rainfall during this season. Wet years are characterized by the weakening of the Mascarene High, strong westerlies from the Congo basin at a low level and di-

vergence of strong easterlies at the upper level. Indian Ocean SST also have a big influence on SON rainfall over the region compared to Atlantic Ocean SST. In addition, there exists a strong positive correlation of SON rainfall with the DMI. DMI has more effect on rainfall over the region than the SOI. Previous studies have also reported the same finding that ENSO or Pacific Ocean has little contribution to the variability of SON rainfall (Omondi et al., 2013; Liebman et al., 2014; Ngarukiyimana et al., 2017). However, a strong relationship is revealed when there is lag in the ENSO events. ENSO and IOD tend to extend the rainfall season of SON and thus study of extreme events may not be well captured by studies focusing on SON. Future studies might need to consider the season of October to December or December to February. Thus, close monitoring of Indian Ocean SST, wind patterns and the pressure systems; Mascarene High and Arabian High is crucial in the updating of seasonal forecasts.

Acknowledgments

Special thanks to Nanjing University of Information Science and Technology for providing a research conducive environment. High gratitude towards the data centers; NOAA, NCEP, ECMWF, the Climate Hazards Center for provision of the datasets employed in the study. The lead author is grateful to Ministry of Commerce of the People's Republic of China for the financial support. Authors would like to thank the editor, and the two anonymous reviewers whose suggestions lead to a substantially improved manuscript.

Compliance with ethical standards

All authors declare no conflict of interest for this study.

References

- Ayugi, B. O., Tan, G., Ongoma, V., & Mafuru, K. B. (2018). Circulations associated with variations in boreal spring rainfall over Kenya. *Earth Systems and Environment*, 2(2), 421-434. <https://doi.org/10.1007/s41748-018-0074-6>
- Ayugi, B., Tan, G., Ullah, W., Boiyo, R., & Ongoma, V. (2019). Inter-comparison of remotely sensed precipitation datasets over Kenya during 1998–2016. *Atmospheric Research*, 225, 96-109. <https://doi.org/10.1016/j.atmosres.2019.03.032>
- Basalirwa, C. P. K. (1995). Delineation of Uganda into climatological rainfall zones using the method of principal component analysis. *International Journal of climatology*, 15(10), 1161-1177. <https://doi.org/10.1002/joc.3370151008>
- Bjornsson, S. & Venegas, H. (1997) A manual for EOF and SVD Analyses of Climatic Data. CGCR Report No. 97-1, McGill University, 8–27.
- Black, E., Slingo, J., & Sperber, K. R. (2003). An observational study of the relationship between excessively strong short rains in coastal East Africa and Indian Ocean SST. *Monthly Weather Review*, 131(1), 74-94. doi:10.1175/1520493(2003)131<0074:AOSOTR>2.0.CO;2
- Copernicus Climate Change Service (C3S). (2017). ERA5: Fifth generation of ECMWF atmospheric reanalyses of the global climate. Copernicus Climate change Service Climate Data Store (CDS). <https://cds.climate.copernicus.edu/cdsapp#!/home>. (Accessed 05.11.2020)
- Dinku, T., Funk, C., Peterson, P., Maidment, R., Tadesse, T., Gadain, H., & Ceccato, P. (2018). Validation of the CHIRPS satellite rainfall estimates over eastern Africa. *Quarterly Journal of the Royal Meteorological Society*, 144, 292-312. DOI: 10.1002/qj.3244
- Dommenget, D., & Latif, M. (2002). A cautionary note on the interpretation of EOFs. *Journal of climate*, 15(2), 216-225.
- Egeru, A., Barasa, B., Nampijja, J., Siya, A., Makooma, M. T., & Majaliwa, M. G. J. (2019). Past, present and future climate trends under varied representative concentration pathways for a sub-humid region in Uganda. *Climate*, 7(3), 35.
- Finney, D. L., Marsham, J. H., Rowell, D. P., Kendon, E. J., Tucker, S. O., Stratton, R. A., & Jackson, L. S. (2020). Effects of explicit convection on future projections of mesoscale circulations, rainfall, and rainfall extremes over Eastern Africa. *Journal of Climate*, 33(7), 2701-2718. DOI: 10.1175/JCLI-D-19-0328.1
- Funk, C., Peterson, P., Landsfeld, M., Pedreros, D., Verdin, J., Shukla, S., Husak, G., Rowland, J., Harrison, L., Hoell, A. & Michaelsen, J. (2015). The climate hazards infrared precipitation with stations—a new environmental record for monitoring extremes. *Scientific data*, 2(1), 1-21. <https://doi.org/10.1038/sdata.2015.66>
- Government of Uganda, GOU. (2015). Economic Assessment of the Impacts of Climate Change in Uganda. Final Study Report. Ministry of Water and Environment, Climate Change Department, Kampala. url: <https://cdkn.org/wp-content/uploads/2015/12/Uganda-CC-economics-Final-Report2.pdf>
- Hastenrath, S., Polzin, D., & Camberlin, P. (2004). Exploring the predictability of the ‘short rains’ at the coast of East Africa. *International Journal of Climatology: A Journal of the Royal Meteorological Society*, 24(11), 1333-1343. doi:10.1002/joc.1070.
- Hoell, A., Funk, C., & Barlow, M. (2014). La Niña diversity and northwest Indian Ocean rim teleconnections. *Climate dynamics*, 43(9-10), 2707-2724. doi:10.1007/s00382-014-2083-y.
- Indeje, M., Semazzi, F. H., & Ogallo, L. J. (2000). ENSO signals in East African rainfall seasons. *International Journal of Climatology: A Journal of the Royal Meteorological Society*, 20(1), 19-46. [https://doi.org/10.1002/\(SICI\)1097-0088\(200001\)20:1<19::AID-JOC449>3.0.CO;2-0](https://doi.org/10.1002/(SICI)1097-0088(200001)20:1<19::AID-JOC449>3.0.CO;2-0)
- Liebmann, B., Hoerling, M. P., Funk, C., Bladé, I., Dole, R. M., Allured, D., Quan X., Pegion, P. & Eischeid, J. K. (2014). Understanding recent eastern Horn of Africa rainfall variability and change. *Journal of Climate*, 27(23), 8630-8645. doi:10.1175/JCLI-D-13-00714.1.
- Limbu, P. T. S., & Guirong, T. (2019). Relationship between the October-December Rainfall in Tanzania and the Walker Circulation Cell over Indian Ocean. *Meteorologische Zeitschrift*, 28(6), 453-469. DOI 10.1127/metz/2019/0939.
- Lorenz, E. N. (1956). Empirical orthogonal functions and statistical weather prediction. Technical report, Statistical Forecast Project Report 1. Department of Meteorology. MIT, 49pp.

- Mafuru, K. B., & Guirong, T. (2020). The influence of ENSO on the upper warm temperature anomaly formation associated with the March–May heavy rainfall events in Tanzania. *International Journal of Climatology*, 40(5), 2745–2763. <https://doi.org/10.1002/joc.6364>
- Makkonen, L. (2006). Plotting positions in extreme value analysis. *Journal of Applied Meteorology and Climatology*, 45(2), 334–340.
- Manatsa, D., Chipindu, B., & Behera, S. K. (2012). Shifts in IOD and their impacts on association with East Africa rainfall. *Theoretical and Applied Climatology*, 110(1), 115–128. doi:10.1007/s00704-012-0610-5.
- Manatsa, D., Morioka, Y., Behera, S. K., Matariira, C. H., & Yamagata, T. (2014). Impact of Mascarene High variability on the East African ‘short rains’. *Climate dynamics*, 42(5–6), 1259–1274. doi:10.1007/s00382-013-1848-z.
- Manatsa, D., Mudavanhu, C., Mushore, T. D., & Mavhura, E. (2016). Linking major shifts in East Africa ‘short rains’ to the Southern Annular Mode. *International Journal of Climatology*, 36(4), 1590–1599. doi:10.1002/joc.4281
- Mutai, C., Polzin, D., & Hastenrath, S. (2012). Diagnosing Kenya rainfall in boreal autumn: Further exploration. *Journal of climate*, 25(12), 4323–4329. doi:10.1175/JCLI-D-11-00414.1.
- Ngarukiyimana, J. P., Fu, Y., Yang, Y., Ogwang, B. A., Ongoma, V., & Ntwali, D. (2018). Dominant atmospheric circulation patterns associated with abnormal rainfall events over Rwanda, East Africa. *International Journal of Climatology*, 38(1), 187–202. doi:10.1002/joc.5169
- Ngoma, H., Wen, W., Ojara, M., & Ayugi, B. (2021). Assessing current and future spatiotemporal precipitation variability and trends over Uganda, East Africa, based on CHIRPS and regional climate model datasets. *Meteorology and Atmospheric Physics*, 1–21. <https://doi.org/10.1007/s00703-021-00784-3>
- Nicholson, S. E., & Kim, J. (1997). The relationship of the El Niño–Southern oscillation to African rainfall. *International Journal of Climatology: A Journal of the Royal Meteorological Society*, 17(2), 117–135. doi:10.1002/(SICI)1097-0088(199702)17:2<117:AID-JOC84>3.0.CO;2-O
- Nicholson, S. E. (1996). A review of climate dynamics and climate variability in eastern Africa. In Johnson T.C. & Odada E.O. (Eds.) *The Limnology, Climatology, and Paleoclimatology of the East African Lakes*, (pp. 25–56), Amsterdam: Gordon and Breach Publ.
- Nicholson, S. E., Leposo, D. & Grist, J.P., (2001). The relationship between El Niño and drought over Botswana, *Journal of Climate*, 14(3), 323–335, doi:10.1175/1520-0442(2001)014<0323:TRBENO>2.0.CO;2.
- Nicholson, S. E. (2015). Long-term variability of the East African ‘short rains’ and its links to large-scale factors. *International Journal of Climatology*, 35(13), 3979–3990. doi:10.1002/joc.4259.
- Nicholson, S. E. (2017). Climate and climatic variability of rainfall over eastern Africa. *Reviews of Geophysics*, 55(3), 590–635. doi:10.1002/2016RG000544
- Nicholson, S. E. (2018). The ITCZ and the seasonal cycle over equatorial Africa. *Bulletin of the American Meteorological Society*, 99(2), 337–348. <https://doi.org/10.1175/BAMS-D-16-0287.1>
- Nsubuga, F. W., & Rautenbach, H. (2018). Climate change and variability: a review of what is known and ought to be known for Uganda. *International Journal of Climate Change Strategies and Management*. Doi 10.1108/IJCCSM-04-2017-0090
- Nsubuga, F.N.W., Olwoch, J. M., Rautenbach, C. D., & Botai, O. J. (2014). Analysis of mid-twentieth century rainfall trends and variability over southwestern Uganda. *Theoretical and applied climatology*, 115(1), 53–71. <https://doi.org/10.1007/s00704-013-0864-6>
- Ogwang, B., Nimusiima, A., Tindamanyire, T., Serwanga, M., Ayesiga, G., Ojara, M., Ssebabi, F., Gugwa, G., Nsubuga, Y., Atim, R., & Aribo, L. (2016). Characteristics and changes in SON rainfall over Uganda (1901–2013). *Journal of Environmental and Agricultural Sciences*, 8, 45–53.
- Ogwang, B. A., Ongoma, V., Xing, L., & Ogou, K. F. (2015). Influence of Mascarene high and Indian Ocean dipole on East African extreme weather events. *Geographica Pannonica*, 19(2), 64–72. <https://doi.org/10.5937/geopan1502064o>
- Ogwang, B. A., Chen, H., Li, X., & Gao, C. (2014). The influence of topography on East African October to December climate: sensitivity experiments with RegCM4. *Advances in Meteorology*. <https://doi.org/10.1155/2014/143917>
- Ogwang, B. A., Guirong, T., & Haishan, C. (2012). Diagnosis of September–November drought and the associated circulation anomalies over Uganda. *Pakistan Journal of Meteorology*, 9(2), 11–24
- Ojara, M. A., Lou, Y., Aribo, L., Namumbya, S., & Uddin, M. J. (2020). Dry spells and probability of rainfall occurrence for Lake Kyoga Basin in Uganda, East Africa. *Natural Hazards*, 100(2), 493–514. <https://doi.org/10.1007/s11069-019-03822-x>
- Ongoma, V., Tan, G., Ogwang, B., & Ngarukiyimana, J. (2015). Diagnosis of seasonal rainfall variability over East Africa: a case study of 2010–2011 drought over Kenya. *Pakistan Journal of Meteorology*, 11(22), 13–21.
- Phillips, J., & McIntyre, B. (2000). ENSO and interannual rainfall variability in Uganda: implications for

- agricultural management. *International Journal of Climatology: A Journal of the Royal Meteorological Society*, 20(2), 171-182.
- Reliefweb., (2020). UgandaKey Message Update: Areas affected by flooding and landslides face deteriorating food security as food prices rise, January 2020. Available at: <https://reliefweb.int/report/uganda/uganda-key-message-update-areas-affected-flooding-and-landslides-face-deteriorating>. (Accessed 18.12.2020).
- Saji, N. H., Goswami, B. N., Vinayachandran, P. N., & Yamagata, T. (1999). A dipole mode in the tropical Indian Ocean. *Nature*, 401(6751), 360-363. <https://doi.org/10.1038/43854>
- Sylla, M. B., Giorgi, F., Coppola, E., & Mariotti, L. (2013). Uncertainties in daily rainfall over Africa: assessment of gridded observation products and evaluation of a regional climate model simulation. *International Journal of Climatology*, 33(7), 1805-1817. <https://doi.org/10.1002/joc.3551>
- Uganda National Meteorological Authority (UNMA). (2019). September to December 2019 seasonal rainfall outlook over Uganda. Available at: <http://www.unma.go.ug>
- Wainwright, C. M., Finney, D. L., Kilavi, M., Black, E., & Marsham, J. H. (2021). Extreme rainfall in East Africa, October 2019–January 2020 and context under future climate change. *Weather*, 76(1), 26-31. doi: 10.1002/wea.3824
- Williams, A. P., & Funk, C. (2011). A westward extension of the warm pool leads to a westward extension of the Walker circulation, drying eastern Africa. *Climate Dynamics*, 37(11-12), 2417-2435. <https://doi.org/10.1007/s00382-010-0984-y>

Influence of Convectively Coupled Equatorial Kelvin Waves on March-May Precipitation over East Africa

Phillip Okello Ochieng^{AB*}, GuirongTan^A, Victor Ongoma^C, Isaiah Nyandega^D

Received: October 08, 2020 | Revised: March 18, 2021 | Accepted: March 21, 2021

doi: 10.5937/gp25-31132

Abstract

Convectively coupled equatorial Kelvin waves (CCEKWs) are those types of equatorially trapped disturbances that propagate eastward and are among the most common intra-seasonal oscillations in the tropics. There exist two-way feedback between the inter-tropical convergence zone (ITCZ) and these equatorially trapped disturbances. Outgoing Longwave Radiation (OLR) was utilized as a proxy for deep convection. For CCEKWs, the modes are located over the West Atlantic, equatorial West Africa, and the Indian Ocean. The influence of other circulations and climate dynamics is studied for finding other drivers of climate within East Africa. The results show a positive relationship between Indian and Atlantic Oceans Sea Surface Temperatures and March-May rainfall over equatorial East Africa over the period of 1980 to 2010. This influence is driven by the Walker circulation and anomalous moisture influx enhanced by winds. Composite analysis reveals strong lower-tropospheric westerlies during the active phase of the CCKWs activities over Equatorial East Africa. The winds are in the opposite direction with the upper-tropospheric winds, which are easterlies. Singular Value Decomposition shows a strong coupling interaction between rainfall over equatorial East Africa and CCKWs. This study concludes that Kelvin waves are not the main factors that influence rainfall during the rainy season. Previous studies show that the main influencing factors are ITCZ, El-Nino Southern Oscillation (ENSO), and tropical anticyclones that borders the African continent. However, CCKWs are a significant factor during the dry seasons.

Keywords: Convectively Coupled Equatorial Kelvin Waves; Inter-Tropical Convergence Zone; Singular Value Decomposition; East Africa; Precipitation

Introduction

The importance of rainfall over East Africa cannot be underscored. Unfortunately, the rain exhibits high spatial and temporal variability. Most of the recent studies in the region (Cattani et al., 2018; Ongoma & Chen, 2017) have focused on the past and future variability of rainfall, giving very little attention to the fac-

tors that modulate the rainfall. Pohl and Camberlin (2006a; 2006b) had reported a more significant effect of ISOs influence on the long rains. Pohl and Camberlin (2006b) described Phases 2 and 3 from the Wheeler-Hendon index, when the convective core is over, using the Intra-Seasonal Oscillations phases established

^A Collaborative Innovation Center on Forecast and Evaluation of Meteorological Disasters, Key Laboratory of Meteorological Disaster, Ministry of Education, Nanjing University of Information Science and Technology, China; tanguirong@nuist.edu.cn

^B Kenya Meteorological Services, Nairobi, Kenya

^C University of the South Pacific, Fiji; victor.ongoma@gmail.com

^D University of Nairobi, Department of Geography and Environmental Studies, Kenya; ianyandega@uonbi.ac.ke

* Corresponding Author: Phillip Okello Ochieng; e-mail: koderaphillips@yahoo.com

by Wheeler and Hendon (2004). Enhanced precipitation over the East African mountains has been associated to Africa and the Indian Ocean.

Convectively coupled Kelvin Waves (CCKWs) are high-frequency intra-seasonal oscillations that extend eastward. They are perhaps among the most critical modes of variability that modulate rainfall in the tropics. They occur along with tropical cyclones and a much broader and smaller Madden – Julian oscillation (MJO) frequency. The movement of heat, humidity, and momentum varies greatly from within and outside the Intertropical Convergence Zone (ITCZ) due to enhanced convection and rainfall, which also affect circulation inside the tropics.

An analysis by Matsuno (1966) documented the near the equator confinement of wider-scale wavelike fluctuations by developing a complete collection of linear wave-mode approaches for shallow water equations upon this equatorial β -plane. Explicitly, this principle of tropical waves starts with the distinction of simple equations, linearized about a primitive state without a vertical shear, which regulates small movements in a three-dimensional stratum atmosphere on an equatorial β -plane, the ‘vertical structure’ formula and the ‘shallow water’ equations (LINDZEN, 1967; Matsuno, 1966).

The zonally (and vertically) propagating, equatorially trapped solutions of the shallow water equations are the equatorial wave modes defined by four parameters: number of the meridional mode, frequency, planetary zonal wavenumber, and ‘equivalent depth of the’ shallow ‘fluid layer. The relative depth is connected to the velocity of the internal gravity wave as a segregation parameter that determines the vertical equation of the structure and the equations of shallow water. Thus, it is also linked to the vertical wavelength

of free (dry) waves and the transverse progression by the equatorial Rossby radius relationship.

The hypothetical dissipation relationship will completely characterize and specify the wave provided by the southern mode number and wave category. Tropical waves are generally assumed to be forced by, and those regulating the natural convection are internal modes with structural elements similar to waves.

These waves produce the highest amplitude signals in outgoing longwave radiation (OLR) data near the equator (Roundy, 2008; Straub & Kiladis, 2002; M. Wheeler & Kiladis, 1999). MacRitchie & Roundy (2012) showed that approximately 62 percent of the precipitation occurring in the negative OLR anomalies of the MJO between 10oN and 10oS over the Indo-Pacific warm pool areas occurs within the negative OLR anomalies of the Kelvin wave band. The result is nearly twice the average precipitation rate per unit area out of Kelvin waves, which is within the active MJO.

The skill of rainfall prediction over the Equatorial East African region falls below expectations most of the time. There is a need for further studies to understand the underlying physical systems that influence ITCZ displacement and, consequently, rainfall. The north-south oscillation of the ITCZ mainly affects the rainfall seasonality over the region. Thus, a discussion about rains over the area is incomplete without mentioning the ITCZ position in a given time. The main aim of this study was to determine the role of convectively coupled equatorial Kelvin waves and other circulation features on the precipitation over the Equatorial East African region. The results of the study aim to improve the on the accuracy of seasonal rainfall predictions which is very important for water resource management and agricultural productivity.

Data and Methods

Study Area

The study area was Equatorial African region located within the grid boxes 25°E-45°E and 5°S-5°N. Although the region of interest is Equatorial East Africa, wave propagation is examined from as far as Atlantic Ocean through Equatorial West/East Africa to the Indian Ocean (60°W to 120°E) to account for the potential wavelength of eastward propagating waves.

East Africa seasonal rainfall pattern is composed of two distinct seasons locally known as the long rains, occurring from March to May (MAM) with peak in April, and the short rains, taking place from October to December (OND) with peak in November as shown in figure.1c. While the long rains are associated with the relatively slow northward movement of

the ITCZ, the short rains are related to a more rapid southward migration of this phenomenon (Walker et al., 2020). Thus, comparing precipitation events during the long rains season tend to be less variable, heavier, and longer in duration, with less interannual variability, and are more likely to be associated with local factors (Mutai & Ward, 2000).

Data

The National Centers for Environmental Prediction (NCEP) and the National Center for Atmospheric Research (NCAR) have carried out a re-analyzed data project based on the Medium Range Forecast (MRF) model (Kalnay et al., 1996). This database is a re-analysis of the global observation network of weather pa-

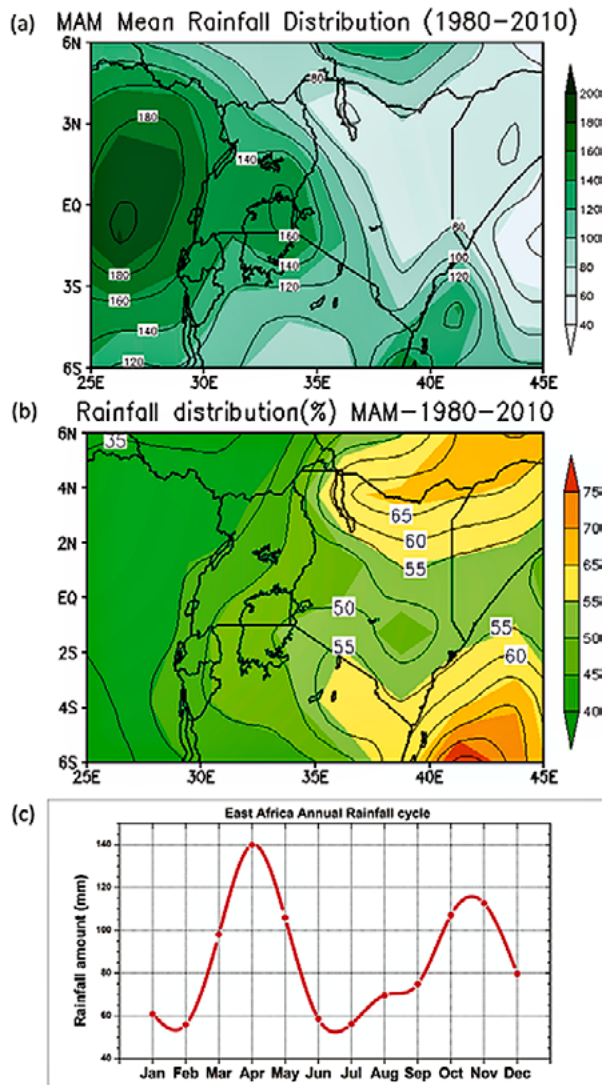


Figure 1. Study area showing the Climatology of March-May rainfall over Equatorial East Africa. a) MAM rainfall distribution in mm/month, b) Percentile distribution of rainfall over equatorial East Africa, c) Annual rainfall cycle of rainfall over equatorial East Africa in mm/month

rameters (wind, temperature, geo-potential height, pressure level humidity, surface area). The data runs

Methods

Wavenumber-frequency Filtering and Wave power Spectral Analysis

The approach used in the first phase of this research is space-time spectrum analysis. This methodology is especially useful for the investigation of zonally moving waves as it decays a data field based on time and longitude into wavenumber and frequency elements for east and westward propagating waves and zone-average fluctuations (Hayashi, 1982). Because we are concerned about synoptic to intra - seasonal time frames, our key findings are centered on spec-

tral amounts which have been determined for several consecutive overlap (by 60 days) of the 96-day sections of the multi-year OLR datasets. The findings are not responsive to such overlaps. To avoid spectral leakage, the first three seasonal cycle harmonics are excluded. During tapering, sophisticated fast Fourier Transforms (FFTs) is conducted in the longitude to determine the Fourier coefficients for each time and latitude. In order to achieve the wavenumber-frequency range for each latitude, additional FFTs are applied in time to these coefficients.

from 1948 to the present. It is reported on a $2.5^\circ \times 2.5^\circ$ grid every six h (00.00, 06.00, 12.00, and 18.00 UTC), on 17 pressure levels from 1000 to 10 hPa, which are adequate resolutions for studying synoptic weather systems (Kalnay et al., 1996).
Outgoing Longwave Radiation (OLR) originates from the Environment Diagnostics Center (CDC). Data is typically collected twice daily from the National Oceanic and Atmospheric Administration (NOAA) polar-orbiting satellite (Gruber & Krueger, 1984) and computed to daily values by Liebmann & Smith (1996). ERA daily data involves the wind zone measured 4 times daily at 0000, 0600, 1200 and 1800 GMT. The data has a spatial resolution of $2.5^\circ \times 2.5^\circ$ and, which covers the period 1980 to 2010.

Tropical Rainfall Measuring Mission (TRMM) data has been used as a proxy for position and strength of ITCZ as rainfall is more closely related to convection. This data set spans from 1998 to the present on 3-hour 0.25° latitudinal-longitude grid systems but has also been weighted for 6-hour 1° latitude-longitude meshes to increase statistical efficiency. TRMM precipitation dataset has been applied by (Cho et al. 2004) to capture equatorial waves. TRMM product 3B42 (Huffman et al., 1997) is used in this study.

The Global Precipitation Climatology Project (GPCP) offers a reliable monthly estimate of global precipitation from the combination of different land and ocean satellite data sets and an overland gauge assessment (Adler et al., 2018). Data from rain sensor locations, satellites and sounding measurements have been combined to measure monthly rainfall on the global 2.5° grid from 1979 to date. A detailed overview of the precipitation available to date across the global oceans provides an accurate integration of satellite-based rainfall estimates. It adds to the study of rainfall over land the required spatial information. Estimates of uncertainties in the rainfall analysis are provided as part of the GPCP items, in addition to the combination of these data sets.

Finally, the OLR power is distributed over all relevant sections of the 31-year period and is again added for latitudes between 15°S and 15°N. The consequent effective bandwidth is 1/96 cycles per day (cpd) in frequency and 1-unit zonal wavenumber. The overall number of degrees of freedom (dof), each latitude, and each (non-overlapping) 96-day section of the 31-year period.

Composite Analysis

Composite assessment includes the detection and analysis of one or more sets of variables identified as per their relationship with essential conditions. The effects of the composites are then used to produce patterns that would hypothesize the phenomenon that could be correlated with individual scenarios.

A time series, hereafter called the CCKW index, was developed based on a selected grid point over equatorial East Africa (0°N, 35°E). The CCKW index comprises all days where the minimum negative Kelvin-filtered OLR variance were less than -1.5 standard deviations as active phase and days where the maximum positive Kelvin-filtered OLR variance were more than +1.5 standard deviations as suppressed phase in magnitude during the 1980-2010 MAM seasons. Lags were then used on this time series in order to exam-

ine propagating characteristics. Day 0 of the CCKW index was taken as the day when the minimum (maximum) Kelvin filtered OLR variance moves over the selected base point. This would show the evolution of precipitation when the various disturbances intensify/weaken.

Singular Value Decomposition

Singular value decomposition (SVD) has been widely used in meteorology since its first application by Prohaska (1976) to study the simultaneous relationships between surface air temperature over the United States of America and sea level pressure patterns. It requires no user-supplied parameters and lacks systematic bias. According to Bretherton et al. (1992) and Wallace et al. (1992), it is perhaps one of the preferable methods to directly produce explicit measures of the derived coupled patterns between two correlated fields.

SVD is a fundamental mathematical (matrix) operation that can be taken as an essential extension to rectangular matrices of square symmetric matrices' diagonalization. The cross-covariance matrix's singular value decomposition identifies pairs of spatial patterns from two data fields that illustrate as much of the mean-squared temporal covariance between the two areas as possible.

Results

Raw Background Power Spectral Analysis

In order to investigate the convective variability associated with equatorial waves, spatial-time power spectral analysis is conducted. Power is shown in the antisymmetric and symmetric OLR components in figure.2. The most striking characteristic of these spectra in wavenumber and frequency is the intensity of the red color. Notable variations can, however, be discerned between eastward and westward and symmetric and antisymmetric elements. The feature with the most power relative to the red background in either part or either propagating direction is the CCKWs, occurring mostly at eastward wavenumbers 2 to 10, and centered at a period of about 2.5-20 days in OLRs, and to a lesser extent in OLR Antisymmetric spectrum. At frequencies less than about 0.3 cpd, there is a more significant occurrence of CCKWs in OLR Symmetric than OLR Anti-symmetric for almost all wavenumbers associated with the Kelvin waves.

Despite these general observed spectral features, the raw power spectra's detailed characteristics are likely to be obstructed by the spectrum's redness. For this reason, we defined a red background spectrum following Wheeler & Kiladis (1999), which we then re-

move from the original ranges, leaving the statistically significant spectral peaks as earlier explained.

The blue lines show filter bands, while the black lines show the dispersion curves of shallow water model Kelvin wave solutions at $\lambda = 5\text{m}$ and $90 = \text{m}$ superimposed on a raw OLR spectrum. The findings are similar to those obtained by Wheeler and Kiladis (1999).

Figure 2. Wavenumber–frequency power spectrum of the symmetric and anti-symmetric component of OLR for 1980–2010, summed from 15°N to 15°S, and plotted as the ratio of the raw OLR power to the power in a smoothed red noise background spectrum during March–May, where the signal is significant at greater than the 95% level

The distribution of Kelvin filtered OLR variance

The geographical distribution of the variance of Kelvin filtered OLR (averaged over 1980-2010 for March-May (MAM), which is the primary rainfall season over East Africa, is shown in figure.3. The overall activity is comparable to previous research findings employing OLR variance filtered for Kelvin waves (Mekonnen et al., 2008; Roundy & Frank, 2004; M. Wheeler et al., 2000; M. Wheeler & Kiladis, 1999). Over the equatorial Indian Ocean, the continent of tropical West Africa, and the central equatorial West Atlantic, peak activity occurs. The behavior of Kelvin waves is also commonly observed between 5°S-5°N over the entire tropical central-to-eastern Atlantic Oceans and 5°S-5°N to 30°E over West Africa. With the exception of tropical West Africa during the MAM season, the variance of Kelvin filtered OLR is not symmetrical with the equator, consistent with the previous Kelvin wave variance (Roundy & Frank, 2004; Straub & Kiladis, 2002). In MAM, the Kelvin wave is most dominant, with its spectral power concentrated, as predicted by linear theory, around the equator (Matsuno, 1966). Throughout the boreal summer, the Kelvin wave remains active, but its amplitude moves far away from the equator of the Northern Hemisphere. This off-equatorial Kelvin wave maximum is correlated with the seasonal ITCZ migration.

Figure 3. Geographical distribution of kelvin filtered OLR variance during MAM

Upper Tropospheric Geopotential (100hPa)

The most robust notable feature of CCKWs over the Western Hemisphere is their upper-level zonal wind signature and geopotential height in figure.4. The upper tropospheric structure of the geopotential field shows an upper-level trough at lag0 days, which then disappears two days after the passage of the CCKWs. At lag-5 days before enacting the CCKWs over east Africa, an upper tropospheric ridge is located over the East Africa region. The rise seems to be quasi-stationary at lag-5 to lag-2 days before shifting eastwards.

At lag-1 days (not shown), the ridge splits into two sections with the left one over South Atlantic Ocean and the equatorial Indian Ocean's right one. At lag+1 day, the upper-level ridge over the Indian Ocean disappears. Simultaneously, one over the Atlantic Ocean does not reach the east African region after the passage of the active phase of the CCKWs. The trough at lag0 days is slightly located to the west of the convec-

Figure 4. Lagged composites of the Upper Tropospheric Geopotential (100 hPa) in meters on selected days based on the CCKW index. The shaded areas show regions significant at greater than 95% confidence level

tive area. Based on the findings in this section, the upper-tropospheric geopotential anomalies that intrude from the extra-tropics tend to force the initial convective anomaly associated with the Kelvin wave. Ventrice et al. (2012) obtained similar findings.

At lag0 days when the suppressed phases of CCKW, contrasting observations are made with the upper-level ridge located on the same position as during the active phase. Similar polar observations are also made on other lag days.

Upper-level Winds (200hPa)

The complex structure of the CCKWs is defined, as shown in figure.5, by upper-level westerlies ahead of the CCKW convectively active period and upper-level easterlies eastward at lag0 days. For the convectively suppressed step of the CCKW, the reverse should therefore be right. It should be remembered that the CCKW-associated upper-level westerly wind anomalies create an atmosphere conducive to the infiltration of extra-tropical waves into the tropics. This corresponds with the results of Ventrice et al. (2012).

Lower tropospheric Winds (850hPa)

As the vector difference between 850 hPa and 200 hPa levels, vertical wind shear is described. It is determined by averaging the CCKW index's set of dates. Composite analysis shows that vertical wind shear decreases before and after the CCKW's convectively active period passes over East Africa as anomalous westerly upper-level winds are opposite in flow with anomalous lower-level easterlies. The atmosphere is moistened by large-scale vertical motions associated with the convectively active process of the CCKWs.

Figure 5. Lagged composites of the Upper Tropospheric winds (200hPa) in m/s on selected days based on the CCKW index. The shadings show areas significant at greater than 95% level for easterly or westerly wind vectors

Figure. 6 indicates the vertical wind shear associated with the CCKWs' active and suppressed process.

Although CCKWs are typically associated with a wind structure at a lower level that is generally opposite to the flow of the upper troposphere, as seen in Figure.5, the zonal wind, temperature, and humidity of these waves have strongly tilted vertical structures (Mekonnen et al., 2008). The phase relationship between the structures of low-level and upper-level winds varies with the phase speed and zonal size of the wave. With the westerly flow at lower speeds, high pressure is collocated and low-pressure is collocated within the easterly flow. The inverse is true for the upper stages. Deep convection warms the mid-to-upper layers of the atmosphere and moistens them.

Over the Atlantic Ocean, the lower tropospheric winds are easterlies before the passage of the active phase of the CCKWs over East Africa. After the path, the winds are predominantly westerlies. The reverse is valid for the Indian Ocean basin. The 850-200hPa vertical wind shear exhibit the reverse patterns. Figure.6 shows the composites of the 850hPa winds on lagged days.

Vertical motions

Vertical motion tested for at over 90% confidence level is shown in Figure.7. At lag0 days, there exists ascending motions below 500-200 hPa thickness in the region over East Africa. On the other hand, there is a downward motion on the East Indian Ocean and the western Atlantic Ocean, which signifies a reverse walker circulation pattern. Similar patterns are observed at lag-1 days (not shown) before the passage of the active phase of Kelvin wave over East Africa. Of significance to note

Figure 6. Lagged composites of the Lower Tropospheric (850hPa) winds (m/s) on the selected days based on the CCKW index (vectors). The shadings show areas significant at greater than 95% level for easterly or westerly wind vectors. Dashed contours represent regions with kelvin OLR variance greater than 400

is at lag-5 days. There is a similar motions pattern over the Atlantic, east Africa, and the Indian Ocean basin, downward motions over East Africa and Indian Ocean areas, and upward motion over East Atlantic.

The vertical motion extends to tropical central Africa at lag-5 days. The circulations associated with vertical movements are in the reverse directions at lag0 days compared to lag-5 days. This circulation pattern

Figure 7. Lagged composites of the vertical cross section of the vertical motions (omega) in (Pa/s*100) based on selected days of the CCKW index, left-active phase and right-suppressed phase. The black streamlines show the directions of the rising and sinking motions. The shadings show areas of significant vertical motion significant at over 80% confidence level

is similar to the Walker circulation, with descending and ascending motions over East Africa and the Indian Ocean. At lag+5 days there are opposite patterns of the vertical movements for the active and the suppressed phases of the CCKW events over the Atlantic and the Indian Ocean basins with no significant motions as from lag+5 days.

The convergence of surface easterlies, which establish themselves in response to the geopotential height fields forced from the extra-tropics, is forced by lower tropospheric upward motion, as discussed earlier. The vertical motion anomalies confirm and spread across the depth of the troposphere as the Kelvin wave's coupled convective and dynamic fields disperse eastward.

Temperature

Figure 8 is a longitude–height cross-section of temperature (contours) with shadings showing regions tested for 95% significance. During the active phase of the CCKWs at lag0 days, the troposphere is cooling up to 400hPa and warming between 300hPa and 200hPa, and the tropopause is cold near and is located

near 100hPa. This temperature profile is consistent with past findings (Wheeler and Kiladis 2000) of convectively coupled tropical waves. There is a warming of the entire troposphere and a cooling of the tropopause at lag-3 and lag-5 the day before the passing of the active period over East Africa.

The low and mid-level alternating heating and cooling observed during the lag0 days indicates that there is a tropospheric heat source that involves both deep convective heating and a second baroclinic heating mode over a cooling framework resulting from stratiform precipitation. The higher troposphere is colder and the sections of the lower troposphere and tropopause are warmer. The temperature response of the atmosphere to the convectively coupled Kelvin wave heating fields tends to be very linear, according to Wheeler et al. (2000). At lag+3 days after the passage of the active CCKW phase over East Africa, the troposphere tends to warm due to the latent heat release through convective heating and cooling at lag+5 days because of the latent heat dissipated during active convection triggered by CCKWs is no longer available within the environment.

Contrasting observations are made during the suppressed phase at lag0 days when the CCKW phase is over East Africa with cooling observed on the upper troposphere at 300–200 hPa levels and

Singular Value Decomposition

The three leading SVD modes of the coupled Kelvin Variance and Rainfall variations account for 74.67% of the total square covariance as shown in figure 9 and

Figure 8. Composite of longitude–height section of air temperature (contoured with shadings showing regions tested for 95% significance on the selected days based on CCKW index, left-active phase and right-suppressed phase

Figure 9. SVD fields of the MAM Kelvin variance. a) SVD1, b) SVD2, c) SVD3 joined lines shows area with positive spatial covariance, dotted lines show areas with negative spatial covariance and the zero contour is marked green

Table 1. Square Covariance Fractions (SCF) explained by each mode and the correlation coefficient (*r*)

Squared covariance	Fraction	Temporal Correlation	Kelvin Variance	Rainfall Variance
Mode 1	37.76	0.54	22.64	21.01
Mode 2	28.79	0.55	16.61	21.04
Mode 3	8.72	0.77	7.40	7.46

figure 10. For simplicity, I labeled the spatial patterns as SVD_k, and the expansion coefficient as svdk, where k=1, 2 and 3.

The square covariance fractions (SCF) explained by each mode and the correlation coefficient (*r*) between the expansion coefficients of the two {svdk (Kelvin Variance) and svdk (rainfall)} variables are shown in Table 1 as indicators of the coupling strength. The first mode has a substantial and extremely significant coupling variation of kelvin and rainfall in East Africa. Contrarily the correlation coefficient associated with the coupling of the modes increases. Although the least variance is demon-

strated by the third SVD mode, its associated coupling coefficient is greater than those of the preceding modes, denoting the potential value of the third mode.

The first couple mode that dominates the variability between the March-May rainfall and the Kelvin variance reveals a positive monopole variability between kelvin variance over central Atlantic and Equatorial West Africa extending to the Indian Ocean basin, with substantial positive rainfall variability. The second couple mode that dominates the variability between the March-May rainfall and the kelvin variance reveals a negative monopole variability between

Figure 10. SVD fields of the MAM rainfall (mm/month) over equatorial East Africa. a) SVD1, b) SVD2, c) SVD3. Red shading shows areas with positive spatial covariance and green shading shows areas with negative spatial covariance

Figure 11. SVD temporal correlation between MAM Kelvin variance (black) and MAM rainfall (mm/month) over equatorial East Africa (dotted-red). (a) SVD1, (b) SVD2, (c) SVD3

Kelvin variance over central Atlantic and Equatorial West Africa extending to the Indian Ocean basin and reduced positive variability of rainfall. The temporal

amplitude of rains and the Kelvin variance correlate very well (>0.5), indicating the relationship's coupled nature as shown in figure 11.

Conclusion and Recommendations

This work has focused on studying the dynamical variability in the entire troposphere up to the tropopause. Understanding the variability of this atmospheric layer on different temporal scales is very important before answering questions such as “Are there any eastward propagating disturbances from the Western Atlantic towards the African region?” or “Does NAO and Atlantic/Indian Ocean SSTs exert have any influence on rainfall over the Equatorial East African region?” can be answered.

A physical understanding of the environmental conditions that cause variability in the intra-seasonal oscillation in the tropics both vertically and horizontally can improve the accuracy of predictions of high-frequency rainfall over equatorial East Africa. These questions have been considered using the NOAA interpolated OLR and NOAA DOE datasets.

Over the equatorial Indian Ocean, the tropical continent of West Africa, and the central equatorial West Atlantic, peak CCKW activity occurs. The activity of Kelvin waves is also generally observed between 5°S - 5°N over the entire tropical central-to-eastern Atlantic Oceans and between 5°S - 5°N and 30°E over West Africa. Compared to other seasons, the CCWKs in MAM are stronger than in Equatorial East Africa.

SST warming near the equator Atlantic implies a conducive background scenario for the propagation of convectively coupled Kelvin waves. Increased SSTs in the Gulf of Guinea often lead in a weakened temperature gradient between the surface of the land and the sea, a characteristic of a weaker monsoon and decreased rainfall over tropical Africa, as shown in previous studies (Ward, 1998). The origin of the CCKWs over tropical Africa is also thought to be on the West tropical Atlantic, as proven by the correlation between Kelvin filtered OLR variance and SSTs. In agreement with Mekonnen et al. (2008), both the Atlantic and Indian Oceans have a positive correlation coefficient depicting a strong coupling between the indices and the rainfall over tropical east Africa.

The upper tropospheric and the lower tropospheric wind fields showed an opposite flow pattern with an upper-level trough seen on the day when the active phase of the CCKW is located over east Africa. This can be attributed to the strong easterly wind shear as observed in the active phase scenarios. CCKWs can also act as a triggering mechanism by enhancing conditions favorable for convection as it passes over a region.

Acknowledgments

The first author is grateful to the Ministry of Commerce of the People's Republic of China (MOFCOM) for sponsoring his MSc studies in China. The authors appreciate the contribution of all the data centers in providing the data free of charge.

References

- Adler, R. F., Sapiano, M. R. P., Huffman, G. J., Wang, J. J., Gu, G., Bolvin, D., Chiu, L., Schneider, U., Becker, A., Nelkin, E., Xie, P., Ferraro, R., & Shin, D. Bin. (2018). The Global Precipitation Climatology Project (GPCP) monthly analysis (New Version 2.3) and a review of 2017 global precipitation. *Atmosphere*, 9(4). <https://doi.org/10.3390/atmos9040138>
- Barnston, A. G., & Livezey, R. E. (1987). Classification, seasonality and persistence of low-frequency atmospheric circulation patterns. *Monthly weather review*, 115(6), 1083-1126. [https://doi.org/10.1175/1520-0493\(1987\)115<1083:CSAPOL>2.0.CO;2](https://doi.org/10.1175/1520-0493(1987)115<1083:CSAPOL>2.0.CO;2)
- Biasutti, M., Battisti, D. S., & Sarachik, E. S. (2003). The annual cycle over the tropical Atlantic, south America, and Africa. *Journal of Climate*, 16(15), 2491-2508. [https://doi.org/10.1175/1520-0442\(2003\)016<2491:TACOTT>2.0.CO;2](https://doi.org/10.1175/1520-0442(2003)016<2491:TACOTT>2.0.CO;2)
- Cattani, E., Merino, A., Guijarro, J. A., & Levizzani, V. (2018). East Africa Rainfall trends and variability 1983-2015 using three long-term satellite products. *Remote Sensing*, 10(6), 1-26. <https://doi.org/10.3390/rs10060931>
- Cattell, R. B. (1966). The scree test for the number of factors. *Multivariate Behavioral Research*, 1(2), 245-276. https://doi.org/10.1207/s15327906mbr0102_10

- Chiang, J. C. H., Kushnir, Y., & Zebiak, S. E. (2000). Interdecadal changes in eastern Pacific ITCZ variability and its influence on the Atlantic ITCZ. *Geophysical Research Letters*, 27(22), 3687–3690. <https://doi.org/10.1029/1999GL011268>
- Cho, H. K., Bowman, K. P., & North, G. R. (2004). Equatorial waves including the Madden-Julian oscillation in TRMM rainfall and OLR data. *Journal of Climate*, 17(22), 4387–4406. <https://doi.org/10.1175/3215.1>
- Convection-2-15Day.Pdf*. (n.d.).
- Dias, J., & Pauluis, O. (2009). Convectively coupled waves propagating along an equatorial ITCZ. *Journal of the Atmospheric Sciences*, 66(8), 2237–2255. <https://doi.org/10.1175/2009JAS3020.1>
- Emanuel, K. A., David Neelin, J., & Bretherton, C. S. (1994). On large-scale circulations in convecting atmospheres. *Quarterly Journal of the Royal Meteorological Society*, 120(519), 1111–1143. <https://doi.org/10.1256/smsqj.51901>
- Finney, D. L., Marsham, J. H., Walker, D. P., Birch, C. E., Woodhams, B. J., Jackson, L. S., & Hardy, S. (2020). The effect of westerlies on East African rainfall and the associated role of tropical cyclones and the Madden–Julian Oscillation. *Quarterly Journal of the Royal Meteorological Society*, 146(727), 647–664. <https://doi.org/10.1002/qj.3698>
- Fu, R., Dickinson, R. E., Chen, M., & Wang, H. (2001). How do tropical sea surface temperatures influence the seasonal distribution of precipitation in the equatorial Amazon? *Journal of Climate*, 14(20), 4003–4026. [https://doi.org/10.1175/1520-0442\(2001\)014<4003:HDTSSST>2.0.CO;2](https://doi.org/10.1175/1520-0442(2001)014<4003:HDTSSST>2.0.CO;2)
- Gruber, A., & Krueger, A. F. (1984). The status of the NOAA outgoing longwave radiation data set. *Bulletin - American Meteorological Society*, 65(9), 958–962. [https://doi.org/10.1175/1520-0477\(1984\)065<0958:TSOTNO>2.0.CO;2](https://doi.org/10.1175/1520-0477(1984)065<0958:TSOTNO>2.0.CO;2)
- Gu, G., & Zhang, C. (2001). A spectrum analysis of synoptic-scale disturbances in the ITCZ. *Journal of Climate*, 14(12), 2725–2739. [https://doi.org/10.1175/1520-0442\(2001\)014<2725:ASAOSS>2.0.CO;2](https://doi.org/10.1175/1520-0442(2001)014<2725:ASAOSS>2.0.CO;2)
- Hayashi, Y. (1982). Space-Time Spectral Analysis and its Applications to Atmospheric Waves. *Journal of the Meteorological Society of Japan. Ser. II*, 60(1), 156–171. https://doi.org/10.2151/jmsj1965.60.1_156
- Huang, B., Banzon, V. F., Freeman, E., Lawrimore, J., Liu, W., Peterson, T. C., Smith, T. M., Thorne, P. W., Woodruff, S. D., & Zhang, H. M. (2015). Extended reconstructed sea surface temperature version 4 (ERSST.v4). Part I: Upgrades and intercomparisons. *Journal of Climate*, 28(3), 911–930. <https://doi.org/10.1175/JCLI-D-14-00006.1>
- Huffman, G. J., Adler, R. F., Arkin, P., Chang, A., Ferraro, R., Gruber, A., Janowiak, J., McNab, A., Rudolf, B., & Schneider, U. (1997). The Global Precipitation Climatology Project (GPCP) Combined Precipitation Dataset. *Bulletin of the American Meteorological Society*, 78(1), 5–20. [https://doi.org/10.1175/1520-0477\(1997\)078<0005:TGPCPG>2.0.CO;2](https://doi.org/10.1175/1520-0477(1997)078<0005:TGPCPG>2.0.CO;2)
- Kalnay, E., Kanamitsu, M., Kistler, R., Collins, W., Deaven, D., Gandin, L., Iredell, M., Saha, S., White, G., Woollen, J. & Joseph, D. (1996). The NCEP/NCAR 40-year reanalysis project. *Bulletin of the American meteorological Society*, 77(3), 437–472. [https://doi.org/10.1175/1520-0477\(1996\)077<0437:TN YRP>2.0.CO;2](https://doi.org/10.1175/1520-0477(1996)077<0437:TN YRP>2.0.CO;2)
- Li, T., & Philander, S. G. H. (1997). On the seasonal cycle of the equatorial Atlantic Ocean. *Journal of Climate*, 10(4), 813–817. [https://doi.org/10.1175/1520-0442\(1997\)010<0813:OTSCOT>2.0.CO;2](https://doi.org/10.1175/1520-0442(1997)010<0813:OTSCOT>2.0.CO;2)
- Lindzen, R. D. (1967). Planetary Waves on Beta-Planets. *Monthly Weather Review*, 95(7), 441–451. [https://doi.org/10.1175/1520-0493\(1967\)095<0441:pwobp>2.3.co;2](https://doi.org/10.1175/1520-0493(1967)095<0441:pwobp>2.3.co;2)
- MacRitchie, K., & Roundy, P. E. (2012). Potential vorticity accumulation following atmospheric Kelvin waves in the active convective region of the MJO. *Journal of the Atmospheric Sciences*, 69(3), 908–914. <https://doi.org/10.1175/JAS-D-11-0231.1>
- Matsuno, T. (1966). Quasi-Geostrophic Motions in the Equatorial Area. *Journal of the Meteorological Society of Japan. Ser. II*, 44(1), 25–43. https://doi.org/10.2151/jmsj1965.44.1_25
- Mekonnen, A., Thorncroft, C. D., & Aiyyer, A. R. (2006). Analysis of convection and its association with African easterly waves. *Journal of Climate*, 19(20), 5405–5421. <https://doi.org/10.1175/JCLI3920.1>
- Mekonnen, A., Thorncroft, C. D., Aiyyer, A. R., & Kiladis, G. N. (2008). Convectively coupled Kelvin waves over tropical Africa during the boreal summer: Structure and variability. *Journal of Climate*, 21(24), 6649–6667. <https://doi.org/10.1175/2008JCLI2008.1>
- Mutai, C. C., & Ward, M. N. (2000). East African rainfall and the tropical circulation/convection on intraseasonal to interannual timescales. *Journal of Climate*, 13(22), 3915–3939. [https://doi.org/10.1175/1520-0442\(2000\)013<3915:EARATT>2.0.CO;2](https://doi.org/10.1175/1520-0442(2000)013<3915:EARATT>2.0.CO;2)
- Ongoma, V., & Chen, H. (2017). Temporal and spatial variability of temperature and precipitation over East Africa from 1951 to 2010. *Meteorology and Atmospheric Physics*, 129(2), 131–144. <https://doi.org/10.1007/s00703-016-0462-0>

- Pohl, B., & Camberlin, P. (2006a). Influence of the Madden-Julian Oscillation on East African rainfall. I: Intraseasonal variability and regional dependency. *Quarterly Journal of the Royal Meteorological Society*, 132(621), 2521–2539. <https://doi.org/10.1256/qj.05.104>
- Pohl, B., & Camberlin, P. (2006b). Influence of the Madden-Julian Oscillation on East African rainfall. II. March-May season extremes and interannual variability. *Quarterly Journal of the Royal Meteorological Society*, 132(621), 2541–2558. <https://doi.org/10.1256/qj.05.223>
- Kanamitsu, M., Ebisuzaki, W., Woollen, J., Yang, S. K., Hnilo, J. J., Fiorino, M., & Potter, G. L. (2002). Ncep-doe amip-ii reanalysis (r-2). *Bulletin of the American Meteorological Society*, 83(11), 1631–1644. <https://doi.org/10.1175/BAMS-83-11>
- Roundy, P. E. (2008). Analysis of convectively coupled Kelvin waves in the Indian ocean MJO. *Journal of the Atmospheric Sciences*, 65(4), 1342–1359. <https://doi.org/10.1175/2007JAS2345.1>
- Roundy, P. E., & Frank, W. M. (2004). A climatology of waves in the equatorial region. *Journal of the Atmospheric Sciences*, 61(17), 2105–2132. [https://doi.org/10.1175/1520-0469\(2004\)061<2105:ACOWIT>2.0.CO;2](https://doi.org/10.1175/1520-0469(2004)061<2105:ACOWIT>2.0.CO;2)
- Schreck, C. J., & Molinari, J. (2011). Tropical cyclogenesis associated with Kelvin waves and the Madden-Julian oscillation. *Monthly Weather Review*, 139(9), 2723–2734. <https://doi.org/10.1175/MWR-D-10-05060.1>
- Straub, K. H., & Kiladis, G. N. (2002). Observations of a convectively coupled Kelvin wave in the eastern Pacific ITCZ. *Journal of the Atmospheric Sciences*, 59(1), 30–53. [https://doi.org/10.1175/1520-0469\(2002\)059<0030:OOACCK>2.0.CO;2](https://doi.org/10.1175/1520-0469(2002)059<0030:OOACCK>2.0.CO;2)
- Ventrice, M. J., Thorncroft, C. D., & Schreck, C. J. (2012). Impacts of convectively coupled kelvin waves on environmental conditions for Atlantic tropical cyclogenesis. *Monthly Weather Review*, 140(7), 2198–2214. <https://doi.org/10.1175/MWR-D-11-00305.1>
- Walker, D. P., Marsham, J. H., Birch, C. E., Scaife, A. A., & Finney, D. L. (2020). Common Mechanism for Interannual and Decadal Variability in the East African Long Rains. *Geophysical Research Letters*, 47(22). <https://doi.org/10.1029/2020GL089182>
- Ward, M. N. (1998). Diagnosis and short-lead time prediction of summer rainfall in tropical North Africa at interannual and multidecadal timescales. *Journal of Climate*, 11(12), 3167–3191. [https://doi.org/10.1175/1520-0442\(1998\)011<3167:DASLTP>2.0.CO;2](https://doi.org/10.1175/1520-0442(1998)011<3167:DASLTP>2.0.CO;2)
- Wheeler, M. C., & Hendon, H. H. (2004). An all-season real-time multivariate MJO index: Development of an index for monitoring and prediction. *Monthly Weather Review*, 132(8), 1917–1932. [https://doi.org/10.1175/1520-0493\(2004\)132<1917:AA RMMI>2.0.CO;2](https://doi.org/10.1175/1520-0493(2004)132<1917:AA RMMI>2.0.CO;2)
- Wheeler, M., & Kiladis, G. N. (1999). Convectively Coupled Equatorial Waves: Analysis of Clouds and Temperature in the Wavenumber-Frequency Domain. *Journal of the Atmospheric Sciences*, 56(3), 374–399. [https://doi.org/10.1175/1520-0469\(1999\)056<0374:CCEWAO>2.0.CO;2](https://doi.org/10.1175/1520-0469(1999)056<0374:CCEWAO>2.0.CO;2)
- Wheeler, M., Kiladis, G. N., & Webster, P. J. (2000). Large-scale dynamical fields associated with convectively coupled equatorial waves. *Journal of the Atmospheric Sciences*, 57(5), 613–640. [https://doi.org/10.1175/1520-0469\(2000\)057<0613:LSDFAW>2.0.CO;2](https://doi.org/10.1175/1520-0469(2000)057<0613:LSDFAW>2.0.CO;2)
- Zhou, L., Wang, S., Du, M., Chen, Q., He, C., Zhang, J., Zhu, Y., & Gong, Y. (2021). The influence of ENSO and MJO on drought in different ecological geographic regions in China. *Remote Sensing*, 13(5), 1–19. <https://doi.org/10.3390/rs13050875>

Summer Thermal Comfort in Russian Big Cities (1966-2015)

Pavel Konstantinov^{A*}, Diana Tattimbetova^A, Mikhail Varentsov^A, Natalia Shartova^A

Received: November 19, 2020 | Revised: March 21, 2021 | Accepted: March 22, 2021

doi: 10.5937/gp25-29440

Abstract

The main goal of the study is the assessment of modern bioclimatic conditions (1966-2015) for determining the level of comfort in large Russian cities based on the observations at the meteorological stations, including Physiological Equivalent Temperature (PET) for the main extent of thermal comfort. According to the distribution of thermal stress events (calculated for meteorological fix hours, 8 times per day) the authors created the comfort diagram for each city during daytime heat wave period and evaluated their comfort conditions. In the current research we are operating with WMO climatic data for eleven biggest cities of the Russian Federation: from the European part (Moscow, Saint-Petersburg, Ekaterinburg, Voronezh, Volgograd, Kazan, Nizhny Novgorod, Perm, Ufa) and from Siberia (Omsk and Krasnoyarsk). The most interesting result of the comparison of the long-period (50 years) urban trends (PET-index and Air Temperature) in different parts of Russia is its extraordinary cross-shaped form in Moscow (in other cities the trends lines are practically parallel to each other). It means that at the level of the average annual values, only in Moscow the PET index (and, hence, potentially the thermal stress) grows faster than the regional climate warms. In other cities this tendency is much weaker (N. Novgorod) or not significant. This interesting tendency is caused by both Moscow related urban planning dynamics in post-USSR period and by regional climate dynamics.

Keywords: Physiological Equivalent Temperature (PET); regional urban climate; urban thermal comfort

Introduction

In recent times, the urban climate studies have inevitably shifted the emphasis towards the problems of sustainable development of (mega)cities. Such concept is closely connected with the studies of the human comfort in large cities in Europe and Asia. It is a rational approach to the resettlement and peaceful co-existence of a large number of people within the confines of a small territory (villages, cities, metropolises, etc.). From this point of view, the cities of the Russian Federation are an ideal monitoring platform, since the concept process of their development has just started. At the same time, it should be taken into account that the Russian Federation is a highly urbanized coun-

try (Kolosov & Nefedova, 2014), and this process has been connected to internal migration of the population since the 1970s.

Rapid urbanization in Russian Federation led to cities growth and its economic advance. Alongside this population of big cities (>1 000 000 inhabitants) is quite vulnerable to heat wave events due to intensive urban heat island event (Kislov & Konstantinov, 2011). In July and August 2010 in the biggest city in Russia – Moscow, where more than 11 million people live, the longest and the strongest heat wave as well as the warmest day (29th of July 2010) were recorded since the meteorological observations in Russia (Konstan-

^A Lomonosov Moscow State University, Faculty of Geography, Leninskie Gory 1 119991; kostadini@mail.ru; diano4ka_07.07.95@mail.ru; mvar91@gmail.com; shartova@yandex.ru

* Corresponding author: Pavel Konstantinov; e-mail: kostadini@mail.ru

tinov et al., 2014). There were close to 11 000 excess deaths from non-accidental causes (predominantly temperature and air pollution) during this period, mainly among people older than 65 years. Increased risks (Zemtsov et al., 2020) also occurred in younger age groups (Shaposhnikov et al., 2014). Thus, the main goal of the study is the assessment of modern bioclimatic conditions (1966-2015) for determining the level of comfort in large Russian cities based on the observations at meteorological stations.

Also, the variety of natural and climatic conditions in the Russian Federation allows to study the bioclimatic characteristics of the large cities (there are 15 cities with more than 1 million inhabitants in Russia) in various subtypes of the temperate zone (from marine to ultracontinental). The similar conditions of planning efforts in these big cities create a uniform

Materials and Methods

This study is based on the characterization of the climatic trends of human thermal comfort and its assessment during heat wave periods. From the standpoint of human health heat wave is a period of time in which an excessive stress of thermoregulation of the body is accessed, as well as an increased risk of morbidity and mortality, especially from respiratory and cardiovascular diseases (Robinson, 2001; Arsenović et al., 2019; Urban et al 2019).

There are many approaches to the definition of heat waves. For this study the most convenient criteria developed by the World Meteorological Organization (WMO) was chosen. According to it, the heat wave is the excess of the maximum temperature for five consecutive days or more at 5°C from the average maximum value for the base period from 1961 to 1990 (Frich et al., 2002)

In this study we choose Physiological Equivalent Temperature (PET) for the main extent of thermal comfort. "Equivalent-physiological temperature for a given place" is the air temperature at which for ordinary room conditions the heat balance of the human body remains unchanged with the internal body temperature and skin temperature for a given situation (Hoppe, 1999) This, however, does not mean that this index can not be applied to the open spaces. On the contrary, it helps a person to compare sensations he/she has in the open air with the room conditions that are familiar to him – some evaluations for Russian Federation were described in paper (Shartova et al., 2018).

The basis for the study was the analysis of standardized data from the regular Roshydromet (Russian WMO meteorological network) over a 50-year period

background of administrative influence on the part of the government. This allows to identify in which geographical regions the traditional type of city management is more successful from a bioclimatic point of view. In other words, in which regions conditions of thermal comfort in cities is a successor of air temperature trends and in which not.

Of course, within the framework of this study, **we accept the hypothesis that changes in the trends of thermal comfort in Russian cities are associated with both the change in the regional climate and with the change of land-use properties in the urban environment.** However, since the natural factor acts with approximately the same strength, noticeable differences in trends (if they are detected) can be generated by the influence of the urban microclimate, which is indirectly related to urban development strategies.

from 1966 to 2015. This was due to the fact that the best quality data of instrumental observations were available during this period. Russia's cities with population of 1 million were chosen as the objects of the research.

In current research we are operating with WMO climatic data for 11 biggest cities of the Russian Federation: from the European part (Moscow, Saint-Petersburg, Ekaterinburg, Voronezh, Volgograd, Kazan, Nizhny Novgorod, Perm, Ufa) and from Siberia (Omsk and Krasnoyarsk). A brief description of each city is given in Table 1.

For calculating PET index we used RayMan model which is widely used in the European practice. For example, with the help of this model the PET index was calculated in Freiburg, Germany, or, more precisely, in the center of this city. The frequency of observed certain gradations of the comfort level by the PET index was calculated with Rayman, as well as the local maps of the bioclimatic comfort of this area (Frohlich & Matzarakis, 2010). The same index was applied in 2010 for the detailed analysis of the bioclimatic conditions of Freiburg for the conditions of the modern climate (period 1961-1990) and the forecast period (2071-2100) based on IPCC scenarios (Matzarakis & Endler, 2010). In general, the results show that the number of days with heat stress conditions has increased.

Another example of using this index with RayMan is the study based on the data analysis of 33,212 hospitalizations among people over 60 years old in São Paulo, Brazil between 2003 and 2007. (Silva & Ribeiro, 2012). The results of the study showed the increase in the probability of hospitalization among the group of people in unsatisfactory socio-economic conditions

Table 1. Main big cities of Russian Federation: geographical overview (Bolshaya..., 2007; Census, 2010)

City	Population	Coordinates	WMO station ID	Köppen climate zone	Basic climatic info
Moscow	11 503 501	55°45'N 37°37'E	27612	Dfb	Coldest month: January (-9.4°C) Warmest month: July (+18.3°C) Average annual rainfall: 684 mm
Saint-Petersburg	4 879 566	59°57'N 30°18'E	26063	Dfb	Coldest month: January (-5°C) Warmest month : July (+18°C) Average annual rainfall: 661 mm
Ekaterinburg	1 349 772	56°50'N 60°35'E	28440	Dfb	Coldest month: January(-12.6°C) Warmest month: July (+19°C) Average annual rainfall: 537 mm
Voronezh	889 680	51°40'N 39°12'E	34123	Dfb	Coldest month: January(-6.1°C) Warmest month: July (+20°C) Average annual rainfall: 587 mm
Volgograd	1 021 215	48°42'N 44°31'E	34560	Dfa	Coldest month: January (-6.3°C) Warmest month: July (+23.6°C) Average annual rainfall: 347 mm
Kazan	1 141 535	55°47'N 49°06'3E	27595	Dfb	Coldest month: January (-10.4°C) Warmest month : July (+20.2°C) Average annual rainfall: 558 mm
Krasnoyarsk	973 826	56°01'N 93°04'E	29572	Dfc	Coldest month: January (-15.5°C) Warmest month : July (+15.7°C) Average annual rainfall: 465 mm
Nizhny Novgorod	1 250 619	56°19'N 44°00'E	27459	Dfb	Coldest month: January (-12°C) Warmest month: July (+18.1°C) Average annual rainfall: 648 mm
Omsk	1 154 116	54°59'N 73°22'E	28698	Dfb	Coldest month: January (-16.3°C) Warmest month : July (+19.6°C) Average annual rainfall: 415mm
Perm	991 162	58°00'N 56°19'E	28224	Dfc	Coldest month: January (-12.6°C) Warmest month : July (+18.6°C) Average annual rainfall: 638 mm
Ufa	1 062 319	54°44'N 56°00'E	28722	Dfb	Coldest month: January (-12.4°C) Warmest month : July (+19.76°C) Average annual rainfall: 590 mm

by 12% with the increase in the value of the bioclimatic index by 10°C.

In this study, we use the Rayman model on a one-dimensional scale, without taking into account environmental obstacles and SVF in WMO-station standard environment.

Since there is no other long-term data for a similar period on the territory of the studied cities, **it is as-**

sumed in the study that the measurement data characterize the city climate quite reliably. According to LCZ climate zones classification (Stewart & Oke, 2012) , WMO station areas in cities, selected for long-term trend investigation (Moscow, Saint-Petersburg, Nizhny Novgorod, Perm, Ekaterinburg and Krasnoyarsk) are situated in Type 6 (Open low-rise) and Type 9 (Sparsely built)– see Fig.1

Figure 1. Satellite images of the cities, considered in the study (taken from Google maps) with locations of the used weather stations indicated by asterisk symbols (right panels). Right panees shows satellite images of the nearest surrounding of the weather stations (area within yellow squares in the left panels)

Results

According to the distribution of thermal stress events it is possible to create comfort diagram for each city during daytime heat wave period (for Moscow and Saint-Petersburg see Fig.2).

This plot shows that in both capitals the greatest frequency during daytime is in strong heat stress area (33.3% and 39.6%). Frequency of extreme heat stress in

Moscow is 13.8% and in Saint-Petersburg 5.3%. The cases of comfortable sensations in the period of heat waves for the whole warm period in Moscow constitute only 6.9%. The lowest frequency is graded as “a slightly cold stress” which corresponds to a slight cold exposure (0.2%).

In general, we can say that in Moscow during the period of heat waves people in 47.5% of cases is vul-

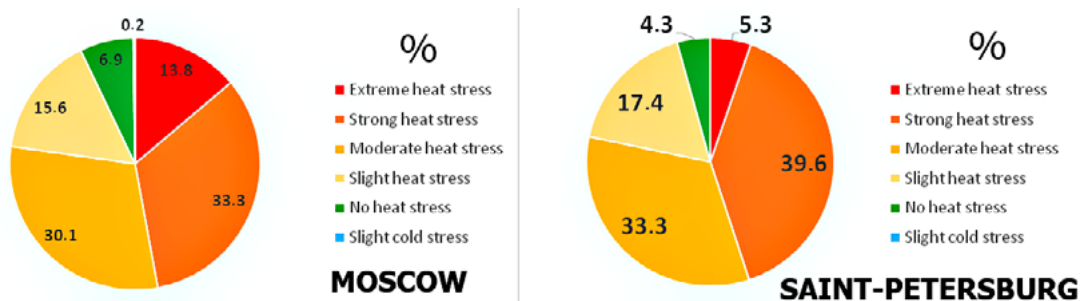


Figure 2. Frequency of PET grades in Moscow and Saint-Petersburg in the day time during heat waves (1966 - 2015 period)

Table 2. Mean-Decade Trends for Air Temperature and for PET in different parts of Russian Federation in 1966-2015

Cities, Russian Federation	Moscow	Saint-Petersburg	Nizhny Novgorod	Perm	Ekaterinburg	Krasnoyarsk
Air temperature linear trend	0.36°C/10yr	0.40°C/10yr	0.38°C/10yr	0.34°C/10yr	0.36°C/10yr	0.29°C/10yr
PET linear trend	0.93°C/10yr	0.25°C/10yr	0.83°C/10yr	0.47°C/10yr	0.54°C/10yr	0.24°C/10yr

nerable to heat stress. In Saint-Petersburg this value is 44.9%

Based on the results obtained in the process of the PET index calculation we plotted a map-diagram which shows the distribution of various degrees of heat stress in 11 large cities of Russia. (Fig.3)

Proceeding from this, we can conclude that the most inclined to heat stress city in the heat waves in the daytime is Volgograd, as Volgograd is one of the hottest cities in Russia. Main PET and air temperature trend results can be briefly summarized in Table 2.

Figure 3. Level of thermal stress in big Russian cities in the day time during heat waves (1966 - 2015 period)

Discussion

So, what if we decide to take a look at long period trends of PET and air temperature in cities of different parts of Russia? We know that climate is changing, air temperature rises in most parts of the Russia (Federal Service for Hydrometeorology and Environmental Monitoring, Roshydromet, 2014). But the thermal comfort is complex characteristic and its trend can clarify the real tendencies of human comfort sensation against the background of regional climate change (see Fig.4)

It is well known that the cities' growth leads to the increase in trends of warming of the local urban climate, which is due to the joint impact of the global climate trends and the impact of the urban heat island (Kataoka et al., 2009). However, practically nothing

is known about the relationship between temperature growth and changes in comfort parameters on the territory of Russia.

The most interesting result of the comparison of the urban trends (PET-index and Air Temperature) in different parts of Russia is its extraordinary cross-shaped form in Moscow (in other cities the trends lines are practically parallel to each other): in further research we plan to investigate such phenomenon by using different thermal comfort indices (UTCI etc) It can be caused just as by Moscow related urban planning dynamics in post-USSR period so by regional climate dynamics. The more detailed analysis of the dynamics of PET-predictors (direct solar radiation, wind speed), indicates that its growth is due to the presence of significant negative trends for wind speed and a score of lower clouds. The obvious, at first glance, the explanation of such well-pronounced wind speed trends - an increase in the roughness in the vicinity of the stations against the background of local land use change. However, the obtained trends for the Moscow region are in good agreement with the estimates from (Federal Service for Hydrometeorology and Environmental Monitoring, Roshydromet, 2014) and (Meshcherskaya, 2004; 2006), according to which the decrease in wind speed with speeds of 0.1-0.5 m/s/10 years over the last decades is typical for the European territory of Russia.

The trend of the decrease in the lower cloudiness in Moscow is making the greatest contribution to the

Figure 4. Linear trends of PET-index (annual mean for warm period) and air temperature (annual mean for warm period) in different parts of Russian Federation in 1966-2015

relative discomfort in summer is manifested more evidently. The similar changes are consistent with the trend of increasing duration sunshine against the background of the increase in the total cloud score for Moscow and Kazan (Gorbarenko et al., 2017; Sidorenko et al., 2012) and the trend of erythema ultraviolet radiation (Chubarova et al., 2018).

We used a small number of cities in our research and can not say about the global trends in the country, nevertheless it is possible to make some valuable conclusions.

The high probability of the heat stress is more evident for large and fast-evolving cities of Central Russia. The faster growth of PET temperatures is observed as compared to air temperatures. This is confirmed by the examples of Moscow and Nizhny Novgorod (PET-warming trend is two times more intensive than thermal one). We can suggest that the cross-shaped form of T and PET can be noticed in Nizhny Novgorod soon.

The maritime climate of Saint Petersburg (the only city with this type of climate among the observed) has the impact on the conditions of thermal comfort. Despite the increase of T the significant changes in PET (feeling of heat for human) did not occur. The probability of heat stress in this city is inconsiderable.

Conclusions

Within the frames of this study, the PET equivalent-physiological temperature index was calculated for each day of the warm period for 11 biggest cities of Russia. Based on the results of the calculations, we have plotted the diagrams with the frequency of occurrence of extreme thermal events during the heat waves for each town.

Also showed that at the level of the average annual values, only in Moscow-city the PET index (and, hence, potentially the thermal stress) grows faster than the regional climate warms ($0.93^{\circ}\text{C}/10\text{yr}$ for PET and $0.36^{\circ}\text{C}/10\text{yr}$ for air temperature). In other cities this tendency is much more weak (N.Novgorod) or

Perm and Yekaterinburg are both located in the area of the Ural Mountains and have similar trends in PET values. We can observe the increase in PET greatly correlated with temperature changes without any unusual effects.

Krasnoyarsk has the most continental climate type among the cities reviewed. We can observe small difference between T and PET in addition to the growth of both parameters. Krasnoyarsk can be considered as the city with the lowest probability of heat stress.

An argumentative issue, of course, is the choice of this particular parameter (the frequencies of PET grades) for determining the relative risk of thermal discomfort phenomenon. However, taking into account the absolute temperature values of thermal waves is also not ideal - because of both the adaptation of the population of more southern regions to hot weather, and the vulnerability of the criterion (Frich et al., 2002) for determining heat waves in the northern regions.

The obtained results can be considered in the further analysis with larger number of weather stations and can used for categorization of cities according to the level and the dynamics of thermal comfort conditions.

not significant. The most inclined to risk city during the heat waves in the daytime is Volgograd, while St. Petersburg can be considered the safest, since the frequency of thermal stress even in this dangerous period does not exceed 5.3% of all the cases.

The main result achieved during the study is the creation of Russia's first comparative climatology of comfort in biggest cities and the determination of the relative danger of heat waves for each of them based on the analysis of 50 year time series, as well as the determination of the dynamics of heat comfort indices for the last 50 years (1966-2015).

Acknowledgments

Research was supported by the grant program of Russian Science Foundation (project no. 17-77-20070 "An initial assessment and projection of the bioclimatic comfort in Russian cities in XXI century against the context of climate change").

Author Contributions

Pavel Konstantinov and Natalia Shartova conceived and designed the experiments; Diana Tattimbetova performed the experiments with Rayman model for warm season periods; Pavel Konstantinov and Mikhail Varentsov analyzed the data; Pavel Konstantinov finally wrote the paper.

References

- Arsenović, D., Lehnert, M., Fiedor, D., Šimáček, P., Středová, H., Středa, T., & Savić, S. (2019). Heat-waves and mortality in Czech cities: A case study for the summers of 2015 and 2016. *Geographica Pannonica*, 23(3), 162-172.
- Osipov, Y. (Ed.) (2007). *Bol'shaya Rossiyskaya entsiklopediya* [The Great Russian Encyclopedia]. Vol. 5. Moscow: Bol'shaya Rossiyskaya entsiklopediya: 710–783 (in Russian).
- Frich, P., Alexander, L. V., Della-Marta, P. M., Gleason, B., Haylock, M., Tank, A. K., & Peterson, T. (2002). Observed coherent changes in climatic extremes during the second half of the twentieth century. *Climate research*, 19(3), 193-212.
- Fröhlich, D., & Matzarakis, A. (2013). Modeling of changes in thermal bioclimate: examples based on urban spaces in Freiburg, Germany. *Theoretical and Applied Climatology*, 111(3), 547-558.
- Kislov, A. V., & Konstantinov, P. I. (2011). Detailed spatial modeling of temperature in Moscow. *Russian Meteorology and Hydrology*, 36(5), 300-306. <https://doi.org/10.3103/S1068373911050037>
- Kolosov, V.A. & Nefedova, T.G. Reg. Res. Russ. (2014) 4: 68. <https://doi.org/10.1134/S2079970514020099>
- Konstantinov, P. I., Varentsov, M. I., & Malinina, E. P. (2014). Modeling of thermal comfort conditions inside the urban boundary layer during Moscow's 2010 summer heat wave (case-study). *Urban Climate*, 10, 563-572.
- Höppe, P. (1999). The physiological equivalent temperature—a universal index for the biometeorological assessment of the thermal environment. *International journal of Biometeorology*, 43(2), 71-75.
- Johansson, E. (2006). Influence of urban geometry on outdoor thermal comfort in a hot dry climate: A study in Fez, Morocco. *Building and environment*, 41(10), 1326-1338.
- Kataoka, K., Matsumoto, F., Ichinose, T., & Taniguchi, M. (2009). Urban warming trends in several large Asian cities over the last 100 years. *Science of the total environment*, 407(9), 3112-3119.
- Matzarakis, A., & Endler, C. (2010). Climate change and thermal bioclimate in cities: impacts and options for adaptation in Freiburg, Germany. *International journal of biometeorology*, 54(4), 479-483.
- Mescherskaya, A. V., Getman, I. F., Borisenko, M. M., & Shevkunova, E. I. (2004). Monitoring of wind-speed in the Volga River catchment and the Ural region in the twentieth century. *Russian Meteorology and Hydrology*, 3, 83-97.
- Mescherskaya, A. V., Eremin, V. V., Baranova, A. A., & Maystrova, V. V. (2006). Change in wind speed in northern Russia in the second half of the twentieth century, from surface and upper air data. *Russian Meteorology and Hydrology*, 9, 46-58..
- Silva, E. N. D., & Ribeiro, H. (2012). Impact of urban atmospheric environment on hospital admissions in the elderly. *Revista de Saúde Pública*, 46(4), 694-701.
- Robinson, P. J. (2001). On the definition of a heat wave. *Journal of Applied Meteorology and Climatology*, 40(4), 762-775.
- Shaposhnikov D, Revich B, Bellander T, et al. Mortality Related to Air Pollution with the Shaposhnikov, D., Revich, B., Bellander, T., Bedada, G. B., Bottai, M., Kharkova, T., Kvasha, E., Lezina, E., Lind, T., Semutnikova, E. & Pershagen, G. (2014). Mortality related to air pollution with the Moscow heat wave and wildfire of 2010. *Epidemiology (Cambridge, Mass.)*, 25(3), 359-364. doi:10.1097/EDE.0000000000000090
- Shartova, N., Shaposhnikov, D., Konstantinov, P., & Revich, B. (2018). Cardiovascular mortality during heat waves in temperate climate: an association with bioclimatic indices. *International Journal of Environmental Health Research*, 28(5), 522–534. <https://doi.org/10.1080/09603123.2018.1495322>
- Stewart, I. D. (2011). A systematic review and scientific critique of methodology in modern urban heat island literature. *International Journal of Climatology*, 31(2), 200-217. doi:10.1002/joc.2141
- Stewart, I. D., & Oke, T. R. (2012). Local climate zones for urban temperature studies. *Bulletin of the American Meteorological Society*, 93(12), 1879-1900. doi:10.1175/BAMS-D-11-00019.1
- Federal Service for Hydrometeorology and Environmental Monitoring (Roshydromet). 2014. The Second Roshydromet Assessment Report on Climate Change and its Consequences in the Russian Federation. General Summary. Moscow: Roshydromet.
- Urban, A., Hondula, D. M., Hanzlíková, H., & Kyselý, J. (2019). The predictability of heat-related mortality in Prague, Czech Republic, during summer 2015—A comparison of selected thermal indices. *International journal of biometeorology*, 63(4), 535-548.
- Zemtsov, S., Shartova, N., Varentsov, M., Konstantinov, P., Kidyayeva, V., Shchur, A., Timonin, S. & Grischchenko, M. (2020). Intraurban social risk and mortality patterns during extreme heat events: A case study of Moscow, 2010-2017. *Health & Place*, 66, 102429. <https://doi.org/10.1016/j.healthplace.2020.102429>

Identification and Geovisualization of Landscape Transformation of Surface Mine Areas in the Đurđevik Coal Basin (Bosnia and Herzegovina)

Sabahudin Smajić^{A*}, Merima Kovačević^A, Dragoslav Pavić^{B, C}

Received: October 30, 2020 | Revised: December 28, 2020 | Accepted: January 11, 2021

doi: 10.5937/gp25-29151

Abstract

The paper researches the landscape transformation of the surface mines of the Đurđevik coal basin (northeastern Bosnia region), where 35.24 Mt of brown coal were produced in the past 74 years, and 227.40 Mm³ of overburden was excavated and disposed of. This type of coal exploitation caused the formation concave and convex of anthropogenic relief forms which ultimately led to significant landscape transformation. These transformations were identified and geovisualized on the basis of field research and comparative GIS analysis of archival maps, satellite images, Digital Elevation Models and plans of this area. As a result of the research, especially comparative GIS analysis of two prepared terrain models of surface mines, the transformation of hypsometry, slope and aspect, hydrographic network, pedological as well as vegetation cover were determined. Obtained geospatial data are geo-visualized in QGIS, and as a result, thematic maps were created to provide insight into the essence of transformations. Therefore, established indicators of landscape transformation can serve as a significant factor in planning the revitalization and land re-cultivation of devastated areas in the Đurđevik coal basin.

Keywords: Landscape transformation; GIS analysis; DEM; geo-visualizations; open pit; Đurđevik coal basin

Introduction

Surface coal mining in the Đurđevik coal basin has a 74-year-long tradition and is the main agent of anthropogenic relief. It started in 1946 at the locality “Kažalj potok” and since then it has been carried out at the following localities: “Živčići”, “Potočari”, “Višća I”, “Brezje”, “Bašigovci”, “Suhodanj” and others, which are closed. Two surface mines are currently active in the Đurđevik coal basin, deep interventions: “Višća II” and “Potočari”, whose annual production

amount is about 500 thousand tons of coal and about 4.20 Mm³ of overburden.

This type of coal exploitation caused the formation anthropogenic relief forms which ultimately led to significant landscape transformation, especially topological (Wu et al., 2019). The transformation of hypsometry, slope and aspect, hydrographic network, pedological as well as vegetation cover was particularly emphasized. Therefore, the characteristics of

^A University of Tuzla, Faculty of Natural Sciences and Mathematics, Department of Geography; sabahudin.smajic@untz.ba; merima.kovacevic@untz.ba

^B University of Novi Sad, Faculty of Sciences, Department of Geography, Tourism and Hotel Management; Trg Dositeja Obradovića 3, 21000 Novi Sad, Serbia; dragoslav.pavic@dgt.uns.ac.rs

^C University of Novi Sad, Faculty of Sciences, Climatology and Hydrology Research Centre

* Corresponding author: Sabahudin Smajić; e-mail: sabahudin.smajic@untz.ba

anthropogenic relief and development tendencies require the research of issues, such as: classification and mapping of shapes, quantitative forecast of transformations, determination of re-cultivation measures, etc. (Dinić, 2007; Smajić et al., 2018).

Identification and geo-visualizations analysis landscape transformation at the spatial and temporal level is possible by comparing the natural and anthropogenic relief on the basis of cartographic material, with the application of GIS technology (Smajić, 2012; Smajić et al., 2018). In the process of landscape modeling of mining areas, the factor significance of 3D modeling and interactive visualization options was also emphasized (Brejcha et al., 2016). Therefore, based on archival topographic maps and the recent ALOS DSM, two DEMs (natural and anthropogenic) of the Đurđevik area were prepared, with whose analysis and comparison, quantified and geo-visualized landscape transformations were identified.

Similar studies analyze the pronounced anthropogenic impact on the natural landscape of mining areas, for example, in the Ruhr District in western Germany (Harnischmacher & Zepp, 2014; Harnischmacher, 2007), the Kolubara basin in Serbia (Dragičević et al., 2012), the Mehedinți County in Romania (Boengiu et al., 2016), Bełchatów Coal Open Mine in central Poland (Jaskulski & Nowak, 2019), Patratu region in India (Pandey & Kumar, 2014) etc. These, as well as numerous other studies, also deal with the topic of design, analysis and comparison of digital terrain models of mining areas. A particularly good example of the identification of landscape topography transformation, based

on a comparative analysis of DEMs, is the Polish open-cast coal mine “Bełchatów”, where topographic changes were found in 75% of the treated area (Jaskulski & Nowak, 2019). Topographic transformations in the area of surface coal mining in the Patratu region were also identified relying on stereographic satellite images using the DEMs comparison. Positive relief changes have been recorded in the landfill area (up to 49 m), while negative ones represent deep depressions (up to 66 m) that become zones of water accumulation (Pandey & Kumar, 2014). Gupta et al. (2014) point out that DEM is generated by synthetic radar interferometry (InSAR) ideal in identifying and estimating altitude changes in mining areas. In this way documented topographic changes in the Indian Jahra field in the period 1996-2004 are ± 40 m. Thomas et al. (2015), on the example of Kerala (India), point out that the application of different terrain models in topographic area analysis is the result of different input data, emphasizing the importance of SRTM and ASTER DEMs in geomorphometric analysis. By comparing the terrain model, e.g. in the Upper Silesian Coal Basin the maximum subsidence above the underground mine galleries of over 30 m (Machowski et al., 2016; Dulias, 2016) and in the Ruhr District over 25 m were determined (Harnischmacher & Zepp, 2014) etc.

In general, the aim of the research is to identify and geo-visualize the achieved level of landscape transformation, especially morphological-hydrographic, areas of surface mines in the Đurđevik coal basin, using field research, methods of comparative analysis of terrain models, and GIS technology.

Study area

The Đurđevik coal basin (13 km²) is located in the municipality of Živinice (Tuzla Canton) in northeastern Bosnia, between 44°23'27" and 44°25'18" N and 18°35'33" and 18°39'48" E. Geotectonic, the area is located in the Spreča paleodepression, within the Bosnian Inner Dinarides (Drešković & Mirić, 2017), and geomorphologically belongs to the macroregion “Mountains and hills, valleys and valleys of northern Bosnia” (Lepirica, 2013). Topographically, the basin is located in the triangle between the rivers Gostelja in the east, Oskova in the north and Djedinska mountain in the southwest, while the western and southern borders are approximately represented by the surrounding settlements (Figure 1).

The basin is open to the northeast, extending approximately in the NW-SE direction for about 5.50 km, while the width is 1-2.50 km. The general direction of Lower Miocene coal seam (14-25 m thick), is NW-SE, while dipping to the SW. The seam most often lies over lumpy marly-sandy clays and gravels,

while the roof is predominantly made up of a series of Lower and Middle Miocene marls and marly limestones (up to 240-300 m thick). Uppermost Pliocene and Quaternary series have a thickness up to 60 m (Arsenović et al., 2016). In the Đurđevik coal basin, a coal seam of different depths has been developed. In the northern part of the basin, the coal seam is shallow and is exploited with surface mining (“Potočari”, “Višća II”, etc.), while the deeper coal reserves in the deposit were exploited in the former open pit “Višća I” in the west, the active open pit “Potočari” (deep interventions) in the north, the former open pits “Živčići”, “Brezje” and “Suhodanje” in the east, and the active underground pit “Đurđevik” in the south (Long-term work program of BCM “Đurđevik”, 2018).

From the foot of Djedinska mountain, the hilly relief forms have a general decline towards Sprečko polje in the north. Mountain streams (Brestovica, Kažalj potok, Višća, etc.) flow in this direction, which used

Figure 1. Location of the study area in Bosnia and Herzegovina (a) and the study area (b)

to flow into the Oskova river, more northern of the exploitation field. The highest terrains are in the western (450 m) and southern (430 m) part of the basin, and the lowest in the Oskova (230 m) and Gostelja (233 m) riverbeds. The average height of the Đurđevik exploitation field is 290.99 m, while the height of the area of surface mines was 235-345 m, and now it is 90-360 m.

Exploitation reserves of brown coal in the basin, intended for surface exploitation, amount to 24.29 Mt, of which the mine “Potočari” owns 10.65 Mt, and “Višća II” 13.64 Mt. With the development of Đurđevik’s surface mines, six hamlets have completely disappeared, and parts of several rural settlements were relocated (Smajić et al., 2009; Smajić, 2012).

Data and methods

In order to realize the set goal of the research, it was necessary to conduct field research and develop a DEM of natural and anthropogenic terrain, the comparison which identified and quantified landscape transformations in the area of surface mines. The geospatial data obtained by the applied GIS methodology were geo-visualized after analytical-synthetic processing. The procedure was realized in several research stages.

First, the available cartographic archival material was inspected, which can be used for vectorization of the necessary contents in order to identify and analyze the condition of the Đurđevik area before surface exploitation. Insight into maps of various scales topographic maps at a scale of 1:25,000 (from 1966) are selected, published by the MGI in Belgrade, while the recent state of the Đurđevik area, viewed on the basis of Google Earth Map (satellite image from 2018), ALOS DSM, JAXA (from 2018) and plans of mining surveying, a scale of 1:2,500 (from 2020). The selected AW3D30 DSM is one of the most accurate, medium-resolution altitude datasets (Florinsky et al., 2018), and uses the Advanced Land Observing Satellite (ALOS) based on stereo mapping from Panchromatic Remote-sensing Instrument for Stereo Mapping (PRISM) (Takaku et al., 2018).

After selecting the cartographic basis, four sheets of TM25, the maps were scanned in raster format with a resolution of 400 dpi, and then filtering and adjusting the raster for better visual appearance, more precise vectorization, as well as georeferencing maps in the coordinate system of appropriate projection were performed. After georeferencing, using the application Google Earth Pro, the boundaries of the Đurđevik exploitation field, of the working area and the parts of surface mines were vectorized. Using QGIS tools, the vectorization of thematic contents (isohypses, watercourses, soil, vegetation, etc.) was also carried out and then on the basis of this vectorization the analysis of average heights, the presence of hypsometric levels, slopes and aspects, disorganization of the river network, devastation of soil and vegetation in the area of surface exploitation were executed. Vectorization of thematic content from the Google Earth Pro satellite image (anthropogenic lakes, relocated watercourses, canals, etc.) was also carried out.

In particular, two digital elevation models of the Đurđevik area were made, from different periods, which well illustrate the transformations of landscape topography. The prepared models were compared using QGIS tools, and the complex analysis is facilitated by a uniform pixel size (10x10 m).

Results and discussion

In the past 74 years, surface exploitation in the Đurđevik coal basin, 35.24 Mt of brown coal was produced, which was mainly used for the needs of the thermal power plant “Tuzla”, and about 227.40 Mm³ of overburden was excavated and disposed of in landfills. This type of exploitation has generated a significant landscape transformation of the Đurđevik coal

basin, especially emphasized in the transformation of morphological, hydrographic, pedogeographic and phytogeographic structure. Areas affected by exploitation are significantly degraded and disturbed by mining operations, so the morphology of the terrain, similar to the neighboring Banovići and Kreka coal basins (Smajić et al., 2018; Smajić & Hadžimustafić,

2016; 2017), represents the integration of natural and newly formed anthropogenic relief forms (floors, excavations, open pits, landfills, etc.). Similarly, in the Ruhr District, the consequences of long-term mining activity are still noticeable today, especially in the form of waste heaps differently integrated into the landscape (Harnischmacher, 2007; Harnischmacher & Zepp, 2014). Specifically, surface exploitation in the Đurđevik coal basin, in addition to several smaller and two larger active open pit mines, formed several external and internal landfills of different dimensions (“Stupnica - T6”, “Suhodanj”, “Brezje”, “Višća”, “Potočari”, “Kažalj”, “Odorovići”, etc.) whose composition is dominated by coal bed sediments, i.e. oligomyocene marls, marly limestones and clays. This tailings material is suitable for biological re-cultivation, especially for plantation cultivation of fruits and vegetables (Salihović & Operta, 2008). GIS analysis of anthropogenic relief of surface mines showed that open pits cover 33.16%, landfills 44.89%, recultivated areas 10.56%, anthropogenic lakes 4.65%, while other parts account for 6.74%. Significant areas of natural soil (861.78 ha) in the newly formed anthropogenic relief in the Đurđevik coal basin were devastated, which disrupted natural pedogenetic processes and vegetation. In this way, podzolic-pseudogley terrace (77.88%) and slope soils (11.29%) and brown acid soils on sandstones (5.94%), brown very shallow and shallow soils on serpentines (3,04%), humus-silicate soils on serpentines (1.03%), pelosols (0.77%) and alluvial-deluvial carbonate-free soils (0.47 ha or 0.05%) were dominantly devastated (The Map of Soil, 1969). Agricultural areas, settlements, forest barren lands and others cover 59.92% of the basin area, while forest phytocenoses predominantly devastated sessile and hornbeam forests (38.19%), and pedunculate and hornbeam forests (1.89%) (The map of actual forest vegetation, 1980).

Coal exploitation at the “Višća II” mine is planned until 2025, and at the “Potočari” mine until 2037. Until then, it is planned to excavate 91.34 Mm³ of overburden and 9.31 Mt of coal, which requires addition-

al expropriation, but also soil devastation. The newly discovered overburden will be partially disposed of in external landfills “Stupnica” and “Višća”, and mostly in internal landfills in the pits of active mines, which will form significant areas of technically re-cultivated soil after the end of disposal. From 2026, more intensive activities are planned for the re-cultivation of devastated areas, primarily the “Stupnica” landfill, the “Potočari” internal landfill, etc. (Long-term work program of BCM “Đurđevik”, 2018).

Morphological transformation

The Đurđevik coal basin is located in the foothills of the Konjuh mountain, which is morphologically represented and surrounded by elevations 338-448 m high (Mramor, Rudine Redžepovac, Gradina, Bjelanovica, Palež, Nišan and others). The relief of the surface mining area is lower, while the area is entirely located in the foothills, and before exploitation it was characterized by a hilly, slightly undulating relief intersected by tributaries of the Oskova and Gostelja rivers, and generally sloping to the north (Figure 2).

The formation of concave and convex anthropogenic relief forms due to exploitation has significantly transformed the morphology of the Đurđevik area. External landfills have covered the natural terrain and flat surfaces have been formed, while active pits and landfills of surface mines are still subject to spatial changes.

Hypsometric transformation

Altitude is a significant microclimatic modifier, and most directly affects the direction of biological re-cultivation of devastated areas. Therefore, a hypsometric analysis of the natural and anthropogenic terrain of surface mines was performed, and a 10-meter digital model of the area was used as a basis (Table 1).

The analysis of DEM natural terrain showed that the lowest hypsometric belt (up to 300 m) covered 77.58% of the area, and the highest of its territory had a height of 280-300 m (37.94%). The belt over 300 m covered 22.42% of the area, while more than half of its

Table 1. Categories and spatial dimensions of elevation

Natural relief			Anthropogenic relief	
Elevation (m)	Area (ha)	Portion (%)	Area (ha)	Portion (%)
- 100	-	-	2.61	0.30
100-200	-	-	63.50	7.37
200-300	668.63	77.58	419.78	48.71
300 -	193.24	22.42	375.89	43.62
Total	861.87	100.00	861.78	100.00

Source: Data obtained by GIS analysis. Cartographic basis: TM 1:25,000 (1966). Belgrade: MGI; Map Satellite (2018). Google Earth; DSM (2018). Tokyo: JAXA.

territory had a height of 300-310 m (52.18%). The average altitude of the natural terrain was 280.16 m, and the absolute altitude difference was 109.84 m (Table 1).

The analysis of DEM anthropogenic terrain showed that the lowest belt (up to 100 m) covers 0.30% of the total area, while the 100-200 m belt covers 7.37%, and the highest territory has a height of 160-200 m (62.18%). The hypsometric belt of 200-300 m covers 48.71% of the area, and the highest territory has a height of 240-300 m (83.97%). The belt over 300 m covers 43.62% of the area, while the highest territory has a height of 300-340 m (96.65%). The average altitude of the anthropogenic terrain is 280.48 m, while the absolute altitude difference of the terrain is 266.32 m. Similarly, the mean height of both terrains of the Polish mine "Bełchatów" is fairly uniform, while the height difference is more emphasized; before the formation of the anthropogenic relief it was 80 m, and now 482 m (Jaskulski & Nowak, 2019).

The results of the comparative analysis of DEM show the uniformity of the average height of both terrains. The southern part of the area, where the landfills are the largest, is characterized by the highest levels (300-360 m), while the northern part, where the open pits are, is significantly lower (90-315 m). The average height of the "Višća II" pit is 235.56 m, the maximum 286.58 m, while the maximum depth is 180 m. The "Potočari" pit has an average height of 214.07 m, a maximum of 298.21 m, while the greatest depth in the central part is 90 m (Figure 2).

External landfills, in the southwestern, southern and southeastern part, covered the parts of the valleys of the Kažalj, Višća, Stupnica, Brnjica and other streams. As a result, flattened surfaces of different volume and degree of re-cultivation were formed. The average height of the re-cultivated landfill "Kažalj" is 310.57 m, maximum 329.16 m, and minimum 264.55 m, while the average height of the landfill "Odorovići" is 325.73 m, maximum 333.83 m, and minimum 310.24 m. The average height of the active landfill "Višća" is 310.16 m, maximum 339.72 m, and minimum 259.19 m, while the average height of the active landfill "Stupnica" is 321.78 m, maximum 356.33 m, and minimum 258.57 m.

Figure 2. Cross-profile (A-B-C-D-E-F) in a section of hypsometric map of the study area

Figure 3. Hypsometric map of natural (up) and anthropogenic (down) relief of the study area

In general, surface exploitation has significantly increased the territory with hypsometric levels up to 240 m and over 320 m, and reduced the territory 240-320 m. This hypsometry is a consequence of excavating the terrain in the open pits area, which continuously lowered the relief, and depositing the overburden on the formed landfills, which caused the elevation of the terrain with a hilly shape (Figure 3). Similarly, the most obvious changes in the area of the mine "Bełchatów" were recorded at sites of large topographic forms of anthropogenic origin: the deepest point in the excavation is lower by 250 m than the original height, while the largest increase in height (by 196 m) occurred in the area of external landfill (Jaskulski & Nowak, 2019). In the Macedonian basin Suvodol, over 140 Mm³ of coal was excavated, which resulted with a depression 50-100 m deep and 3 km in diameter, while a landfill grows nearby as a typical anthropogenic hill (Dragičević & Milevski 2010).

Slope transformation

The slope of the terrain is a significant indicator of the morphological structure of the area. The distribution and coverage of slope categories is an indicator of the scope and intensity of morphostructural and exogeomorphological processes, but also of the future influences of these processes on the characteristics and interdependence of denudation and accumulation (Radoš et al., 2012). Therefore, slope models of natu-

Table 2. Categories and spatial dimensions of slopes

Inclination (°)	Natural relief		Anthropogenic relief	
	Area (ha)	Portion (%)	Area (ha)	Portion (%)
0-1°	136.16	15.80	125.35	14.54
1-3°	163.27	18.94	167.96	19.49
3-5°	117.46	13.63	106.33	12.34
5-8°	159.59	18.52	106.90	12.40
8-12°	159.75	18.54	103.86	12.05
12-16°	73.43	8.52	70.88	8.22
16-20°	34.87	4.05	54.50	6.32
20-30°	16.65	1.93	87.89	10.20
30-40°	0.62	0.07	30.88	3.58
> 40°	-	-	7.30	0.85
Total	861.80	100.00	861.86	100.00

Source: Same as table 1.

ral and anthropogenic terrain of surface mines have been developed. In the process of terrain slope identification, methods and algorithms integrated into the QGIS program were used, and ten slope classes were singled out (Table 2).

The GIS analysis of natural terrain model showed that slopes up to 5° were spread over 48.37% of the territory, which was characterized by weaker leaching and the appearance of smaller gullies, as well as a significant increase in leaching power and erosive processes, resulting in linear erosion. Slopes of 5-12° are

spread to 37.06%, while slopes of 12-20° are spread to 12.57% of the territory. In general, the morphology of the area was dominated by sloping plains, and quite sloping and slopes morphogenetically shaped by slope processes, while flat surfaces and gentle slopes were significantly represented. On a slope over 20°, there was 2.00% of the territory affected by intensive slope processes, where as a result strong erosion caused the outbreak of the parent rock substrate to the surface in some places. The area was dominated by medium steep and slightly steep slopes (Table 2, Figure 4).

The GIS analysis of the anthropogenic terrain model showed that slopes up to 5° are spread on 46.37% of the territory, slopes 5-12° on 24.45%, while slopes of 12-20° on 14.54% of the area. Morphologically, the area is dominated by sloping plains and flattened surfaces, and almost equally represented mild and quite sloping. On a slope over 20°, there is 14.63% of the territory affected by intensive slope processes, where medium steep slopes also dominate, with a significant share of steep slopes.

The results of the comparative analysis of the slope model show a significant decrease in the territory of the Đurđevik coal basin with slope up to 16°, except for the category 1-3°, and an increase in the territory over 16°. The decrease of the territory in the category of 5-8° (6.12%) and 8-12° (6.49%) was especially emphasized, and the increase in the category of 20-30° (8.27%) and 30-40° (3.51%). In general, the trend of increasing height differences and the slope of the terrain affected by exploitation is emphasized.

Aspect transformation

Terrain aspect is a significant indicator of morphological and climatic transformation of the area. Its influence on geomorphological processes is emphasized, because slopes of different aspects differentially ab-

Figure 4. The slope map of natural (up) and anthropogenic (down) relief of the study area

Table 3. Aspect categories and their spatial coverage

Aspect	Natural relief		Anthropogenic relief	
	Area (ha)	Portion (%)	Area (ha)	Portion (%)
N (337.5-22.5°)	262.46	30.45	188.94	21.92
NE (22.5-67.5°)	130.38	15.12	114.59	13.30
E (67.5-112.5°)	106.70	12.38	111.54	12.94
SE (112.5-157.5°)	93.43	10.84	101.05	11.73
S (157.5-202.5°)	26.20	3.04	84.57	9.81
SW (202.5-247.5°)	6.79	0.79	62.60	7.26
W (247.5-292.5°)	56.24	6.52	79.57	9.23
NW (292.5-337.5°)	179.85	20.86	118.95	13.80
Total	862.04	100.00	861.82	100.00

Source: Same as table 1.

sorb short-wave radiation, which affects the characteristics of climatic elements as exogenous-geomorphological agents (Radoš et al., 2012). Therefore, a GIS analysis of the spatial orientation of the natural and anthropogenic relief of surface mines was performed. In the aspect identification process, methods and algorithms integrated into the QGIS program were used, where the aspect values were expressed as azimuths (0-360°) and differentiated in eight equal intervals (Table 3).

The natural terrain of the Đurđevik area was characterized by the shadiest aspects, while the anthropogenic ones also have the most represented shady aspects,

with an emphasized increase in the territory with E, SE, S, SW and W aspects (Table 3; Figure 5). Specifically, with the GIS analysis of the natural terrain model, shady aspects were found and made 66.43% of the territory, and sunny 14.67%, while eastern aspects (12.38%) were more represented than western ones (6.52%). The analysis of the anthropogenic terrain model showed that the shady aspects characterize almost half of the territory (49.02%), the sunny 28.80%, while the eastern aspects (12.94%) are significantly more represented than the western ones (9.23%).

The results of the comparative analysis of aspect models show a decrease in the Đurđevik territory with shady (17.41%), and an increase with sunny (14.13%), eastern (0.56%) and western aspect (2.71%). These transformations are a consequence of the formation of anthropogenic relief of significantly different and more homogeneous aspects in relation to the natural relief. As the biological re-cultivation on the slopes of the completed landfills is conditioned by the slope and aspect, the orientation of the terrain is a significant factor in planning and selecting the type of re-cultivation of the devastated areas of the Đurđevik site. Since in areas with higher insolation, the aspect effect of the slope is more emphasized, landfills should be formed with a larger number of final slopes with northern aspect, and less with southern aspect. However, if due to the amount of overburden and the inclusion of the landfill in the existing terrain it is not possible to avoid sunny aspects, slopes should be provided with a more moderate slope to mitigate insolation consequences (Knežiček et al., 2006; Smajić et al., 2018).

Hydrographical transformation

The hydrographic backbone of the Đurđevik coal basin is the river Oskova, a left tributary of the Spreča, with its tributaries. Oskova and its tributary Gostelja frame the basin on the north and east sides, respectively, from the main collecting arteries of surface

Figure 5. The aspect map of natural (up) and anthropogenic (down) relief of the study area

water (Figure 6). According to morphometric measurements, 25.45 km of watercourses touched the exploitation field in Oskova, and 24.71 km in Gostelja.

The results of the GIS analysis of four sheets of a topographic map, scale 1:25,000, show that the watershed between Oskova and Gostelja used to run through the central part of the area earlier, in a south-north direction. All watercourses of the researched area flowed in this direction, which before exploitation, north of the exploitation field, flowed into Oskova, while today they are significantly disorganized. In particular, the river network of the area affected by the exploitation consisted of several watercourses, the sources which are located south and southwest along the perimeter of the exploitation field. Their length in the area of mines, according to the natural relief, was 34.08 km, and the density of the river network was 3.95 km/km². The length of watercourses with constant water yield was 16.94 km or 1.97 km/km², and occasional 17.14 km or 1.99 km/km². The area between Kažalj stream and Gostelja was predominantly characterized by a centrifugal type of river network. The total length of watercourses within the exploitation field was 50.17 km, while 67.93% of their length was destroyed by surface exploitation. In the northwestern area, the 765.67 m long Oskova stream has been relocated (Figure 6). Similar but more intense river transformations affected the Kolubara basin, when the river of the same name was diverted to the tributary Peštan, which resulted in increased coastal erosion, lateral migration of the river flow, loss of land, etc. (Dragičević et al. 2017; Dragičević et al. 2012).

Surface exploitation in the Đurđevik coal basin resulted in 40.09 ha of anthropogenic lakes (Figure 6). The largest is Lake Odorovići, whose area is 10.82 ha, and the length of the shore is about 3.20 km. The lake was formed in 1979 due to the partitioning of the valley of the Kažalj stream with the overburden of a landfill of the same name. It is located at an altitude of 320.00 m, between the hamlets of Kupjerusi in the east, Odorovići in the west, and the re-cultivated landfill "Kažalj" in the north, while on the south side several mountain streams flow into the lake. The depth of the lake is 22.50 m, while the length of the water mirror in the north-south direction is 797.11 m, and the width in the east-west direction is 308.64 m. The emphasized annual oscillation of the lake level is mainly conditioned by the pluviometric regime and evaporation, and it is especially pronounced during the summer period when the water level drops for 1.5 m, while the oscillations of levels in drier years are possible up to 3 m.

The second largest is Lake Bašigovci (8.22 ha), formed in 1985 in the pit of the surface mine "Bašigovci", which has been completely transformed

Figure 6. Digital Elevation Model of natural (up) and anthropogenic (down) relief of the study area

into a sports and recreational complex by the regulation plan. For example, the positive practice of using anthropogenic reservoirs for tourism purposes, which should be pursued, is visible in the German lignite basin Lower Lusatian where 9.75 thousand ha are currently under water (Deshaies, 2020), in the Šaleška valley in Slovenia 200 ha (Šterbenk, 2006) etc. The length of the shore of Bašigovačko Lake is 1.37 km, the length in the north-south direction is 393.32 m, while the width in the east-west direction is 333.38 m. This lake is located at an altitude of 250.50 m, while the maximum depth of the lake is 45.50 m. The lake is dominantly filled with groundwater and less with surface water from the immediate catchment area, it has an overflow system in the northeast, so the annual oscillations of water levels are not significantly pronounced.

The third largest in this basin is Lake Suhodanj with an area of 7.90 ha. The lake was formed in 1988 in the landfill area of the former open pit mine Suhodanj, and due to the partitioning of the Brnjica stream valley by the Stupnica landfill. The level of the lake is at a height of 293.00 m, while its depth is 15 m. The length of the shore of this lake is 1.43 km, the length in the east-west direction is 404.97 m, while the width in the north-south direction is 351.07 m. The Stupnica landfill is quite porous, and the lake water sinks significantly through the marly limestones embankment and flows into the Gostelja river. The annual oscillations

tion of the lake level is significant, in the summer period the water level is lower than the spring by about 1 m, while the oscillations of the levels in drier years are possible by 2-3 m.

Lake Čenda is much smaller with an area of 3.20 ha; it is located at an altitude of 269.20 m, between the hamlets of Čenda in the south, Jahić in the east and Beširević in the northeast, and the landfill of the former open mine “Višća I” in the west. The lake was formed in 1982, and its depth is 26.70 m. The length of the shore of this lake is 1.10 km, the length in the north-south direction is 299.31 m, while the width in the east-west direction is 196.36 m.

In the western part of the area there is Lake Brestovica with an area of 3.28 ha. The lake was formed in the period 1974-1982 due to the partitioning of the

Brestovica stream valley by the landfill “Kažalj”. The length of the shore of this lake is 797.12 m, the length in the east-west direction is 273.51 m, the width in the north-south direction is 195.95 m, while the depth of the lake is 4 m. The annual oscillation of the lake level is conditioned by the pluviometric regime mainly, by the evaporation and sinking of the lake water through the landfill, and this is especially pronounced in summer when the water level drops by 0.60 m on average, although larger oscillations are also possible. In the area of Odžak and Šahići there are also several smaller anthropogenic lakes with an area of up to one hectare. Some of these lakes in the Đurđevik coal basin have existed for many years, have a natural tributary and an overflow system, and have formed their own water regime.

Conclusion

Based on the comparative analysis of DEM natural and anthropogenic terrain, the paper identifies and geovisualizes the landscape transformation of the surface mine area in the Đurđevik coal basin. The results of the research show that 861.78 ha of natural surface were devastated in the past 74 years, and that complex concave and convex anthropogenic relief forms were formed, which significantly transform the Đurđevik landscape. Comparative analysis of DEMs determined the trend of increasing height differences and the slope of the terrain affected by exploitation. The uniformity of the average height of both terrains was emphasized, while the increase in the height difference of the anthropogenic terrain was higher by 156.48 m than the natural one. The territory with hypsometric levels up to 240 m and over 320 m was increased, and 240-320 m was reduced.

The territory of the basin with slope up to 16° has been significantly reduced, except in the category 1-3°, while territory with slope over 16° increased. The territory with slope category 5-8° and 8-12° has been especially reduced, while territory with slope 20-30° and 30-40° increased. The homogeneity of the exposition structure of the anthropogenic relief was emphasized,

the territory with shady aspect was reduced, and it was increased with sunny, eastern and western aspect.

Surface mines also disrupted the orographic watershed between Oskova and Gostelja, while the river network, whose density was 3.95 km/km², was completely disorganized. This completely disrupted the natural potamological function of the watercourse of this area; 16.94 km of permanent and 17.14 km of occasional watercourses were completely destroyed, 765.67 m of the Oskova river were relocated, 40.09 ha of anthropogenic reservoirs were formed, etc.

In general, the most obvious landscape transformations occurred at locations of large topographic forms of anthropogenic origin. The largest height difference was found in the active open pits “Potočari” (230 m) and “Višća II” (106 m), and in the landfills “Stupnica” (100 m), “Višća” (80 m) etc.

As the Đurđevik mine is legally obliged to recultivate the devastated terrain due to coal exploitation, identified and geovisualized indicators of landscape transformation of surface mine areas can be of great importance when planning and performing land recultivation of devastated areas, but also the final design of the post-exploitation landscape.

Acknowledgements

The paper was created within the framework of the research project “Recent physical-geographic changes in Đurđevik basin caused by surface exploitation of coal”, which was approved and funded under Program 4, Internal Call of the University of Tuzla for financing/co-financing of projects in the field of science of importance for the Federation B&H in 2019, entitled “Support for research of importance for the Federation in 2019.” (No. 01-6211-1-IV/19) from 26.11.2019.

References

- Arsenović, S., Urošević, M., Sretenović, B., Cvetkov, V., & Životić, D. (2016). Modelling of a coal seam of the deposit Đurđevik (BiH) by means of 2D reflection seismic imaging. *Journal of Geophysics and Engineering*, 13(3), 422-428. <https://doi.org/10.1088/1742-2132/13/3/422>
- Boengiu, S., Ionuș, O., & Marinescu, E. (2016). Man-made changes of the relief due to the mining activities within Husnicioara open pit (Mehedinți County, Romania). *Procedia Environmental Sciences*, 32, 256-263. <https://doi.org/10.1016/j.proenv.2016.03.030>
- Brejcha, M., Staňková, H., & Černota, P. (2016). Landscape modelling of past, present and future state of areas affected by mining. *Perspectives in Science*, 7, 151-155. <https://doi.org/10.1016/j.pisc.2015.11.024>
- Deshaies, M. (2020). Metamorphosis of Mining Landscapes in the Lower Lusatian Lignite Basin (Germany): New uses and new image of a mining region. *Les Cahiers de la recherche architecturale urbaine et paysagère*, 7. <https://doi.org/10.4000/craup.4018>
- Dinić, J. (2007). *Čovek i reljef* [People and relief]. Belgrade: Serbian Geographical Society. (in Serbian)
- Dragičević, S., Pripužić, M., Živković, N., Novković, I., Kostadinov, S., Langović, M., Milojković, B., & Čvorović, Z. (2017). Spatial and Temporal Variability of Bank Erosion during the Period 1930-2016: Case Study-Kolubara River Basin (Serbia). *Water*, 9(10), 748. <https://doi.org/10.3390/w9100748>
- Dragičević, S., Živković, N., Roksandić, M., Kostadinov, S., Novković, I., Tošić, R., Stepić, M., Dragičević, M., & Blagojević, B. (2012). Land Use Changes and Environmental Problems Caused by Bank Erosion: A Case Study of the Kolubara River Basin in Serbia. In Appiah-Opoku, S. (Ed.). *Environmental Land Use Planning*, (pp. 3-20). <https://dx.doi.org/10.5772/50580>
- Dragičević, S., & Milevski, I. (2010). Human Impact on the Landscape - examples from Serbia and Macedonia. In Zlatić, M. (Ed.) *Global Change - Challenges for soil management*. Germany: Catena Verlag GmbH, 298-309.
- Drešković, N., & Mirić, R. (2017). *Regionalna geografija Bosne i Hercegovine I* [Regional Geography of Bosnia and Herzegovina I]. Sarajevo: Faculty of Science, University of Sarajevo. (in Bosnian)
- Dulias, R. (2016). Anthropogenic Landforms in the Upper Silesian Coal Basin. In: *The Impact of Mining on the Landscape. Environmental Science and Engineering*. (pp. 51-82). Cham: Springer. https://doi.org/10.1007/978-3-319-29541-1_3
- Florinsky, I.V., Skrypitsyna, T.N., & Luschkova, O.S. (2018). Comparative accuracy of the AW3D30 DSM, ASTER GDEM, and SRTM1 DEM: A case study on the Zaoksky testing ground, Central European Russia, *Remote Sensing Letters*, 9(7), 706-714. <https://doi.org/10.1080/2150704X.2018.1468098>
- Gupta, M., Mohanty, K.K., Kumar, D., & Banerjee, R. (2014). Monitoring surface elevation changes in Jharia coalfield, India using synthetic aperture radar interferometry. *Environmental Earth Sciences*, 71, 2875-2883. <https://doi.org/10.1007/s12665-013-2664-9>
- Harnischmacher, S., & Zepp, H. (2014). Mining and its impact on the earth surface in the Ruhr District (Germany). *Zeitschrift für Geomorphologie, Suppl.* 58(3), 3-22. <https://doi.org/10.1127/0372-8854/2013/S-00131>
- Harnischmacher, S. (2007). Anthropogenic impacts in the Ruhr District (Germany): A contribution to anthropogeomorphology in a former mining region. *Geografia Fisica e Dinamica Quaternaria*, 30(2), 185-192.
- Jaskulski, M., & Nowak, T. (2019). Transformations of Landscape Topography of the Bełchatów Coal Mine (Central Poland) and the Surrounding Area Based on DEM Analysis. *ISPRS International Journal of Geo-Information*, 8(9), 403. <https://doi.org/10.3390/ijgi8090403>
- Knežiček, Ž., Uljić, H., & Husagić, R. (2006). *Oblikovanje i prenamjena prostora površinskih kopova lignite* [Shaping and changing areas of lignite open pits]. Tuzla: Mining Institute. (in Bosnian)
- Lepirica, A. (2013). *Geomorfologija Bosne i Hercegovine* [Geomorphology of Bosnia and Herzegovina]. Sarajevo: Sarajevo Publishing. (in Bosnian)
- Machowski, R., Rzetala, M.A., Rzetala, M., & Solarški, M. (2016). Geomorphological and Hydrological Effects of Subsidence and Land use Change in Industrial and Urban Areas. *Land Degradation & Development*, 27(7), 1740-1752. <https://doi.org/10.1002/ldr.2475>
- Pandey, A.C., & Kumar, A. (2014). Analysing topographical changes in open cast coal-mining region of Patratu, Jharkhand using CARTOSAT-I Stereopair satellite images. *Geocarto International*, 29(7), 731-744. <https://doi.org/10.1080/10106049.2013.838309>
- Radoš, D., Lozić, S., & Šiljeg, A. (2012). Morphometrical Characteristics of the Broader Area of Duvanjsko Polje, Bosnia and Herzegovina. *Geoadria*, 17(2), 177-207.
- Salihović, S., Musić, O., & Operta, M. (2008): Ispitivanje jalovinskih materijala na području Tuzlanskog kantona u svrhu korištenja za tehničku i biološku rekultivaciju na primjeru PK Višća i

- Šikulje [Testing of tailings materials in the Tuzla Canton for the purpose of use for technical and biological reclamation on the example of the open pits Višća and Šikulje]. *Proceedings of the 2nd Congress of Geographers of Bosnia and Herzegovina* (pp. 461-470). Neum: Geographical Society in the Federation of B&H. (in Bosnian with English abstract)
- Smajić, S., Kulenović, S., & Pavić, D. (2009). Geographical Consequences of the Surface Exploitation of Coal on the Area of Tuzla Basin. *Geographica Pannonica*, 13(2), 32-40.
- Smajić, S., Hadžimustafić, E., & Kadušić, A. (2018). Identification and geovisualization of morphological-hydrographic changes in the area of the open pit "Turija". *Revija za geografiju*, 13(2), 39-58.
- Smajić, S. (2012). *Geografske promjene na prostoru Tuzlanskog bazena uzrokovane površinskom eksploatacijom uglja* [Geographical changes in the Tuzla Basin area caused by surface coal mining] (Doctoral dissertation). University of Tuzla, Faculty of Science, Tuzla. (in Bosnian)
- Smajić, S., & Hadžimustafić, E. (2016). Recentne morfološko-hidrografske promjene na području površinskih kopova sjevernog krekanskog sinklinorijuma [Recent morphological-hydrographic changes in the area of surface mines of the northern Kreka's synclinorium]. *Proceedings of the Faculty of Science, Volume Geography*, 12, 5-22. (in Bosnian with English abstract)
- Smajić, S., & Hadžimustafić, E. (2017). Morfološko-hidrografske promjene u južnom dijelu banovičkog basena uzrokovane površinskom eksploatacijom uglja [Morphological-hydrographic changes in the southern part of the Banovići basin caused by surface coal mining]. *Proceedings of the 4th Congress of Geographers of Bosnia and Herzegovina* (pp. 554-567). Sarajevo: Geographical Society in the Federation of B&H. (in Bosnian with English abstract)
- Takaku, J., Tadono, T., Tsutsui, K., & Ichikawa, M. (2018). Quality Improvements of 'AW3D' Global DSM Derived from ALOS PRISM. *Proceedings IGARSS 2018 - 2018 IEEE International Geoscience and Remote Sensing Symposium* (pp. 1612-1615), 22-27 July 2018, Valencia, Spain. doi: 10.1109/IGARSS.2018.8518360
- Thomas, J., Prasannakumar, V., & Vineetha, P. (2015). Suitability of spaceborne digital elevation models of differentscales in topographic analysis: an example from Kerala, India. *Environmental Earth Sciences*, 73, 1245-1263. <https://doi.org/10.1007/s12665-014-3478-0>
- Šterbenk, E. (2006). Uspješan program oporavka okoliša za područja pogođena negativnim utjecajem rudarstva, energetike i industrije, temelj za razvoj turizma (primjer Šaleške doline - Slovenija) [Successful environmental recovery program for areas affected by the negative impact of mining, energy and industry, the basis for tourism development: example of the Šaleška valley - Slovenia]. *Proceedings - International scientific seminar "Tourism as a factor of regional development"* (pp. 253-260). Tuzla: University of Tuzla. (in Bosnian with English abstract)
- Wu, Z., Lei, S., Lu, Q., & Bian, Z. (2019). Impacts of Large-Scale Open-Pit Coal Base on the Landscape Ecological Health of Semi-Arid Grasslands. *Remote Sensing*, 11(15), 1820. <https://doi.org/10.3390/rs11151820>
- ≈
- ALOS AW3D30 DSM (2018). Japan Aerospace Exploration Agency (JAXA). Tokyo.
- Data base (2020). Federal Geodetic Administration (FGA). Sarajevo.
- Long-term work program of BCM "Đurđevik", 2017-2032. (2018). Đurđevik: BCM.
- Map Satellite (2018). Google Earth Proo.
- Situational plans "Potočari" and "Višća II" (2020). Scale 1:2,500. Đurđevik: BCM.
- The Map of Soil (1969). Scale 1:50,000. Sarajevo: The Institute for Agriculture and Soil.
- The map of actual forest vegetation of Bosnia and Herzegovina (1980). Scale 1:500,000. Sarajevo: The Faculty of Forestry.
- Topographic map (1956). Scale 1:50,000. Belgrade: Military Geographical Institute.
- Topographic map (1966). Scale 1:25,000, section Šerići-1381, Živinice-1382, Banovići-1446, Đurđevik-1447. Belgrade: Military Geographical Institute.

The Nexus of Tourism Spending with Economic Performance: A Panel Data Analysis for the Eurozone Area

Ageliki Anagnostou^A, George Ekonomou^{B,C}, Dimitris Kallioras^{D*}

Received: November 23, 2020 | Revised: January 24, 2021 | Accepted: January 25, 2021

doi: 10.5937/gp25-29541

Abstract

The paper investigates the nexus of tourism spending (i.e. leisure and business tourism spending) with economic performance (i.e. GDP and employment) for the Eurozone countries, during the period 2000-2018, employing sophisticated panel data analysis techniques. The issue is salient, given that within the Eurozone economic space the abolition of border impediments has released dynamics and brought into surface a new mix of opportunities, threats and challenges that has been changing the balance between centripetal and centrifugal forces. The findings of the paper identify the long-run equilibrium and confirm the bi-directional relationships among the variables considered, thus contributing to the discussion on the relationship between tourism and economic performance.

Keywords: business tourism spending; leisure tourism spending; GDP; employment; panel data analysis; Eurozone area

Introduction

The tourism industry pursues paths to develop markets that are both promising, in terms of demand, and challenging, in terms of supply (Tsui et al., 2017; WTTC, 2019). Thus, tourism may create opportunities, especially concerning the gross domestic product (GDP) and employment, with positive externalities and multiplicative effects (Khan et al., 1995; Chao et al., 2006). In an era of globalization, and under volatile market conditions, such a perspective becomes of paramount importance. This is especially so within economic integration schemes.

Business and leisure tourism spending represent a couple of major, profitable, and popular market seg-

ments within tourism industry (WTTC, 2019). Both segments may consider as natural developments of networking and alliances at the interface of open and integrated economies. Given the ever-increasing demand for travelling to international destinations, identified growth patterns in the tourism sector may, apparently, indicate the ever-growing competition among destinations (Lim & Won, 2020). Hence, emphasis must be placed on identifying patterns that consider tourism spending not only as a mere macroeconomic variable but also – and most importantly – as a (or the) key factor that may generate positive externalities and multiplicative effects in the national economies.

^A University of Thessaly, Department of Economics; aganag@uth.gr

^B Agricultural University of Athens, Department of Management Economy and Communications of Cultural and Tourism Units; goikonomoug@aua.gr

^C University of Thessaly, Department of Planning and Regional Development; goikonomou@uth.gr

^D University of Thessaly, Department of Planning and Regional Development; Pedion Areos, PO 38334, Volos, Greece dkallior@uth.gr; <https://orcid.org/0000-0003-3060-3745>

* Corresponding Author: Dimitris Kallioras; e-mail: dkallior@uth.gr; phone: (+30)2421074484, fax: (+30)2421074385

The paper investigates the nexus of business and leisure tourism spending with GDP and employment for the Eurozone area. To this end, the paper employs sophisticated panel data analysis techniques (i.e. unit root, cointegration, and causality analyses). The issue is salient given that within the EU economic space – and much more within the Eurozone economic space – the abolition of border impediments has released dynamics and brought into surface a new mix of opportunities, threats and challenges that has been changing the balance between centripetal and centrifugal forces (Kallioras et al., 2009 and 2017; Petrakos et al., 2011; Anagnostou et al., 2016). The findings of the paper identify the long-run equi-

librium and confirm the bi-directional relationships among the variables considered, thus contributing to the discussion on the relationship between tourism and economic performance. The analysis covers the period 2000-2018 and utilizes data obtained from the World Travel & Tourism Council (WTTC) and the World Bank. The findings of the paper offer clear-cut policy suggestions.

The remainder of the paper is as follows. Section 2 reviews the literature on the causal relationships between tourism and economic growth. Section 3 presents the data and deploys the methodology. Section 4 performs the empirical analysis and discusses the findings. Section 5 offers the conclusions.

Theoretical Background

The relationship between tourism and economic growth is defined (Oh, 2005; Tugcu, 2014) in terms of four related hypotheses. The “tourism-led economic growth” (“TLEG”) hypothesis indicates a uni-directional causality between tourism expansion and economic growth, in the sense that the expansion of tourism strengthens economic growth. Thus, national governments may boost growth through subsidizing the tourism sector. In contrast, insufficient tourism policies or external shocks may hinder national economic growth prospects. The “economy-driven tourism growth” (“EDTG”) or “reverse” hypothesis indicates a uni-directional causality running from economic growth to tourism expansion. Tourism plays an important – but not the primary – role in economic growth. Thus, national governments may, also, boost growth through subsidizing other sectors or leading industries. The “feedback” or “reciprocal” hypothesis indicates a bi-directional, reciprocal, causality between tourism expansion and economic growth. Tourism expansion affects economic growth, and vice versa. This means that tourism expansion policies may boost economic growth and higher economic growth may boost tourism expansion, in a self-sustained fashion. The “neutrality” hypothesis discloses the absence of any type of causality between tourism expansion and economic growth. Thus, tourism expansion is not a driver of economic growth and economic growth has no impact on tourism.

Against the backdrop of the four hypotheses that define the relationship between tourism and economic growth, the issue has been gaining increasing attention in the corresponding literature (Dwyer et al., 2004; Lee & Chang, 2008; Pablo-Romero et al., 2013; de Vita & Kyaw, 2016; *inter alia*). Yet, concerning the Eurozone countries only some sporadic studies, that mostly focus on the Mediterranean countries, exist. These studies,

using a wide array of methodological approaches, covering different time periods, and utilizing different variables, provide, rather, inconsistent results. The “TLEG” hypothesis has been confirmed for Cyprus (Chou, 2013), for France (Tugcu, 2014; Demirhan, 2016), for Greece (Ivanov & Webster, 2007; Soukiazis & Proença, 2008; Eeckels et al., 2012), for Italy (Soukiazis & Proença, 2008; Cortes-Jimenez & Pulina, 2010; Tugcu, 2014; Demirhan, 2016), for Latvia (Chou, 2013), for Portugal (Soukiazis & Proença, 2008; Neves et al., 2015; Cerdeira & Bento, 2016; Demirhan, 2016), for Slovakia (Chou, 2013), and for Spain (Balaguer & Cantavella-Jordá, 2002; Novak et al., 2007; Soukiazis & Proença, 2008; Tugcu, 2014). Yet, the “TLEG” hypothesis has been rejected for Cyprus (Ivanov & Webster, 2007), and for Spain (Ivanov & Webster, 2007). The “EDTG” hypothesis has been confirmed for Cyprus (Katircioğlu, 2009a), for Malta (Tugcu, 2014), for Slovakia (Škrinjarić, 2019), and for Slovenia (Tugcu, 2014; Gričar et al., 2016; Škrinjarić, 2019). The “feedback” hypothesis has been confirmed for Estonia (Chou, 2013), for France (Tugcu, 2014), for Greece (Dritsakis, 2004; Tugcu, 2014), for Italy (Massidda & Mattana, 2013), for Malta (Katircioğlu, 2009b), and for Spain (Cortes-Jimenez & Pulina, 2010). The “neutrality hypothesis” has been confirmed for Estonia (Chou, 2013), for Greece (Kasimati, 2011; Tugcu, 2014; Demirhan, 2016), for Malta (Tugcu, 2014), for Slovenia (Tugcu, 2014), and for Spain (Demirhan, 2016). Unstable and/or weak relations have been found for Austria, for Cyprus, for Germany, for Greece, for Italy, for the Netherlands, for Portugal, and for Spain (Dragouni et al., 2013; Antonakakis et al., 2015a & 2015b).

There is, apparently, no concrete body of empirical literature on the relationship between tourism and economic growth for the Eurozone countries, and much more for the Eurozone area as a whole. The paper paves the road for a broad and comprehensive

understanding on the issue through the treatment of the Eurozone area as a unified, integrated, area, through the decomposition of the tourism industry

into the segments of business and leisure tourism, and through the study of economic performance both in terms of GDP and employment.

Data

The study compiles and utilizes a balanced panel dataset for the Eurozone countries, namely: Austria, Belgium, Cyprus, Estonia, Finland, France, Germany, Greece, Ireland, Italy, Latvia, Lithuania, Luxembourg, Malta, the Netherlands, Portugal, Slovakia, Slovenia, and Spain. Towards investigating the nexus of busi-

ness and leisure tourism spending with GDP and employment, the paper employs the following variables: GDP (*gdp*), employment (*empl*), business tourism spending (*bts*), and leisure tourism spending (*lts*) (Table 1). The variables are expressed in logarithmic terms.

Table 1. Presentation of the variables

Variable	Acronym	Definition	Measurement	Source
GDP	<i>gdp</i>	GDP	€	World Bank
employment	<i>empl</i>	employed people aged 15-67	no. of employees	World Bank
business tourism spending	<i>bts</i>	spending on business travel	€	WTTC
leisure tourism spending	<i>lts</i>	spending on leisure travel	€	WTTC

Sources: WTTC / World Bank

Methodology

The paper investigates the nexus of business and leisure tourism spending with GDP and employment for the Eurozone countries, during the period 2000-2018. Towards examining the dynamic causal relationships between tourism spending variables and economic performance variables, the paper employs sophisticated, established, panel analysis techniques. Particularly, the empirical analysis is performed as follows: Initially, panel unit root tests for each series are undertaken, testing for the order of integration on the variables considered (i.e. *gdp*, *empl*, *bts*, and *lts*). Then, having integration of order 1 ($I(1)$) in each series, panel cointegration tests are employed to investigate the existence of a long-run relationship between the sets of the variables considered. If the series of the variables considered are cointegrated, the long-run cointegration vector is estimated. Finally, if a long-run relationship between the sets of the variables considered is found to exist, and having estimated the corresponding long-run cointegration vectors, dynamic panel causality tests are applied to evaluate the corresponding short-run cointegration and the direction of the corresponding causality.

Panel Unit Root Tests

The first step of the empirical analysis is to conduct a series of panel unit root tests to determine the order of integration of the panel variables. Particularly, the paper employs five non-parametric unit root tests, name-

ly: the LLC test (Levin et al., 2002), the Breitung test (Breitung, 2000), the IPS test (Im et al., 2003), the ADF-Fisher test (Maddala and Wu, 1999), and the PP-Fisher test (Choi, 2001). The first three tests assume a common unit root process across countries, while the other two assume individual unit root processes. All the aforementioned tests have the null hypothesis of unit roots.

Panel Cointegration Tests

Having established $I(1)$ in the panel dataset, the second step of the empirical analysis is to determine whether long-run relationships exist. The paper employs the ADF-Fisher test (Maddala and Wu, 1999). The latter is a Johansen Fisher-type test (Johansen, 1988) that combines tests from individual cross-sections to obtain a test statistic for the full panel. It is a non-parametric test that does not assume homogeneity in the coefficients. Having established that the series of the variables considered are cointegrated, the paper estimates the corresponding long-run cointegration vectors.

The long-run equilibrium relationship, given by the error correction terms (ECTs), is a measure of the extent by which the observed values in time $t-1$ deviate from the long-run equilibrium relationship. Since the variables are cointegrated, any such deviation at time $t-1$ should induce changes in the values of the variables in the next time point to force the variables back to the long-run equilibrium relationship. The following two equations are estimated:

$$lgdp_{it}(lempl_{it}) = \alpha_{1,i} + \delta_{1,t} + \beta_{1,i}lbt_{it}(llts_{it}) + \eta_{i,t} \quad (1)$$

$$lbt_{it}(llts_{it}) = \alpha_{2,i} + \delta_{2,t} + \beta_{2,i}lgdp_{it}(lempl_{it}) + \phi_{i,t} \quad (2)$$

where $i=1,\dots,19$ refers to each country in the panel dataset, $t=2000,\dots,2018$ denotes each year considered, $\alpha_{1,i}$ and $\alpha_{2,i}$ are the country-specific fixed effects, $\delta_{1,t}$ and $\delta_{2,t}$ are the time-specific fixed effects, $\beta_{1,i}$ and $\beta_{2,i}$ are the coefficients, $\eta_{i,t}$ and $\phi_{i,t}$ are the disturbance terms, which follow the normal probability distribution with zero mean and constant variance, $lgdp$, $lempl$, lbt , and $llts$ are the natural logarithms of GDP, employment, business tourism spending, and leisure tourism spending, respectively. Since, all variables are expressed in natural logarithms, the estimated long-run coefficients may interpret as elasticities.

The long-run cointegration vector is estimated using the panel dynamic ordinary least squares (DOLS) estimation method (Mark & Sul, 2003). The DOLS estimates are used in order to obtain the residuals as the ECTs. The DOLS estimator corrects standard ordinary least squares (OLS) estimator for bias induced by endogeneity and serial correlation on the leads and lags of the first-differenced regressors to control for potential endogeneities. Then, the OLS estimator is applied using the residuals from the first-step regression. Following Engle & Yoo (1987), the Akaike information criterion (AIC) (Akaike, 1974) is used to determine the optimal specifications of equations (1) and (2).

Panel Causality Tests

The ADF-Fisher test (Maddala & Wu, 1999) only indicates whether (or not) the variables are cointegrated and whether (or not) a long-run relationship exists between them. It does not indicate the direction of causality. Thus, having estimated equations (1) and (2) for each pair of the variables considered, and obtaining the estimated residuals ($\eta_{i,t}$ and $\phi_{i,t}$), the paper proceeds in estimating the panel-based vector error-correction model (VECM) (Engle & Granger, 1987) with the one-period lagged residuals (Holtz-Eakin et al., 1988). The panel-based VECM consists of the following two equations:

$$\Delta lgdp_{i,t}(\Delta lempl_{i,t}) = \alpha_{1,i} + \sum_{k=1}^h \theta_{1,1,i,k} \Delta lgdp_{i,t-k}(\Delta lempl_{i,t-k}) + \sum_{k=1}^h \theta_{1,2,i,k} \Delta lbt_{i,t-k}(\Delta llts_{i,t-k}) + \lambda_{1,i} \eta_{i,t} + u_{1,i,t} \quad (3)$$

$$\Delta lbt_{i,t}(\Delta llts_{i,t}) = \alpha_{2,i} + \sum_{k=1}^h \theta_{2,1,i,k} \Delta lbt_{i,t-k}(\Delta llts_{i,t-k}) + \sum_{k=1}^h \theta_{2,2,i,k} \Delta lgdp_{i,t-k}(\Delta lempl_{i,t-k}) + \lambda_{2,i} \phi_{i,t} + u_{2,i,t} \quad (4)$$

where $lgdp$, $lempl$, lbt , and $llts$ are the natural logarithms of GDP, employment, business tourism spending, and leisure tourism spending, respectively, Δ is the difference operator, $\eta_{i,t}$ and $\phi_{i,t}$ are the lagged residuals derived from the long-run cointegrating relationships in equations (1) and (2), $\theta_{1,1,i,k}$, $\theta_{1,2,i,k}$, $\theta_{2,1,i,k}$, and $\theta_{2,2,i,k}$ are the short-run adjustment coefficients, $\lambda_{1,i}$ and $\lambda_{2,i}$ measure how fast the values of the variables of the system come back to the long-run equilibrium levels when they deviate from them, k denotes lag length, $u_{1,i,t}$ and $u_{2,i,t}$ are the disturbance terms assumed to be uncorrelated with mean zero.

By using the variables in their differenced form, the paper takes care of the OLS estimation problem, which is due to the correlation between country-specific effects and explanatory variables. Nevertheless, differencing introduces the problem of simultaneity because the lagged dependent variables are correlated with the differenced ECTs. Furthermore, heteroscedasticity in the errors across the cross-section members is expected to occur. Hence, the application of an instrumental variable estimator, to cope with these problems, is necessary. A widely-used estimator is the panel GMM estimator (Arellano & Bond, 1991). In the system of equations (3) and (4), pre-determined lags of the system variables are used as instruments to obtain consistent results. Following, again, Engle & Yoo (1987), the paper uses the AIC (Akaike, 1974) to determine the optimal specifications of equations (3) and (4).

The source of causation can be identified by testing the significance of the coefficients of the independent variables, $\Delta lgdp_{i,t-k}$ ($\Delta lempl_{i,t-k}$) and $\Delta lbt_{i,t-k}$ ($\Delta llts_{i,t-k}$), in equations (3) and (4). Checking for short-run causality, the null hypothesis is tested to detect whether short-run causality runs from $\Delta lgdp_{i,t-k}$ ($\Delta lempl_{i,t-k}$) ($H_0: \theta_{1,2,i,k}=0, \forall_{i,k}$) and/or from $\Delta lbt_{i,t-k}$ ($\Delta llts_{i,t-k}$) ($H_0: \theta_{2,2,i,k}=0, \forall_{i,k}$). Checking for long-run causality, the significance of the speed of adjustment is tested (whether $\lambda_{1,i} = 0$ and $\lambda_{2,i} = 0$). Checking for strong causality, joint tests are applied by including the coefficients of the explanatory variables and the respective ECT of each equation. This specific notion of causality denotes which variables bear the burden of a short-run adjustment to re-establish a long-run equilibrium, following a shock to the system (Asafu-Adjaye, 2000; Oh & Lee, 2004a & 2004b). Since all variables are represented in a stationary form, standard Wald F-tests (Wald, 1945) can be used when testing the various null hypotheses.

Results

Panel Unit Root Tests' Results

The empirical analysis begins with conducting the LLC test (Levin et al., 2002), the Breitung test (Breitung, 2000), the IPS test (Im et al., 2003), the ADF-Fisher test (Maddala & Wu, 1999), and the PP-Fisher test (Choi, 2001). As it can be inferred from the tests' statistics (Tables 2A and 2B), the unit root hypothesis cannot be rejected. Particularly, in almost all cases, three out of the five or four out of the five unit root tests conducted report evidence of unit roots. Thus, from the unit roots tests, it can be concluded that the variables considered are $I(1)$. This indicates a possible long-run cointegrating relation.

Panel Cointegration Tests' Results

Having established for the different sets of variables, the existence of long-term relationships is examined by employing the ADF-Fisher test (Maddala & Wu, 1999). The results show (Table 3) that the trace statistic and the maximum eigenvalue statistic of the null hy-

pothesis are statistically significant for all sets of variables. This means that the null hypothesis is rejected, at the 5% significance level, indicating that there is a cointegration relationship between the pairs of the variables considered. Indeed, the empirical realizations of the trace statistic and the maximum eigenvalue statistic provide evidence in favor of a long-run relationship.

The long-run cointegrating relationships in equations (1) and (2) are estimated using the DOLS estimator (Mark & Sul, 2003) to correct standard OLS for the bias induced by endogeneity and serial correlation. The long-run elasticity estimation results (Tables 4A and 4B) indicate that the coefficients of both expenditure proxies are positive and statistically significant at the 5% level for all dependent variables. Specifically, both affect and in a positive way. Particularly, an increase in by 1% increases and by 0.724% and 0.075%, respectively, while an increase in by 1% increases and by 0.767% and 0.082% respectively. Also,

Table 2A. Panel unit root test results (levels)

Variable		levels				
		LLC Test	Breitung Test	IPS Test	ADF-Fisher Test	PP-test Test
lgdp	Statistic	-2.48	1.48	1.73	21.42	19.08
	Prob.	0.01**	0.93	0.96	0.99	1.00
lemp	Statistic	-0.52	3.06	1.29	22.05	31.63
	Prob.	0.30	1.00	0.90	0.98	0.76
lbts	Statistic	-0.71	1.51	1.01	29.78	50.48
	Prob.	0.24	0.93	0.84	0.83	0.08
llts	Statistic	-2.00	3.66	1.40	32.16	45.44
	Prob.	0.02**	1.00	0.92	0.74	0.19

** indicates statistical significance at the 5% level.

Source: Authors' elaboration

Table 2B. Panel unit root test results (1st differences)

Variable		1st differences				
		LLC Test	Breitung Test	IPS Test	ADF-Fisher Test	Fisher-type Test
lgdp	Statistic	-6.13	-4.60	-1.67	57.06	83.65
	Prob.	0.00**	0.00**	0.05**	0.02**	0.00**
lemp	Statistic	-4.77	-3.14	-1.54	55.28	83.31
	Prob.	0.00**	0.00**	0.06	0.03**	0.00**
lbts	Statistic	-11.27	-8.62	-7.35	115.12	147.45
	Prob.	0.00**	0.00**	0.00**	0.00**	0.00**
llts	Statistic	-11.16	-8.17	-6.45	108.24	173.89
	Prob.	0.00**	0.00**	0.00**	0.00**	0.00**

** indicates statistical significance at the 5% level.

Source: Authors' elaboration

Table 3. ADF-Fisher panel cointegration test results

Variables		Fisher statistics (from trace test)	p-value	Fisher statistics (from maximum eigenvalue test)	p-value
lgdp & lbts	none	207.4**	0.00	188.3**	0.00
	at most 1	84.08	0.00	84.08	0.00
lgdp & llts	none	109.7**	0.00	99.27**	0.00
	at most 1	60.51	0.01	60.51	0.01
lemp & lbts	none	142.3**	0.00	127.5**	0.00
	at most 1	70.22	0.00	70.22	0.00
lemp & llts	none	101.9**	0.00	84.05**	0.00
	at most 1	71.11	0.00	71.11	0.00

** indicates rejection of the null hypothesis of no cointegration at least at the 5% level of statistical significance. For each data set, in each panel, the null hypothesis () is tested using the observed trace statistic and maximum eigenvalue statistic. If the null hypothesis is rejected, the alternative hypothesis () is examined.

Source: Authors' elaboration

Table 4A. Long-run elasticity estimation results (estimations of equation 1)

Independent Variables	lgdp		lemp	
	estimates	t-stat	estimates	t-stat
lbts	0.724	11.250**	0.075	2.604**
llts	0.767	15.418**	0.082	3.239**

** denotes statistical significance at the 5% level.

Source: Authors' elaboration

Table 4B. Long-run elasticity estimation results (estimations of equation 2)

Independent Variables	lbts		llts	
	estimates	t-stat	estimates	t-stat
lgdp	0.909	12.905**	0.977	17.195**
lemp	0.892	2.186**	0.826	1.780*

** and * denote statistical significance at the 5% and 10% level, respectively.

Source: Authors' elaboration

both and affect and in a positive way. Particularly, an increase in by 1% increases and by 0.909% and 0.977%, respectively, while an increase in by 1% increases and by 0.892% and 0.826%, respectively.

Panel Causality Tests' Results

The long-run causal relationships between the pairs of the variables considered is examined with the use of panel VECM. Defining the lagged residuals (,) from the estimated long-run cointegration equations (i.e. equations 3 and 4), the VECMs are estimated for the different variable sets (Tables 5A and 5B). The results indicate the short-run and long-run Granger causality tests (Granger, 1969). The optimal lag structure of one year is chosen using the AIC (Akaike, 1974). Short-run causality is determined by

the statistical significance of the estimated coefficients of the first differences of variables. Long-run causality is determined by the statistical significance of the respective ECTs, using t-tests. The coefficients of the ECTs give the adjustment rate at which short-run dynamics converge to the long-run equilibrium relationship.

The ECTs are statistically significant and negative in all cases, indicating a long-run relationship of all the pairs of the variables considered. Particularly, it comes that both business tourism spending and leisure tourism spending are statistically significant determinants of GDP and employment, and vice versa. Thus, the "feedback" or "reciprocal" hypothesis is confirmed for the Eurozone countries during the period under consideration.

Table 5A. Panel VECM estimation results (estimations of equation 3)

Dependent Variable		Independent Variable	Coefficient	t-statistic
$\Delta l g d p$	SR	$\Delta l b t s$	0.201	10.397**
	LR	ECT	-0.135	-5.450**
$\Delta l e m p l$	SR	$\Delta l b t s$	0.086	8.520**
	LR	ECT	-0.150	-5.494**
$\Delta l r g d p$	SR	$\Delta l l t s$	0.455	15.390**
	LR	ECT	-0.115	-4.920**
$\Delta l e m p l$	SR	$\Delta l l t s$	0.165	10.532**
	LR	ECT	-0.190	-7.860**

SR and LR denote short-run and long-run, respectively.

** denotes statistical significance at the 5% level.

Source: Authors' elaboration

Table 5B. Panel VECM estimation results (estimations of equation 4)

Dependent Variable		Independent Variable	Coefficient	t-statistic
$\Delta l b t s$	SR	$\Delta l g d p$	1.212	11.273**
	LR	ECT	-0.261	-6.188**
$\Delta l b t s$	SR	$\Delta l e m p l$	1.335	5.891**
	LR	ECT	-0.171	-5.282**
$\Delta l l t s$	SR	$\Delta l g d p$	0.776	14.570**
	LR	ECT	-0.181	-5.837**
$\Delta l l t s$	SR	$\Delta l e m p l$	1.015	8.983**
	LR	ECT	-0.078	-3.306**

SR and LR denote short-run and long-run, respectively.

** denotes statistical significance at the 5% level.

Source: Authors' elaboration

Conclusions

The paper investigates the nexus of business and leisure tourism spending with GDP and employment for the Eurozone countries, during the period 2000-2018, employing sophisticated, established, panel data analysis techniques. The findings of the paper indicate that both business tourism spending and leisure tourism spending are statistically significant determinants of GDP and employment, and vice versa, thus confirming the “feedback” or “reciprocal” hypothesis. Particularly, the findings of the paper indicate a bi-directional, reciprocal, causality between business tourism spending and leisure tourism spending, on the one hand, and GDP and employment, on the other.

The findings of the paper call for a set of well-targeted and carefully-designed policy interventions focusing on promoting both business tourism and leisure tourism. This is so as tourism expansion policies may

boost economic growth and higher economic growth may boost tourism expansion, in a self-sustained fashion. Tourism planners ought to demonstrate openness in new trends and challenges to meet visitors' needs and demands, whereas, at the same time, economists and entrepreneurs should embed innovation in investment plans concerning the provision of services, facilities, and infrastructure to enhance tourism expansion through memorable tourism experiences. This is, apparently, not an easy-to-achieve task, considering that exogenous economic shocks (COVID-19 is the most notable one) lead to pressures on tourism and economic activity. Overall, it remains to be seen whether and to what extent the individual economies of the Eurozone have the same capacity to reap the benefits of tourism expansion. To this end, the paper sets the basis for further empirical research.

References

- Akaike, H. (1974). A new look at the statistical model identification. *IEEE Transactions on Automatic Control*, 19, 716-723. DOI: 10.1109/TAC.1974.1100705
- Anagnostou, A., Kallioras, D., & Kollias, C. (2016). Governance convergence among the EU28? *Social Indicators Research*, 129(1), 133-146. <https://doi.org/10.1007/s11205-015-1095-2>
- Antonakakis, N., Dragouni, M., & Filis, G. (2015a). Tourism and growth: The times they are a-changing. *Annals of Tourism Research*, 50, 159-172. DOI: 10.1016/j.annals.2014.11.008
- Antonakakis, N., Dragouni, M., & Filis, G. (2015b). How strong is the linkage between tourism and economic growth in Europe? *Economic Modelling*, 44, 142-155. <https://doi.org/10.1016/j.econmod.2014.10.018>
- Arellano, M., & Bond, S.R. (1991). Some tests of specification for panel data: Monte Carlo evidence and an application to employment equations. *Review of Economic Studies*, 58, 277-297. <https://doi.org/10.2307/2297968>
- Asafu-Adjaye, J. (2000). The relationship between energy consumption, energy prices and economic growth: Time series evidence from Asian developing countries. *Energy Economics*, 22, 615-625. [https://doi.org/10.1016/S0140-9883\(00\)00050-5](https://doi.org/10.1016/S0140-9883(00)00050-5)
- Balaguer, J., & Cantavella-Jorda, M. (2002). Tourism as a long-run economic growth factor: The Spanish case. *Applied Economics*, 34, 877-884. <https://doi.org/10.1080/00036840110058923>
- Breitung, J. (2000). The local power of some unit root tests for panel data. *Advances in Econometrics*, 15, 161-177. [https://doi.org/10.1016/S0731-9053\(00\)15006-6](https://doi.org/10.1016/S0731-9053(00)15006-6)
- Cerdeira Bento, J.P. (2016). Tourism and economic growth in Portugal: An empirical investigation of causal links. *Tourism and Management Studies*, 12(1), 164-171. DOI: 10.18089/tms.2016.12117
- Chao, C.-C., Hazari, B.R., Laffargue, J.-P., Sgro, P.M., & Yu, E.S.H. (2006). Tourism, Dutch disease and welfare in an open dynamic economy. *Japanese Economic Review*, 57(4), 501-515. <https://doi.org/10.1111/j.1468-5876.2006.00400.x>
- Choi, I. (2006). Unit root tests for panel data. *Journal of International Money and Finance*, 20, 249-272. [https://doi.org/10.1016/S0261-5606\(00\)00048-6](https://doi.org/10.1016/S0261-5606(00)00048-6)
- Chou, M.C. (2013). Does tourism development promote economic growth in transition countries? A panel data analysis. *Economic Modelling*, 33: 226-232. <https://doi.org/10.1016/j.econmod.2013.04.024>
- Cortes-Jimenez, I., & Pulina, M. (2010). Inbound tourism and long-run economic growth. *Current Issues in Tourism*, 13(1), 61-74. <https://doi.org/10.1080/13683500802684411>
- Demirhan, B. (2016). Tourism-Led Growth Hypothesis in Mediterranean Countries: Evidence from a panel cointegration and Error Correction Model. *Applied Economics and Finance*, 3(1), 38-53. DOI: 10.11114/aef.v3i1.1207
- De Vita, G., & Kyaw, K.S. (2016). Tourism development and growth. *Annals of Tourism Research*, 60, 23-26. <https://doi.org/10.1016/j.annals.2016.05.011>
- Dickey, D.A., & Fuller, W.A. (1979). Distribution of the estimators for autoregressive time series with a unit root. *Journal of the American Statistical Association*, 74, 417-431. <https://doi.org/10.2307/2286348>
- Dragouni, M., Filis, G., & Antonakakis, N. (2013). Time-varying interdependencies of tourism and economic growth: Evidence from European countries. *MPRA Papers*, 48715. <https://mpra.ub.uni-muenchen.de/48715/>
- Dritsakis, N. (2004). Tourism as a long-run economic growth factor: An empirical investigation for Greece using causality analysis. *Tourism Economics*, 10(3), 305-316. DOI: 10.5367/0000000041895094
- Dwyer, L., Forsyth, P., & Spurr, R. (2004). Evaluating tourism's economic effects: New and old approaches. *Tourism Management*, 25(3) 307-317. [https://doi.org/10.1016/S0261-5177\(03\)00131-6](https://doi.org/10.1016/S0261-5177(03)00131-6)
- Eeckels, B., Filis, G., & Leo, C. (2012). Tourism income and economic growth in Greece: Empirical evidence from their cyclical components. *Tourism Economics*, 18(4), 817-834. <https://doi.org/10.5367/te.2012.0148>
- Engle, R.F., & Granger, C.W.J. (1987). Cointegration and error-correction: representation, estimation and testing. *Econometrica*, 55: 251-276. <https://doi.org/10.2307/1913236>
- Engle, R.F., & Yoo, B.S. (1987). Forecasting and testing in co-integrated systems. *Journal of Econometrics*, 35, 143-159. [https://doi.org/10.1016/0304-4076\(87\)90085-6](https://doi.org/10.1016/0304-4076(87)90085-6)
- Granger, C. (1964). Investigating causal relations by econometric models and cross-spectral methods. *Econometrica*, 37(3), 424-438. <https://doi.org/10.2307/1912791>
- Gričar, S., Bojnec, S., Karadžić, V., & Rakočević, S. (2016). Comparative analysis of tourism-led growth in Slovenia and Montenegro. *Managing Global Transitions*, 14(1), 75-92.
- Holtz-Eakin, D. (1988). Testing for individual effects in autoregressive models. *Journal of Econometrics*, 39, 297-308. [https://doi.org/10.1016/0304-4076\(88\)90060-7](https://doi.org/10.1016/0304-4076(88)90060-7)

- Im, K.S., Pesaran, M.H., & Shin, Y. (2003). Testing for unit roots in heterogeneous panels. *Journal of Econometrics*, 115, 53-74. [https://doi.org/10.1016/S0304-4076\(03\)00092-7](https://doi.org/10.1016/S0304-4076(03)00092-7)
- Ivanov, S., & Webster, C. (2007). Measuring the impact of tourism on economic growth. *Tourism Economics*, Vol. 13, No. 3, pp. 379-388. <https://doi.org/10.5367/000000007781497773>
- Johansen, S. (1988). Statistical analysis of cointegration vectors. *Journal of Economics Dynamic and Control*, 12, 231-254. [https://doi.org/10.1016/0165-1889\(88\)90041-3](https://doi.org/10.1016/0165-1889(88)90041-3)
- Kallioras, D., Gkotinakou, G., & Fardas, M. (2017). Detecting trends of convergence among the Eurozone countries in terms of economic freedom. *International Journal of Economics and Finance Studies*, 9(1), 33-47.
- Kallioras, D., Topaloglou, L., & Venieris, S. (2009). Tracing the determinants of economic cross-border interaction in the European Union. *Spatium*, 21, 1-10. DOI: 10.2298/SPAT0921001K
- Kasimati, E. (2011). Economic impact of tourism on Greece's economy: Cointegration and causality analysis. *International Research Journal of Finance and Economics*, 79, 79-85.
- Katircioğlu, S.T. (2009a). Tourism, trade and growth: The case of Cyprus. *Applied Economics*, 41(21), 2741-2750. <https://doi.org/10.1080/00036840701335512>
- Katircioğlu, S.T. (2009b). Testing the tourism-led growth hypothesis: The case of Malta. *Acta Oeconomica*, 59(3), 331-343. DOI: 10.1556/AO-econ.59.2009.3.4
- Khan, H., Phang, S., & Toh, R. (1995). The multiplier effect: Singapore's hospitality industry. *Cornell Hotel and Restaurant Administration Quarterly*, 36, 64-69. <https://doi.org/10.1177/001088049503600121>
- Lee, C.C., & Chang, C. (2008). Tourism development and economic growth: A closer look at panels. *Tourism Management*, 29, 180-192. <https://doi.org/10.1016/j.tourman.2007.02.013>
- Levin, A., Lin, C.F., & Chu, C. (2002). Unit root tests in panel data: asymptotic and finite sample properties. *Journal of Econometrics*, 108, 1-24. [https://doi.org/10.1016/S0304-4076\(01\)00098-7](https://doi.org/10.1016/S0304-4076(01)00098-7)
- Lim, J., & Won, D. (2020). How Las Vegas' tourism could survive an economic crisis? *Cities*, 100, 102643. <https://doi.org/10.1016/j.cities.2020.102643>
- Maddala, G.S., & Wu, S. (1999). A comparative study of unit root tests with panel data and a new simple test. *Oxford Bulletin of Economics and Statistics*, 61(S1), 631-652. <https://doi.org/10.1111/1468-0084.0610s1631>
- Mark, N.C., & Sul, D. (2003). Cointegration vector estimation by panel DOLS and long-run money demand. *Oxford Bulletin of Economics and Statistics*, 65(5), 655-680. <https://doi.org/10.1111/j.1468-0084.2003.00066.x>
- Massidda, C., & Mattana, P. (2013). A SVECM analysis of the relationship between international tourism arrivals, GDP and trade in Italy. *Journal of Travel Research*, 52(1), 93-105. <https://doi.org/10.1177/0047287512457262>
- Neves, D.C., Fernandes, A.J., & Pereira, E.T. (2015). Determinants of touristic attraction in Portuguese regions and their impact on GDP. *Tourism Economics*, 21(3), 629-648. DOI: 10.5367/te.2013.0361
- Nowak, J.J. (2007). Tourism capital, good imports and economic growth: Theory and evidence for Spain. *Tourism Economics*, 13(4), 515-536. <https://doi.org/10.5367/000000007782696113>
- Oh, C.O. (2005). The contribution of tourism development to economic growth in the Korean economy. *Tourism Management*, 26(1), 39-44. <https://doi.org/10.1016/j.tourman.2003.09.014>
- Oh, W., & Lee, K. (2004a). Causal relationship between energy consumption and GDP revisited: The case of Korea 1970-1999. *Energy Economics*, 26(1), 51-59. [https://doi.org/10.1016/S0140-9883\(03\)00030-6](https://doi.org/10.1016/S0140-9883(03)00030-6)
- Oh, W., & Lee, K. (2004b). Energy consumption and economic growth in Korea: Testing the causality relation. *Journal of Policy Modeling*, 26, 973-981. <https://doi.org/10.1016/j.jpolmod.2004.06.003>
- Pablo-Romero, M.P., & Molina, J.A. (2013). Tourism and economic growth: A review of empirical literature. *Tourism Management Perspectives*, 8, 28-41. <https://doi.org/10.1016/j.tmp.2013.05.006>
- Petrakos, G., Kallioras, D., & Anagnostou, A. (2011). Regional convergence and growth in Europe: Understanding patterns and determinants. *European Urban and Regional Studies*, 18(4), 375-391. <https://doi.org/10.1177/0969776411407809>
- Škrinjarić, T. (2019). Examining the causal relationship between tourism and economic growth: Spillover Index approach for selected CEE and SEE countries. *Economies*, 7(1), 19. <https://doi.org/10.3390/economies7010019>
- Soukiazis, E., & Proença, S. (2008). Tourism as an alternative source of regional growth in Portugal: A panel data analysis at NUTS II and III levels. *Portuguese Economic Journal*, 7, 43-61. DOI: 10.1007/s10258-007-0022-0
- Tsui, K., Hasan, M., Tan, D., Lau, O., & Balli, F. (2017). New Zealand business tourism: Exploring the impact of economic policy uncertainties. *Tourism Economics*, 24, 386-417. <https://doi.org/10.1177/1354816617731387>
- Tugcu, C.T. (2014). Tourism and economic growth nexus revisited: A panel causality analysis for the case of the Mediterranean region. *Tourism Man-*

agement, 42, 207-212. <https://doi.org/10.1016/j.tourman.2013.12.007>

Wald, A. (1945). Sequential tests of statistical hypotheses. *Annals of Mathematics*, 16(2), 117-186. doi: 10.1214/aoms/1177731118

World Tourism Travel Council (2019). *Travel and tourism economic impact 2019 world*, World Travel & Tourism Council (WTTC), London.